Summer 2014

Synthesis and properties of transition-metal arsenide nanostructures: from superparamagnetism to superconductivity

Prachi Desai

Recommended Citation

SYNTHESIS AND PROPERTIES OF TRANSITION-METAL ARSENIDE

NANOSTRUCTURES: FROM SUPERPARAMAGNETISM TO

SUPERCONDUCTIVITY

by

PRACHI DESAI

A DISSERTATION

Presented to the Faculty of the Graduate School of the

MISSOURI UNIVERSITY OF SCIENCE AND TECHNOLOGY

In Partial Fulfillment of the Requirements for the Degree

DOCTOR OF PHILOSOPHY

in

CHEMISTRY

2014

Approved by:
Manashi Nath, Advisor
Wayne Huebner
Jay Switzer
Pericles Stavropoulos
Jeffery Winiarz

PUBLICATION DISSERTATION OPTION

This dissertation is prepared in the style of the Chemistry of Materials (American Chemical Society) journal, NanoResearch (Springer) journal, Journal of Experimental Nanoscience (Taylor and Francis) and Materials Science and Engineering:B (Elsevier). This dissertation includes an article as Paper I that has been published in Chem. Mater. (31-64). Paper II is an article that has been submitted to NanoResearch (65- 92). Paper III has been submitted to Journal of Experimental Nanoscience (93-110) and Paper IV is prepared to be submitted to Materials Science and Engineering: B (111-119).

Appendix A contains unpublished results on LiFeAs nanostructure synthesis and characterization.

Appendix B contains unpublished results on Bi_2Se_3 electrodeposition conditions.

ABSTRACT

This dissertation study focuses on developing new protocols for synthesis of nanostructured transition-metal pnictides including superconducting LiFeAs and studying their structure- property relationship. Nanostructured materials are known to differ in properties compared to their bulk counterparts owing to enhanced surface area and increased packing efficiency in devices. Synthetic chemistry skills and nanofabrication techniques like wet chemistry, electrodeposition, solvothermal, hydrothermal and lithography, are extremely useful for creating nanostructures of these functional materials. This is a challenging task simply because maintaining the phase composition same as that of the bulk material along with achieving nanostructures (nanoparticles, nanowires, nanopillars etc.) simultaneously is not easy. Papers I and II showcase novel synthesis methods for E based pnictides [EPn where $E = 1^{st}$ row transition elements and Pn = P, As etc.]. The superparamagnetism of transition-metal pnictides (e.g. FeAs, CoAs) nanomaterials obtained by this method have interesting magnetic features like high blocking temperatures and inter-particle magnetic exchange. Paper III, shows the concept of generalized protocol of EAs synthesis and discusses the principles behind this method. This protocol has been tested for applicability to not only FeAs, but also MnAs , CoAs and CrAs systems. Generalization of this method along with the discovery of superparamagnetic FeAs is one of the key findings of this research work. Alongside, paper IV shows the formation of Co_3O_4 nanowires through solid-solid conversion route aided by sacrificial templates.

ACKNOWLEDGMENTS

TABLE OF CONTENTS

LIST OF ILLUSTRATIONS

PAPER II

LIST OF TABLES

1. INTRODUCTION

1.1 MAIN-GROUP METAL PNICTIDES

Metal pnictides are compounds formed when the metals in the periodic table combine with the anions of group 15 (previously referred to as Group VA) in the -3 and -5 oxidation states. The term "pnictide" comes from the Latin word pnictogen[1] that means foul smelling, since most of these compounds carried unpleasant smells. Solid state chemistry of the pnictides is very old and dates back over a century. However, recent interest in metal pnictides grew with the discovery of novel optical properties in semiconducting pnictides such as GaN,[2] GaP,[3] $GaAs$,[4] InP, $InAs$[5] etc. Metal pnictides include binaries, ternary and quaternary compositions such as APn, A-B-C-Pn, where A, B are elements that belong to main group as well as transition-metals and Pn = As, P, while C = other charge compensating ions. Amongst the pnictides, nitride chemistry of these compounds has grown since the turn of the 20th century led by pioneers such as Juza, Jack, Marchand, Rabenau and others.[6] Research in the binary pnictides date back over 100 years, whereby, work led by Zintl and others have contributed significantly towards developing a fair amount of understanding of these metal pnictides.[7] Zintl was the first to recognize that alkali and alkaline earth metals combine with group 14 and 15 elements to form compounds that can be considered stoichiometric salts. For example, he showed that magnesium usually combines with the metalloids of group 14 or 15 to form compounds such as Mg_3XZ (X = P, As, Sb, Bi), Z is a semi metal or main group metal and MgX (X = Si, Ge, Sn and Pb). However, families of known metal pnictides compounds were relatively few and less populated and the study of metal pnictides were mostly confined to the main group metal pnictides with the group 13 metal pnictides

occupying a major chunk of research activities. In late 2008, the discovery of high temperature superconductivity in iron pnictides led to the explosion of interest in transition metal arsenides and phosphides. Based on the specific transition metal chemistry these materials were guaranteed to show interesting magnetic properties interwoven into the pnictide chemistry. The synthesis and importance of such pnictides and especially the transition-metal pnictides is the broad scope of this research work. Pnictides have proven their worth as functional materials for a wide plethora of applications, and developing methodologies for creating nanostructures of such pnictides through simple, reproducible technique, is the specific objective of this research.

1.1.1. Metal Nitrides. Most of the metal pnictides show semiconducting properties where the specific characteristics are influenced strongly by the nature of pnictide ion. The metal nitrides of the group 13 elements (AlN,[8] GaN and InN) represent an important trio of semiconductors because of their direct band gaps which span the range 1.95-6.2 eV, including the whole of the visible region and extending well out into the UV range.[9] Alkali metal nitrides like Li_3N have also found niche applications as electrodes in reversible hydrogen storage.[10] It may also be used as starting material for binary and ternary nitride synthesis. PtN has been synthesized by Gregoryanz et al. as one of the novel noble metal nitrides.[11] IrN_2 and OsN_2[12] emerged as super hard materials that found refractory uses. Such refractory metal nitride coatings find numerous applications in cutting tools, wear resistant parts, and the jewelry industry. Recent investigations have disclosed interesting applications of thin films of refractory metal nitrides in microelectronics. The metal nitride layer in silicon acts as a barrier dielectric that serves to improve the properties of the electronic MEMS devices. Superconductivity has also

been observed in nitrides which are hard like NbN, HfN, ZrN.[13] These are also used as refractory materials owing to high bulk moduli. Mixed metal oxynitrides and metal oxynitrides constitute an important branch of metal nitrides because of various applications in energy storage, electro-conductive films, as gate dielectric oxides. The observed ordering and stability of these oxynitrides at high temperatures provide superior device properties. Hetrostructures of alloy metal nitrides and advances in thin film deposition methods have yielded new applications to the metal nitrides. Such hetrostructures can be integrated within the device structure. Enhanced electron mobility and piezoelectric properties have been observed in A1GaN/GaN heterostructures.[14] The heterostructuring in these nitrides is found useful to enhance the band gap and provide different colors for the applications like LEDs based on band gap tuning.

     1.1.2. Metal Phosphides. The main-group metal phosphides are compounds formed with anions, P^{3-} and a less electronegative metal. The important main group metal phosphides include Na_3P, Ca_3P_2, GaP, InP, Cu_3P Cu_3P_2, AlP, Mg_3P_2 etc. Among these AlP and Ca_3P_2 are poisonous and are used as rodenticides. GaP (indirect band gap 2.25eV) and InP (1.27eV) are semiconductors at room temperatures. GaP[15] and InP[16] form the core components of LEDs and their bandgaps can be tuned very precisely with doping in the semiconductor lattice. This band gap tuning is useful in improving and altering the emission and electronic transport properties of the metal phosphides. For example, in order to attain high efficiencies of green light by LEDs, it was observed GaP nanowires having pure hexagonal crystal structure exhibited conversion of indirect band gap (cubic phase) to direct upon nanostructuring.[17] In particular InP has emerged as an important solar cell material. Highly reactive heavy alkali metal phosphides have been

prepared by Englich et al. by treating trimethylsilyl-substituted phosphines with alkali metal *tert*-butyl alcoholates.[18] Modified InP@ZnS nanocrystals[19] have shown to have efficient emission properties in the blue to near IR region. The relatively large number of reports and interest in phosphides has been ignited in parts by the availability of phosphide precursors like trioctylphosphine (TOP) and trioctylphosphine oxide (TOPO).[20]

1.1.3. Metal Arsenides. GaAs with zinc blende structure is one of the most important arsenide semiconductors as it has higher electron mobility and less noise at high operating frequencies when compared to silicon which is the material of choice for making high frequency transistors. GaAs is a direct band-gap semiconductor with E_g= 1.42eV. Currently, these semiconductors are generally useful in the form of thin films. However, the future holds a lot of promise for nanoparticles GaAs especially quantum dots based on their very efficient electronic and optical properties in the nanoscale regime.[21] InAs is a direct bandgap semiconductor with a bandgap of 0.35eV. Other arsenides like GaInAs with zinc blende structure and a bandgap of 0.74eV, constitutes an important component of detectors, photodiodes and solar cells.

1.2. TRANSITION-METAL PNICTIDES

The transition-metal pnictides (both arsenides and phosphides) have gained recent importance following the discovery of superconductivity in Fe-based pnictide superconductors.[22] This discovery, however, has re-kindled an already active *albeit* less pronounced research field thriving on the novelties associated with *d*-electron configuration of the central atom in the transition metal pnictides. These transition metal

pnictides had been studied with respect to their important magnetic properties which were later correlated with their role in superconductivity in the Fe-based superconductors where they act as charge storing layer. Additionally, they have also shown promise as catalysts in HDS (hydrodesulphurization) and HDN (hydrodenitrogenation) of organic chemicals,[23] and as electro catalysts. These includes the binary, EAs , ternary compositions like $LnEPn$[24] (where E = transition elements of the 1st row, Ln =lanthanides and Pn = pnictides, respectively), and quaternary compositions.[25]

The binary EAs are formed when transition metals in +3 oxidation states combine with -3 oxidation state of As. Figure 1.1 highlights the position of transition elements in the periodic table with partially filled 3d shell that constitutes the transition metal of the binary arsenides discussed here in this work.

Figure 1.1: Binary transition-metal arsenides discussed in this work

The other important transition-metal pnictides include RhP_3, RuP, Ru_2P, Pd_3P, Pd_5P_2, Ni_2P, MoP and other ternary composition containing mixed cations like $NiFeP$, $CoMnP$, etc. RhP_3 is a better catalyst for HDS as compared to Rh metal.[26] $Ru_2P/MCM-41$ and $RuP/MCM-41$ catalysts can be synthesized by thermal decomposition of ruthenium chloride and hypophosphite precursors. These supported catalysts showed higher activites than the $Ru/MCM-41$.[27]

In 1967 Howe et al. had discussed the electronic properties of first row transition elements as binaries compounds with chalcogenides and pnictides. Both these families have a wide range of electronic and magnetic properties.[28] Busch and Hullinger found that FeAs and CrAs are semiconducting with activation energy (band gaps) of $\sim 0.1 eV$ for the former. Selte and Krejhaus et al. have investigated crystal structures and magnetic properties of the arsenides by neutron diffraction and magnetometry, in order to provide the first detailed account of the magnetic ordering observed in these compounds[29]. Kauzlarich et al. have also reported observing unusual magnetic properties and structures of $Ca_{14}MnSb_{11}$ and $Ca_{21}Mn_4Sb_{18}$.[30] These transition metal pnictides also show interesting electrochemical properties based on their facile redox chemistry. Monconduit and group have discussed the reactivity of the ternary transition-metal pnictides in Li_xMPn_4 (M = Ti, V; Pn = P, As) towards Li and found that these materials show high specific capacities ($500 < C < 1000$ $mAhg^{-1}$) in their first charge/discharge cycles which are held on to 80% after 20 cycles and are very promising as negative electrode material in Li-ion battery.[31]

Magnetic properties of these transition-metal pnictides makes them unique and very useful for applications like magnetic refrigeration which is based on the

magnetocaloric effect (MCE) and have recently demonstrated promise as an alternative to conventional vapor-cycle refrigeration. For a material that displays the MCE, alignment of randomly oriented magnetic moments by an external magnetic field results in heating. This heat can then be removed from the MCE material to the ambient atmosphere by heat transfer. If the magnetic field is subsequently turned off, the magnetic moments randomize again, which leads to heat withdrawal by the material and cooling of the surrounding below the ambient temperature. $MnFeP_{0.45}As_{0.55}$ is one such material that has a Curie temperature of ~300 K and allows magnetic refrigeration at room temperature.[32, 33] The magnetocaloric effect is intricately dependent on the structural parameters, as well as the magnetic exchange interactions within the crystal lattice. For bulk EAs the density functional calculations investigated the structural and magnetic properties of TiAs, FeAs, CoAs, CrAs and provided a theoretical framework for their study. It was shown that the electronic density of states of VAs, CrAs, and MnAs satisfy the Stoner criterion and hence give rise to a half metallic-ferromagnetic ground state (exceptions being MnP and MnAs). Typically, the binary transition-metal pnictides crystallize in 5 structure types:

1. **face-centered cubic** NaCl-type (for ScAs);

2. **hexagonal TiP-**type (for TiAs and ZrAs, HfAs);

3. **orthorhombic MnP-**type (for VAs, CrAs, FeAs, CoAs and RuAs);

4. **hexagonal NiAs type** (for MnAs and NiAs);

5. **tetragonal NbAs-type** structure (for NbAs and TaAs).

As mentioned in the preceding sections, the transition metal pnictides obtained a major thrust following the discovery of superconductivity in LaFePO in 2006.[34] This initial report of superconductivity in a rather unexpected Fe containing composition led to a flurry of research activities which resulted in identification of several other superconducting compositions within these Fe based pnictides, specifically arsenides (Figure 1.2).[35] The continued interest in these Fe-based superconductors was sustained by the exhibition of high T_c (critical temperature for superconductivity) which could be altered by changing the Ln ion as well as doping in the pnictide positions. Apart from the Fe-based pnictides, skutterudites such as $La_{0.8}Rh_4P_{12}$ were also shown to have a superconducting T_c of 13.6 K.[36] The observance of superconductivity and related magnetism in the transition-metal pnictides has been studied by Ivanovskii[37] and Goodenough[38] for both arsenides and phosphides.
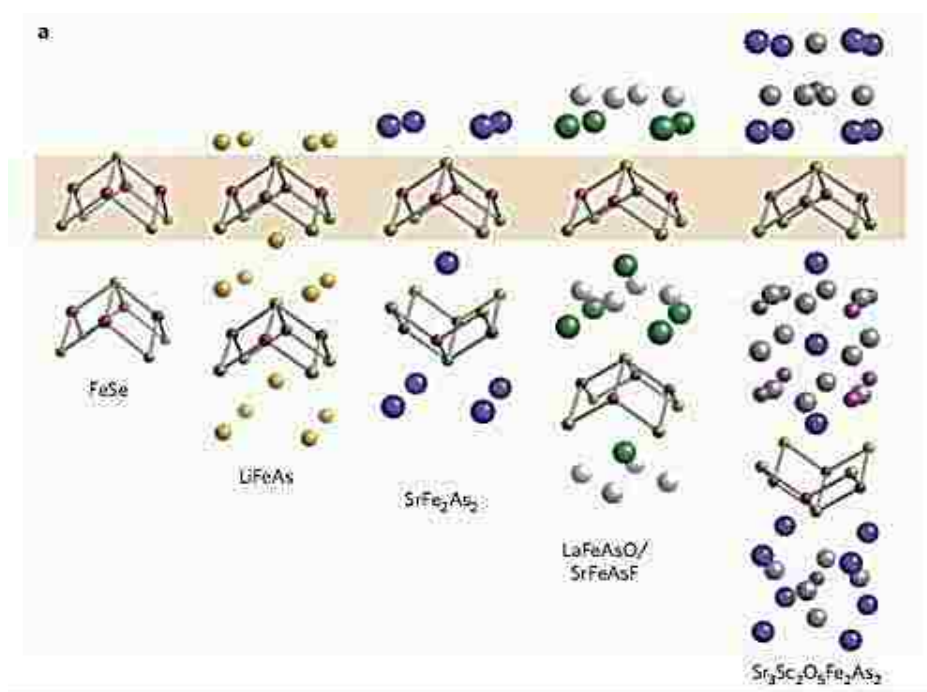
Figure 1.2: The five tetragonal structures exhibited by different families of the Fe-based superconductors[35]

The Fe-based superconductors were typically classified as [1111], [122] and [111] families, generic for LnFePO, $BaFe_2As_2$, and LiFeAs, respectively. Other than the pnictides, the Fe-chalcogenide based superconductors like FeSe have also exhibited unconventional superconductivity and are included in this family. The quartenary [1111] pnictides include compounds with compositions like $LnEPn$O (where $Ln=$ Rare earth, $E =$ transition metal and $Pn =$ Pnictogen) with ZrSiCuAs type layered crystal structure. Single crystalline quaternary LaFePO is superconducting at 6.6 K.[39] These are the first candidates to be studied amongst the iron- based superconductors. It has been observed that the crystal structures of these compounds have a significant influence on the superconductivity. These oxypnictides contains an alternate stacking of FeP layers with La_2O_3. It has been shown that the effect of doping and pressure application in these oxypnictides raises the critical temperatures up to 55K.[40] Therefore, many isostructural compounds with rich chemical compositions were synthesized, e.g., LaAgSO, LnCuSeO, LNEPO ($E =$ transition metal), LnEAsO, LnESbO, UCuPO, BaCuSF, SrZnPF, CeMnSiH, etc. It is possible that here superconductivity is associated with oxygen vacancies that dope a small fraction of the compound with charge carriers. This can be verified by 10-20% substitution of the oxide ions by the fluoride. This superconductivity and T_c enhancement was in direct competition with some fullerides and MgB_2.

The other ternary member of the iron- based superconductor is also isoelectronic $BaFe_2As_2$ (122). The common structural motif in these was the FeAs layers alternating with Ba ions. The critical T_c in $BaFe_2As_2$ goes as high as 39 K due to doping $Ba_{(1-x)}K_{(x)}Fe_2As_2$.[41] It has been observed that all the Fe-based pnictide superconductors exhibit a crystal structure containing similar motifs as the [1111] family, $viz.$ the anionic Fe-Pn layers alternating with the cationic layers. In [1111] family the cationic layer is

made by edge-sharing of the Ln_2O_3 polyhedra, while for the [122] and [111] families, simple cations occupy the interstitial space between the anionic layers (Figure 1.2).

LiFeAs, of the iron- based superconductor family which has Fe_2As_2 layers and intercalated Li ions to give the Cu_2Sb type tetragonal structure. The superconducting T_c found in pure phase LiFeAs was 18 K as found by Wang et al.in 2008.[42] The binary arsenide layers in these iron based superconductors are known to provide crucial support to superconductivity similar to the Cu_2O layers in cooperate superconductors. The crystal structure of LiFeAs is anti-PbFCl-type, layered tetragonal structure with $P_{4/nmm}$ space group.

It is known that pressure tends to decrease the magnetic transition temperature in the doped or undoped compounds. The application of pressure changes the interatomic distance and modifies the electronic and phonon spectra of a solid without including any chemical complexity. Pressure can also create new ground states in these compounds. The other source of pressure is chemical pressure induced by doping with smaller ions which can bring about the lattice contraction in these layered compounds. For example, In $BaFe_2As_2$ when As is doped with smaller P a reduction in volume of the cell along with lattice contraction occurs. The superconducting T_c increases with pressure for under doped FeAs-pnictides, remains constant for optimal doping and decreases linearly in the over doped region. The [111] family of Fe-based superconductors however, shows the most pronounced pressure effect second only to the chalcogenide superconductors.[43] In these compounds it is known that the superconducting T_c decreases linearly with pressure at the rate of -1.5 K/GPa. The possible explanation of this effect in LiFeAs is due to short lattice constants due to small Li^+ size. LiFeAs has the smallest volume and therefore, it

can be considered as a "high pressure" analog of the undoped FeAs compounds[44]. The other member of the [111] superconductors is NaFeAs which is isotypic to LiFeAs. In NaFeAs the FeAs tetrahedral is distorted giving rise to two different As-Fe-As bond angles making the compressed tetrahedron in the basal plane which is a direct consequence of accommodating the larger Na^+. Physical pressure application in this system causes the distortion to disappear and thus raises the T_c to 33K, no further tetrahedral compression can be performed in the LiFeAs system. This result is of great consequence to a nanochemist since nanostructuring often confines the crystal in small volumes and either enhancement or suppression of superconductivity can be observed if these bulk superconductors are nanostructured. These observations will provide very valuable insights into the working principle of these unconventional superconductors as well as their structure-property correlation.

1.3. NANOSTRUCTURED TRANSITION-METAL PNICTIDES

Nanomaterials science and technology has been on the forefront of materials science ever since its conception and the expectations that they can indeed change the world. Most of this expectation is attributed to the effect of reduced dimensions on the fundamental, intrinsic properties of the materials. Properties that are associated with the electrons and their mobilities within the materials, are the ones that are most prominently altered/enhanced in the nanostructures. Accordingly, magnetism and superconductivity are expected to show unique features accompanying the reduction in material's dimension. Nanostructuring of a superconductor causes artificial potential wells wherein superconducting flux lines are confined. The topology of nanostructures provides the

boundary conditions to the potential wells causing a change in properties much similar to quantum confinement. This is called the "quantum size effect" in superconductors. In the nanoscale parameters like penetration depth (λ_L), coherence length (ξ_0) and Anderson's criteria are perturbed and thus provides an insightful way to understand the underlying principle of superconductivity. It is important to know that the ground state properties of a superconductor change when the dimensions become less than the characteristic length scales, such as the penetration depth and coherence length. Anderson had predicted in 1959 that there is a third length scale that controls the superconducting order parameter in nano-sized superconductors. According to the Anderson's criterion, there is a complete destabilization of superconductivity for grain sizes at which the energy level spacing (arising from quantum size effects in small particles) becomes equal to the superconducting energy gap, $\Delta(0)$. This criterion has since been experimentally verified in many elemental superconductors.[45] The other factor that influences superconductivity is the length of the superconducting wave function. This is the second fundamental length scale in a superconductor, and was introduced initially by Pippard.[46] He argued that the superconducting wave function should have a characteristic dimension ξo which can be estimated from the uncertainty principle. For example in In nanoparticles it has been observed that 5% increase in T_c and 400 times increase in H_c for 39 nm particles is possible on reducing the dimensions from bulk In.[47] On the contrary, quantum suppression of superconductivity has been predicted by Bezrydin by thermally activated phase slips in Mo-Ge alloy ultrathin nanowires.[48] In Al nanoparticles suppression of superconductivity is observed when size reaches 10 nm, mainly due to the increase in electronic energy level gap in comparison to superconducting gap.[49] Shell effects have

been observed in Sn nanoparticles which also enhance superconductivity.[50] A

suppression of superconductivity was observed in MgB_2 nanowires (T_c = 33 K) as

compared to bulk MgB_2 (T_c = 39 K).[51] All these factors such as size, surface effects,

doping, flux pinning and lattice deformities caused by nanostructuring can potentially

alter the superconducting parameters and even give rise to higher transition temperatures

compared to the bulk state. Fe-based chalcogenide superconductors have lived up to this

promise, whereby, recent results showed that the T_c could be increased significantly

through extreme confinement of FeSe within the nanoparticles.[52] The effect of

nanostructuring of LiFeAs or LaFeAsO on superconducting T_c has not been observed till

now owing to lack of synthesis methods for making these compounds in the nanoscale.

Nano-magnetism is the field of magnetic phenomena occurring at the submicron

range. Many of the binary transition-metal pnictides have significant magnetic

interactions. The magnetic interactions are also influenced by the nanostructuring of the

binary transition-metal arsenides. In ferromagnetic nanomaterials, reduction in material

dimension below a certain threshold limit (critical size) leads to confinement of the spins

in a single magnetic domain. This type of confinement causes the magnetic particles to

behave as monodomain magnetic clusters leading to superparamagnetic behavior.

Normally in bulk ferromagnets, there are regions where the magnetization in each

domain is not of the same magnitude and/or direction. This non- uniformity is referred to

as magnetic anisotropy and this leads us into the concept of preferred axis of

magnetization. Hence, for an isotropic nanoparticle containing in the monodomain size

range there may not be any magnetic anisotropy but for spindle shaped/oblong/prolate

nanorods or nanowires, the anisotropy may be different in X-Y directions depending

upon the direction of lower energy. The anisotropy is represented by the constant K, also known as magnetocrystalline anisotropy constant. Also, new magnetic properties emerge when the grain or particle size for a bulk ferromagnet matches the "magnetic domain" size. At that point the individual particle behaves like a paramagnet but with very high magnetic moment and saturation magnetization thus being referred to as "superparamagnetism". This kind of transformation will be further discussed and forms the core of this dissertation. Nanostructuring also causes breaking of electron pairing and hence make surface magnetic phenomenon more prominent, frequently causing the conventional antiferromagnets and ferrimagnets to show unique features.

Nanostructuring of transition-metal pnictides especially phosphides has been investigated by various groups. Magnetic susceptibility data on dodecylamine-capped FeP nanoparticles suggested that the moments within each particle were coupled anti-ferromagnetically and that there was no evidence of a Néel transition, in contrast to bulk FeP.[53] Brock et al. have developed arrested precipitation methods for synthesis of FeP, Fe_2P, MnP, MnAs and Ni_2P nanoparticles with narrow size distribution.[54,55, 56] In case of MnP, the nanoparticles were found to be superparamagnetic below T_c with no evidence of a metamagnetic transition, as was observed in bulk (microcrystalline) MnP. Similarly, MnP nanorods[57] were observed to be ferromagnetic, with a coercive field of 4200 Oe at 10 K and a blocking temperature of 250.4 K at 500 Oe. The introduction of shape anisotropy into nanoparticles of MnP had little or no influence on the magnetic properties, suggesting that the inherent magnetocrystalline anisotropy was the dominating influence. In MnAs nanoparticles a suppression of the magnetostructural transition was noted which is also prevalent in the bulk MnAs.[58] A conversion of Fe nanoparticles into

Fe_2P and FeP has been carried out by Muthuswamay *et. al,* they found that Fe_2P rods were ferromagnetic with a Curie temperature between 215 and 220 K and exhibited a blocking temperature of 179 K, whereas bulk FeP is a metamagnet with a Néel temperature of 120 K.[54] These reports suggested that due to nanostructuring nanoparticles of transition-metal pnictides adopt new magnetic properties which may serve for new applications.

Recently magnetic nanomaterials have found a lot of applications in wide range of fields including (i) in biomedical fields as contrast enhancing agents for MRI imaging and for magnetic fluid hyperthermia agents for cancer treatment; (ii) as ferrofluids; (iii) as single bit memory units in magnetic storage devices; and (iv) as dilute magnetic semiconductors for spintronic devices. The potential for such wide range applications provides a major technological driving force for the exploration of magnetic nanomaterials in all aspects of research and development.[59]

The superparamagnets have been sought after for use in magnetic storage devices where each monodomain particle is used as a bit, and the reduced size of the nanoparticles makes it possible to pack large densities of such bits thereby increasing the efficiency of data storage. However, higher data storage densities also require beating the superparamagnetic limit. In particular, when the magnetic energy stored in a small, nanoscale particles is comparable to the thermal energy, a nanomagnet may become non-magnetic (superparamagnetic) above so-called "blocking temperature" T_B. Since T_B is a size dependent parameter, the size of the nanoparticles will be have to be small (below critical size) and each nanoparticle will have to be isolated (i.e. non-interacting) from each other to prevent changes in moment via crosstalk. This isolation of the

superparamagnetic particles is achieved through several ways. One of the favored ways to achieve this has been pinning the magnetic moments through ordering the superparamagnetic nanostructures in an array and embedding them in anti-ferromagnetic matrices. This technique has yielded in delayed onset of superparamagnetism and can result in higher storage densities through interparticle ordering in low applied magnetic field. This kind of architectural control can be achieved by the application of the magnetic field or slow evaporation or dip pen lithography etc.

1.4. SYNTHETIC METHODS

No matter what the applications of nanotechnology are, the need for novel, facile and scalable methods of nanomaterial synthesis are always necessary to realize the expectations of the nanotechnology revolution. Advances and improvements in nanomaterials synthesis were the major focus of nanomaterials chemistry in the last 20 years. Many methods have been established, standardized and adopted that enable micrograms to milligrams-scale synthesis at both bench scale and industrial scale. In general, nanomaterials synthesis can be broadly classified into two categories: (i) *top-down* approach where materials in the bulk size are fragmented and scaled down to nanometer dimension; and (ii) *bottom-up* approach where nanomaterials are built through chemical assembly of atomic and molecular building blocks.[60] While *top-down* approach preserves the composition of the materials very precisely, it is the *bottom-up* approach that has been of more interest to the materials chemists, since it gives the opportunity to create innovative nanostructures of unique composition and tune their properties very

precisely. Hence, as a chemist, the *bottom-up* approach is most lucrative to create the various nanostructures including the pnictides

In the case of binary pnictides, Bawendi and co-workers have studied the mechanism for the formation of InP quantum dots (QDs) by the reaction of indium(III) myristate, tris(trimethylsilyl)phosphine (TMS)$_3$P and octylamine in sealed NMR tubes, analyzing the intermediates using 1H NMR spectroscopy.[61] The same group also made InP nanocrystals (NCs) from the same precursors in supercritical octane at 320ºC using a microfluidic reactor.[62] Further modification of the same method yielded core-shell InAs@ ZnCdS QDs.[63] The process involved a two-step conversion; reaction of indium(III) myristate with octadecylamine (ODE), TOP and (TMS)3As at 230ºC resulted in the formation of the InAs core, followed by the slow addition of dimethyl cadmium, diethyl zinc and(TMS)$_3$S resulting in the deposition of the alloy shell. Mocatta et al. explored the room temperature *n*- and *p*-type doping of InAs NCs with Cu or Ag by the addition of the corresponding metal salts dissolved in a mixture of toluene, dodecylamine and didodecyldimethylammonium bromide to 4 nm InAs NCs in toluene.[64] Similarly, Tamang et al. demonstrated the aqueous phase transfer of InP/ZnS QDs using hydrophilic thiols such as cysteine, thioglycolic acid, dihydrolipoic acid, 3-mercaptopropanoic acid and 11-mercaptoundecanoic acid.[65] Cadmium phosphide (Cd$_3$P$_2$) QDs were synthesized by the injection of [(TMS)3P] dispersed in TOP and ODE into cadmium oleate in ODE at temperatures of 25, 80, 120 and 150 ºC.[66] Harris and co-workers reported the synthesis of cadmium arsenide(Cd$_3$As$_2$) QDs by the fast injection of tris(trimethylsilyl)arsine [(TMS)$_3$As]in TOP into the solution containing cadmium(II) myristate and ODE at 175 ºC, which initiated the formation of small particles of Cd$_3$As$_2$ (2 nm).[67]

Cobalt phosphide (Co_2P) nanowires have been synthesized by a one-pot colloidal reaction of cobalt oleate in TOP at 290 ºC or 320 ºC.[68] Ternary cobalt iron phosphide nanostructures were synthesized by the reaction of iron(III) oleate and cobalt(II) oleate with TOP in the presence of oleyl amine.[69] Single-source precursors were also employed for the growth of cobalt phosphide materials. Co_2P or CoP nanoparticles (5 nm) were obtained by the injection of cobalt diselenophosphinate $[Co(Se_2PR_2)_2]$ (R=^{i}Pr, Ph and t-Bu) precursor dissolved in TOP to TOPO or HDA at 300ºC after 60 and 150 minutes respectively. In this study, the thermolysis of the $Co(C_5H_7O_2)_2$ precursor in TOPO at 350 ºC for 6 min produced Co nanoparticles. When the reaction time was increased to 5 h, most of the Co nanoparticles were converted into Co_2P.[70]

Schaak and co-workers have devised a general method of converting metal nanoparticles to form transition metal phosphides such as Ni_2P, PtP_2, Rh_2P, PdP_2, Pd_5P_2, and Au_2P_3 by reacting with TOP in a hot solvent (290−360 °C). It was also observed that in this method nanostructures such as hollow spheres can be easily made using a Kirkendall-type mechanism, which utilized metal nanoparticles as reactive templates.[71, 72] With this study it was established that TOP can be used as an appropriate precursor for the conversion of a metal nanoparticle to metal phosphide. Nanoparticles of Fe phosphide were prepared through reductive annealing of nanoparticulate Fe phosphate precursors cast onto atomically flat mica surfaces.[73] This route appears to be general for a range of transition metals and pnictogens and avoided the use of highly toxic and pyrophoric agents such as $Pn(SiMe_3)_3$ (Pn = P, As), which are commonly employed in the synthesis of pnictide nanoparticles.

FeP nanoparticles were synthesized by the reaction of Fe(III) acetylacetonate with tris(trimethylsilyl)phosphine at 240-320° using trioctylphosphine oxide (TOPO) as a solvent and dodecylamine, myristic acid (MA), or hexylphosphonic acid (HPA) as additional capping groups (ligands).[54] Mechanochemical reaction between transition metal and pnictogen powders was also performed by Kim et al. It was concluded that the reaction enthalpy and particle size influence both the reaction path and rate. However in most experiments this yielded only micron sized particles.[74] Lu et. al. have made FeAs nanoparticles sonochemically from transition metal chlorides and arsenic, while Zhang and coworkers made FeAs nanocrystals from reductive recombination of $FeCl_3$ and $AsCl_3$ at 150 —180 °C.[75] However, these reports did not provide any details about the magnetic nature of the FeAs nanoparticles, and also the morphology was very ill-defined. The dearth of synthetic strategies towards formation of arsenide nanostructures through solution chemistry is mainly due to the toxicity of many of the volatile As-precursors like $AsCl_3$, AsH_3 and even metallic As, which may be acting as an obstacle. Recently triphenylarsine (TPA) has been used as As precursor for the growth of InAs[76] and GaAs.[76] Under solid-state conditions and refluxing in benzene respectively, TPA as a precursor addresses the toxicity related issues and is a much more lucrative As precursor in lieu of its ease of handling, moderate reactivity and less toxicity. Mesh like nanostructured CoAs has also been synthesized by Lu and Xie et al.[77] Thin films of CoAs by using metal-organic complex 1,3-bis(tert-butyl)-2-112 [tetracarbonyl-cobalt(-1)]-1,3,2-diazarsolidine were also synthesized by Klingan et al. in 1995 using the CVD method.[78] However, these conventional methods, even though yields compositionally pure samples, are not very amenable to morphology control.

In our work the synthesis of FeAs@C^{79} nanoparticles was carried out in a N$_2$ filled glove box containing less than 1 ppm of O$_2$. 1 mM of triphenylarsine and 5 mM of HDA was weighed and added to a three-neck round bottom flask equipped with a magnetic stir bar and air condenser. The mixture was slowly heated to 325° C during which the reactants slowly melted and the colorless mixture refluxed in its own vapors. 1 mM of Fe(CO)$_5$ maintained at room temperature was then injected using a syringe pump into the hot HDA + TPA mixture. Upon addition of Fe(CO)$_5$ the solution immediately turned black with rapid evolution of gases. After 5 min the gases subsided and the black solution was left to reflux for 3 hrs. After 3 hrs. the heating was stopped and the reaction was cooled down to room temperature. The process was optimized for all the other metal carbonyls (Mn, Cr, Co). Figure 1.3 shows the pictorial representation of the technique. *Tm* stands for transition metal.
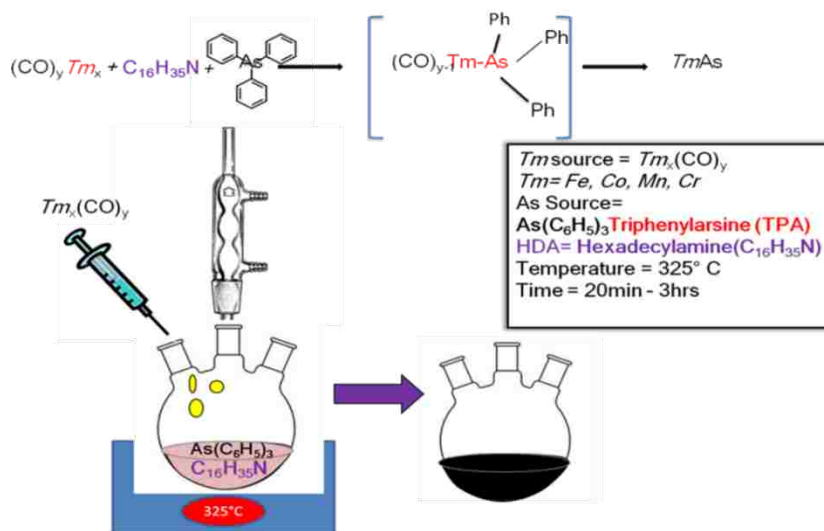
Figure 1.3: Experimental set up for the arsenide synthesis along with the plausible chemical conversion

For the synthesis of nanostructured LiFeAs a new method was developed by a combination of solution phase method and ceramic method of powder synthesis. This was termed at the sacrificial template method. Figure 1.4 shows the central idea behind the method. The first step in this approach was the synthesis of nanoparticulate FeAs.
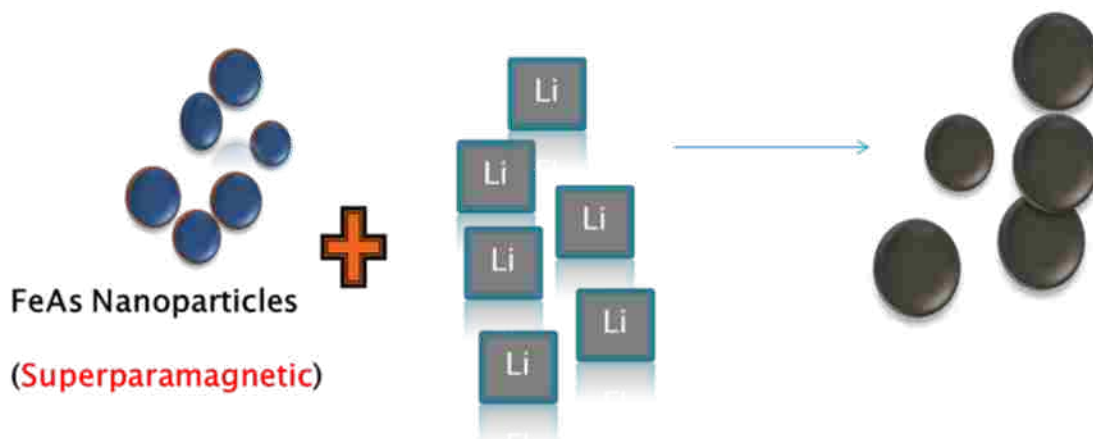
Figure 1.4: Schematic showing the central idea behind the sacrificial template technique

Secondly, these nanoparticles were made to react with large excess of bulk Lithium metal in in order to form the nanostructured LiFeAs. Recently electrochemical reduction of FeAs has been tried by Chen et al. using $LiPF_6$ as a source of Li ions. They found that a thin layer of LiFeAs can be formed on the surface of the FeAs electrode. The thin film of LiFeAs did not however reflect a change in particle size or superconducting T_c but it proved the possibility of synthesizing these nanoparticles from FeAs nanoparticles by the sacrificial template approach. The conceptual description of sacrificial template is that the FeAs nanoparticles act as a soft morphology-directing template which gets consumed in the reaction. One of the biggest advantages of using sacrificial template is that there is no necessity of template removal and it yields a very

uniform product with respect to morphology. Many other researchers have utilized these sacrificial templates to guide nanostructures morphology. For example, Gates et al. converted single crystalline nanowires of Ag_2Se by reacting $AgNO_3$ with Se nanowires[80]. The Se nanowires were supported on TEM grids and dispersed in water. Thus the shape of the resulting product nanowires is predetermined by the shape of Se nanowires.

The stoichiometry is taken care by the chemical reactions.

Se(s) (**Nanowires**) + $6Ag^+$ + $3H_2O$ →$2Ag_2Se$ (s) (**Nanowires**) + Ag_2SeO_3+ $6H^+$

Similarly, carbon nanotubes have been used as templates for Si_3N_4

3 SiO (g) + 3C (s)(nanotubes) + $2N_2$(g) → Si_3N_4(s) (Nanowires) + 3CO(g)[81]
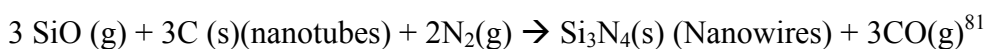
The formation of CdTe nanowires by consumption of Cd(OH)Cl

$CdCl_2$ + NaOH → Cd(OH)Cl

Cd(OH)Cl + NaHTe → CdTe (s) (**nanowires**)[82]
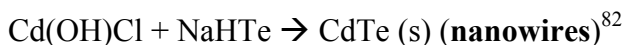
1.5. RESEARCH PROBLEM

After reflecting on the topics in the introduction, binary transition metal arsenides, high temperature superconductors and consequences of nanostructuring, it can be stated that the research problem covered here is the conversion of nanoparticles of binary transition metal pnictides, specifically FeAs into ternary LiFeAs. Furthermore, based on the work done it can be summarized that this dissertation aims to address the study of transition-metal pnictide nanostructures and their properties. The sacrificial template approach is developed and it is found as a viable method for complex inorganic compound nanostructures synthesis. This has been achieved by a combination of solution–phase synthesis of the binary arsenide and solid state synthesis methods which

forms the backbone of nanopowder synthesis. Important properties of pnictides like superparamagnetism emerge and a case for their conversion into superconducting LiFeAs nanostructures can be made.

This study provided us a chance for developing new methods for nanostructure synthesis different from the traditional methods of synthesis. This dissertation is an attempt to present the possible pathways/ protocols for such a synthesis further validated by characterization techniques like XRD, STEM SEM etc. The upcoming chapters will undertake the journey towards LiFeAs synthesis and bittersweet side findings achieved till date in this process.

BIBLIOGRAPHY

1. Girolami, G. S., Origin of the terms pnictogen and pnictide. *J. Chem. Edu.* **2009,** *86* , 1200- 1201.

2. Micic, O.; Ahrenkiel, S.; Bertram, D.; Nozik, A., Synthesis, structure, and optical properties of colloidal GaN quantum dots. *Appl.Phys. Lett.* **1999,** *75*, 478-480.

3. Kawashima, T.; Yoshikawa, H.; Adachi, S.; Fuke, S.; Ohtsuka, K., Optical properties of hexagonal GaN. *J.Appl.Phys.* **1997,** *82* (7), 3528-3535.

4. Blakemore, J., Semiconducting and other major properties of gallium arsenide. *J. Appl. Phys.* **1982,** *53* (10), R123-R181.

5. Gaponenko, S. V., *Optical properties of semiconductor nanocrystals*. Cambridge university press: 1998; Vol. 23.

6. Cameron, J. M.; Hughes, R. W.; Zhao, Y.; Gregory, D. H., Ternary and higher pnictides; prospects for new materials and applications. *Chem. Soc. Rev.* **2011,** *40* , 4099-4118.

7. Kauzlarich, S. M., A Rational Approach to Solid State Synthesis—The Zintl Concept. *Comments Inorg.Chem.* **1990,** *10*, 75-88

8. Meng, F.; Estruga, M.; Forticaux, A.; Morin, S. A.; Wu, Q.; Hu, Z.; Jin, S., Formation of Stacking Faults and the Screw Dislocation-Driven Growth: A Case Study of Aluminum Nitride Nanowires. *ACS Nano* **2013,** *7*, 11369-11378.

9. Rinke, P.; Winkelnkemper, M.; Qteish, A.; Bimberg, D.; Neugebauer, J.; Scheffler, M., Consistent set of band parameters for the group-III nitrides AlN, GaN, and InN. *Phys. Rev. B* **2008,** *77*, 075202-075214.

10. Westerwaal, R.; Haije, W., Evaluation solid-state hydrogen storage systems. *Hydrogen and Clean Fossil Fuels, ECN* **2008**, 2-75.

11. Gregoryanz, E.; Sanloup, C.; Somayazulu, M.; Badro, J.; Fiquet, G.; Mao, H.-K.; Hemley, R. J., Synthesis and characterization of a binary noble metal nitride. *Nature Mater.* **2004,** *3*, 294-297.

12. Young, A. F.; Sanloup, C.; Gregoryanz, E.; Scandolo, S.; Hemley, R. J.; Mao, H. K., Synthesis of novel transition metal nitrides IrN2 and OsN2. *Phys. Rev. Lett.* **2006,** *96* 155501- 155504.

13.   Chen, X.-J.; Struzhkin, V. V.; Wu, Z.; Somayazulu, M.; Qian, J.; Kung, S.; Christensen, A. N.; Zhao, Y.; Cohen, R. E.; Mao, H.-k.; Hemley, R. J., Hard superconducting nitrides. *Proc. Natl. Acad. Sci. U.S.A.* **2005,** *102* , 3198-3201.

14.   Shealy, J. R.; Prunty, T. R.; Chumbes, E. M.; Ridley, B. K., Growth and passivation of AlGaN/GaN heterostructures. *J.Cryst. Growth* **2003,** *250* , 7-13.

15.   Li, S.; Van Zee, R. J.; Weltner, W., Far-infrared spectra of small gallium phosphide, arsenide, and antimonide molecules in rare-gas matrixes at 4 K. *J. Phys. Chem.* **1993,** *97* , 11393-11396.

16.   Weinberg, I., InP solar cells for use in space. *Solar Cells* **1990,** *29* , 225-244.

17.   Assali, S.; Zardo, I.; Plissard, S.; Kriegner, D.; Verheijen, M. A.; Bauer, G.; Meijerink, A.; Belabbes, A.; Bechstedt, F.; Haverkort, J. E. M.; Bakkers, E. P. A. M., Direct Band Gap Wurtzite Gallium Phosphide Nanowires. *Nano Lett.* **2013,** *13* , 1559-1563.

18.   Englich, U.; Hassler, K.; Ruhlandt-Senge, K.; Uhlig, F., A Convenient Synthetic Strategy toward Heavy Alkali Metal Bis(trimethylsilyl)phosphides: Crystal Structures of the Ladder-Type Polymers [A(thf)P(SiMe$_3$)$_2$]$_\infty$ (A = K, Rb, Cs). *Inorg.Chem.* **1998,** *37* , 3532-3537.

19.   (a) Ryu, E.; Kim, S.; Jang, E.; Jun, S.; Jang, H.; Kim, B.; Kim, S.-W., Step-Wise Synthesis of InP/ZnS Core−Shell Quantum Dots and the Role of Zinc Acetate. *Chem. Mater.* **2009,** *21* , 573-575; (b) Xie, R.; Battaglia, D.; Peng, X., Colloidal InP Nanocrystals as Efficient Emitters Covering Blue to Near-Infrared. *J.Am.Chem.Soc.***2007,** *129*, 15432-15433.

20.   Henkes, A. E.; Schaak, R. E., Trioctylphosphine: A General Phosphorus Source for the Low-Temperature Conversion of Metals into Metal Phosphides. *Chem. Mater.* **2007,** *19*, 4234-4242.

21.   Nozik, A. J.; Beard, M. C.; Luther, J. M.; Law, M.; Ellingson, R. J.; Johnson, J. C., Semiconductor Quantum Dots and Quantum Dot Arrays and Applications of Multiple Exciton Generation to Third-Generation Photovoltaic Solar Cells. *Chem.Rev.* **2010,** *110*, 6873-6890.

22.   Kamihara, Y.; Hiramatsu, H.; Hirano, M.; Kawamura, R.; Yanagi, H.; Kamiya, T.; Hosono, H., Iron-based layered superconductor: LaOFeP. *J.Am.Chem.Soc.***2006,** *128* , 10012-10013.

23.   Landau, M. V.; Herskowitz, M.; Hoffman, T.; Fuks, D.; Liverts, E.; Vingurt, D.; Froumin, N., Ultradeep Hydrodesulfurization and Adsorptive Desulfurization of Diesel Fuel on Metal-Rich Nickel Phosphides. *Ind. Eng. Chem. Res.* **1996,** *48* , 5239-5249.

24. Stoyko, S. S.; Khatun, M.; Mar, A., Ternary Arsenides A2Zn5As4 (A = K, Rb): Zintl Phases Built from Stellae Quadrangulae. *Inorg.Chem.* **2012,** *51*, 9517-9521.

25. Khatun, M.; Stoyko, S. S.; Mar, A., Quaternary Arsenides $AM_{1.5}Tt_{0.5}As_2$ (A = Na, K, Rb; M = Zn, Cd; Tt = Si, Ge, Sn): Size Effects in $CaAl_2Si_2$- and $ThCr_2Si_2$-Type Structures. *Inorg.Chem.* **2013,** *52*, 3148-3158.

26. Kanda, Y.; Ichiki, T.; Kayaoka, S.; Sawada, A.; Sugioka, M.; Uemichi, Y., Preparation of Highly Active Noble Metal Phosphide Catalysts: Effect of Precursors on the Formation of the Active Phase and Hydrodesulfurization Activity. *Chem. Lett.* **2013,** *42*, 404-406.

27. Guan, Q.; Sun, C.; Li, R.; Li, W., The synthesis and investigation of ruthenium phosphide catalysts. *Catal. Commun.* **2011,** *14*, 114-117.

28. Howe, A.; Fensham, P., Electronic properties of binary compounds of the first-row transition metals. *Chem. Soc. Rev.* **1967,** *21*, 507-524.

29. (a) Selte, K.; Kjekshus, A., Crystal structure of FeAs. *Acta Chem. Scand.* **1969,** *23*, 2047-54; (b) Jeffries, J. R.; Butch, N. P.; Cynn, H.; Saha, S. R.; Kirshenbaum, K.; Weir, S. T.; Vohra, Y. K.; Paglione, J., The interplay between magnetism, structure, and strong electron-phonon coupling in binary FeAs under pressure. *Phys.Rev.B.***2010,** *83***,** 134520

30. Young, D. M.; Kauzlarich, S. M., Preparation, Structure, and Electronic Properties of $Ca_{11}MSb_9$ (M = Al, Ga, In). *Chem. Mater.* **1995,** *7*, 206-9.

31. (a) Monconduit, L.; Gillot, F.; Doublet, M.; Lemoigno, F., Lithium insertion/deinsertion mechanisms in the transition metal pnictides Li_xMPn_4. *Ionics* **2003,** *9*, 56-63; (b) Boyanov, S.; Bernardi, J.; Gillot, F.; Dupont, L.; Womes, M.; Tarascon, J.-M.; Monconduit, L.; Doublet, M.-L., FeP: another attractive anode for the Li-ion battery enlisting a reversible two-step insertion/conversion process. *Chem. Mater.* **2006,** *18*, 3531-3538.

32. Balli, M.; Fruchart, D.; Gignoux, D.; Zach, R., The "colossal" magnetocaloric effect in $Mn_{1-x}Fe_xAs$: What are we really measuring? *Appl.Phys. Lett.* **2009,** *95*, 072509-072509-3.

33. Shen, B.; Sun, J.; Hu, F.; Zhang, H.; Cheng, Z., Recent progress in exploring magnetocaloric materials. *Adv.Mater.***2009,** *21*, 4545-4564.

34. McQueen, T.; Regulacio, M.; Williams, A.; Huang, Q.; Lynn, J.; Hor, Y.; West, D.; Green, M.; Cava, R., Intrinsic properties of stoichiometric LaFePO. *Phys. Rev. B* **2008,** *78*, 024521.

35. Paglione, J.; Greene, R. L., High-temperature superconductivity in iron-based materials. *Nat. Phys.* **2010,** *6* , 645-658.

36. Imai, M.; Akaishi, M.; Sadki, E.; Aoyagi, T.; Kimura, T.; Shirotani, I., Superconducting properties of filled skutterudite $La_{0.8}$ Rh_4 P_{12}. *Phys. Rev. B* **2007,** *75*, 184535.

37. Ivanovskii, A. L., New high-temperature superconductors based on rare-earth and transition metal oxyarsenides and related phases: synthesis, properties and simulations. *Phys Usp.* **2008,** *51* , 1229.

38. Goodenough, J., Interpretation of structure and magnetism in transition-metal pnictides M_2X and $(M_{1-x}M'_x)_2X$ *J. Solid State Chem.* **1973,** *7* , 428-447.

39. Baumbach, R.; Hamlin, J.; Shu, L.; Zocco, D.; Crisosto, N.; Maple, M., Superconductivity in LnFePO (Ln= La, Pr and Nd) single crystals. *New J. Phys.***2009,** *11*, 025018.

40. Kito, H.; Eisaki, H.; Iyo, A., Superconductivity at 54 K in F-Free $NdFeAsO_{1-y}$. *J. Phys. Soc. Jpn.* **2008,** *77,* 063707

41. Rotter, M.; Tegel, M.; Johrendt, D., Superconductivity at 38 K in the iron arsenide $(Ba_{1-x} K_x) Fe_2 As_2$. *Phys.Rev. Lett.* **2008,** *101* , 107006.

42. Wang, X.; Liu, Q.; Lv, Y.; Gao, W.; Yang, L.; Yu, R.; Li, F.; Jin, C., The superconductivity at 18 K in LiFeAs system. *Solid State Commun.* **2008,** *148* , 538-540.

43. Aswathy, P.; Anooja, J.; Sarun, P.; Syamaprasad, U., An overview on iron based superconductors. *Supercond. Sci. Technol.* **2010,** *23*, 073001.

44. Gooch, M.; Lv, B.; Tapp, J. H.; Tang, Z.; Lorenz, B.; Guloy, A. M.; Chu, P. C., Pressure shift of the superconducting Tc of LiFeAs. *Europhys. Lett.* **2009,** *85* , 27005.

45. Oppenmann, R., Anderson localization problems in gapless superconducting phases. *Physica A* **1990,** *167* , 301-312.

46. Pippard, A., Field variation of the superconducting penetration depth. *Proc. R. Soc. A* **1950,** *203* , 210-223.

47. Li, W.-H.; Yang, C.; Tsao, F.; Wu, S.; Huang, P.; Chung, M.; Yao, Y., Enhancement of superconductivity by the small size effect in In nanoparticles. *Phys. Rev. B* **2005,** *72* , 214516.

48. Bezryadin, A.; Lau, C.; Tinkham, M., Quantum suppression of superconductivity in ultrathin nanowires. *Nature* **2000,** *404* , 971-974.

49. Ralph, D.; Black, C.; Tinkham, M., Gate-voltage studies of discrete electronic states in aluminum nanoparticles. *Phys.Rev. Lett.* **1997,** *78* , 4087.

50. Bose, S.; García-García, A. M.; Ugeda, M. M.; Urbina, J. D.; Michaelis, C. H.; Brihuega, I.; Kern, K., Observation of shell effects in superconducting nanoparticles of Sn. *Nat. Mater.* **2010,** *9* , 550-554.

51. Wu, Y.; Messer, B.; Yang, P., Superconducting MgB_2 Nanowires. *Adv. Mater.* **2001,** *13* , 1487.

52. Mishra, S.; Song, K.; Ghosh, K. C.; Nath, M., Enhancement of Superconducting T c (33 K) by Entrapment of FeSe in Carbon Coated $Au–Pd_{17}Se_{15}$ Nanoparticles. *ACS Nano* **2014,** *8*, 2077-2086.

53. Perera, S. C.; Fodor, P. S.; Tsoi, G. M.; Wenger, L. E.; Brock, S. L., Application of de-silylation strategies to the preparation of transition metal pnictide nanocrystals: the case of FeP. *Chem. Mater.* **2003,** *15*, 4034-4038.

54. Muthuswamy, E.; Kharel, P. R.; Lawes, G.; Brock, S. L., Control of phase in phosphide nanoparticles produced by metal nanoparticle transformation: Fe_2P and FeP. *ACS Nano* **2009,** *3* , 2383-2393.

55. Perera, S. C.; Tsoi, G.; Wenger, L. E.; Brock, S. L., Synthesis of MnP nanocrystals by treatment of metal carbonyl complexes with phosphines: A new, versatile route to nanoscale transition metal phosphides. *J.Am.Chem.Soc.* **2003,** *125*, 13960-13961.

56. Senevirathne, K.; Burns, A. W.; Bussell, M. E.; Brock, S. L., Synthesis and characterization of discrete nickel phosphide nanoparticles: effect of surface ligation chemistry on catalytic hydrodesulfurization of thiophene. *Adv. Funct. Mater.* **2007,** *17* , 3933-3939.

57. Gregg, K. A.; Perera, S. C.; Lawes, G.; Shinozaki, S.; Brock, S. L., Controlled synthesis of MnP nanorods: Effect of shape anisotropy on magnetization. *Chem. Mater.* **2006,** *18* , 879-886.

58. Tian, P.; Zhang, Y.; Senevirathne, K.; Brock, S. L.; Dixit, A.; Lawes, G.; Billinge, S. J., Diverse structural and magnetic properties of differently prepared MnAs nanoparticles. *ACS Nano* **2011,** *5* , 2970-2978.

59. Pecharsky, V. K.; Gschneidner, K. A., Magnetocaloric materials. *Handbook of Magnetism and Advanced Magnetic Materials* **2007**.

60.   Edelstein, A. S.; Cammaratra, R., *Nanomaterials: Synthesis, properties and applications*. CRC Press: 1998.

61.   Allen, P. M.; Walker, B. J.; Bawendi, M. G., Mechanistic insights into the formation of InP quantum dots. *Angew. Chem. Int. Ed.* **2010,** *49* (4), 760-762.

62.   Baek, J.; Allen, P. M.; Bawendi, M. G.; Jensen, K. F., Investigation of Indium Phosphide Nanocrystal Synthesis Using a High-Temperature and High-Pressure Continuous Flow Microreactor. *Angew. Chem.* **2011,** *123* (3), 653-656.

63.   Allen, P. M.; Liu, W.; Chauhan, V. P.; Lee, J.; Ting, A. Y.; Fukumura, D.; Jain, R. K.; Bawendi, M. G., InAs (ZnCdS) quantum dots optimized for biological imaging in the near-infrared. *J.Am.Chem.Soc.***2009,** *132* , 470-471.

64.   Mocatta, D.; Cohen, G.; Schattner, J.; Millo, O.; Rabani, E.; Banin, U., Heavily doped semiconductor nanocrystal quantum dots. *Science,* **2011,** *332* , 77-81.

65.   Tamang, S.; Beaune, G. g.; Texier, I.; Reiss, P., Aqueous phase transfer of InP/ZnS nanocrystals conserving fluorescence and high colloidal stability. *ACS Nano* **2011,** *5* , 9392-9402.

66.   Miao, S.; Hickey, S. G.; Rellinghaus, B.; Waurisch, C.; Eychmüller, A., Synthesis and characterization of cadmium phosphide quantum dots emitting in the visible red to near-infrared. *J.Am.Chem.Soc.***2010,** *132* , 5613-5615.

67.   Harris, D. K.; Allen, P. M.; Han, H.-S.; Walker, B. J.; Lee, J.; Bawendi, M. G., Synthesis of cadmium arsenide quantum dots luminescent in the infrared. *J.Am.Chem.Soc.* **2011,** *133* , 4676-4679.

68.   Li, Y.; Malik, M. A.; O'Brien, P., Synthesis of Single-Crystalline CoP Nanowires by a One-Pot Metal−Organic Route. *J.Am.Chem.Soc.***2005,** *127*, 16020-16021.

69.   Ye, E.; Zhang, S. Y.; Lim, S. H.; Bosman, M.; Zhang, Z.; Win, K. Y.; Han, M. Y., Ternary cobalt–iron phosphide nanocrystals with controlled compositions, properties, and morphologies from nanorods and nanorice to split nanostructures. *Chem. Eur. J.* **2011,** *17*, 5982-5988.

70.   Zhang, H.; Ha, D.-H.; Hovden, R.; Kourkoutis, L. F.; Robinson, R. D., Controlled Synthesis of Uniform Cobalt Phosphide Hyperbranched Nanocrystals Using Tri-n-octylphosphine Oxide as a Phosphorus Source. *Nano Lett.* **2010,** *11* , 188-197.

71.   Chiang, R.-K.; Chiang, R.-T., Formation of Hollow Ni_2P Nanoparticles Based on the Nanoscale Kirkendall Effect. *Inorg.Chem.* **2006,** *46*, 369-371.

72. Barry, B. M.; Gillan, E. G., Low-Temperature Solvothermal Synthesis of Phosphorus-Rich Transition-Metal Phosphides. *Chem. Mater.* **2008,** *20* , 2618-2620.

73. Stamm, K. L.; Garno, J. C.; Liu, G.-y.; Brock, S. L., A General Methodology for the Synthesis of Transition Metal Pnictide Nanoparticles from Pnictate Precursors and Its Application to Iron−Phosphorus Phases. *J.Am.Chem.Soc.* **2003,** *125* , 4038-4039.

74. Kim, Y. K.; Cho, Y. W., Synthesis of transition metal pnictide nanocrystalline powders by mechanochemical reaction. J. Alloys Compd. **2005,** *393* , 211-218.

75. Zhang, X. M.; Wang, C.; Qian, X. F.; Xie, Y.; Qian, Y. T., Synthesis of Nanocrystalline Iron Monoarsenide via a Reductive Recombination Pathway. *J. Solid State Chem.* **1999,** *144* , 237-239.

76. Wang, J.; Yang, Q., A developed Ullmann reaction to III–V semiconductor nanocrystals in sealed vacuum tubes. *Dalton Transactions* **2008,** (43), 6060-6066.

77. Xie, Y.; Lu, J.; Yan, P.; Jiang, X.; Qian, Y., A safe low temperature route to nanocrystalline transition metal arsenides. *Chem. Lett.* **2000,** , 114-115.

78. Klingan, F.; x; Robert; Miehr, A.; Fischer, R. A.; Herrmann, W. A., Thin films of CoAs from low‐temperature metalorganic chemical vapor deposition of a novel single‐source precursor compound. *Appl.Phys. Lett.* **1995,** *67* , 822-824.

79. Desai, P.; Song, K.; Koza, J.; Pariti, A.; Nath, M., Soft-Chemical Synthetic Route to Superparamagnetic FeAs@C Core–Shell Nanoparticles Exhibiting High Blocking Temperature. *Chem. Mater.* **2013,** *25* , 1510-1518.

80. Gates, B.; Wu, Y.; Yin, Y.; Yang, P.; Xia, Y., Single-crystalline nanowires of Ag2Se can be synthesized by templating against nanowires of trigonal Se. *J.Am.Chem.Soc.* **2001,** *123*, 11500-11501.

81. Han, W.; Fan, S.; Li, Q.; Gu, B.; Zhang, X.; Yu, D., Synthesis of silicon nitride nanorods using carbon nanotube as a template. *Appl.Phys. Lett.* **1997,** *71* , 2271-2273.

82. Shim, H.-S.; Shinde, V. R.; Kim, J. W.; Gujar, T. P.; Joo, O.-S.; Kim, H. J.; Kim, W. B., Diameter-tunable CdSe nanotubes from facile solution-based selenization of Cd(OH)₂ nanowire bundles for photoelectrochemical cells. *Chem. Mater.* **2009,** *21* , 1875-1883.

PAPER

I. SOFT CHEMICAL SYNTHETIC ROUTE TO SUPERPARAMAGNETIC FeAs@C CORE-SHELL NANOPARTICLES EXHIBITING HIGH BLOCKING TEMPERATURE

Prachi Desai[a,‡] **Kai Song,**[b#] **Jakub Koza,**[a] **Akshay Pariti**[c]**, Manashi Nath** [a,‡,*]
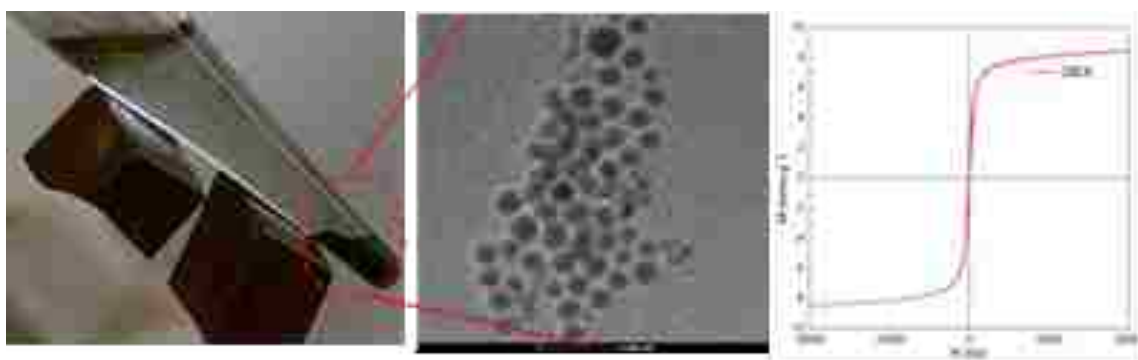
[a] Department of Chemistry, Missouri University of Science and Technology, Rolla, MO 65409.

[b] Materials Research Centre, Missouri University of Science and Technology, Rolla, MO 65409; [#]presently at FEI Company, 5350 NE Dawson Creek Drive, Hillsboro, Oregon 97124.

[c] Department of Chemical and Biochemical Engineering, Missouri University of Science and Technology, Rolla, MO 65409.

1. ABSTRACT

Superparamagnetic FeAs nanoparticles with a fairly high blocking temperature (T_B) have been synthesized through a new solvent-less hot injection precipitation technique. The synthesis involved usage of triphenylarsine (TPA) as a novel As precursor, which reacts with Fe(CO)5 by ligand displacement at moderate temperatures (300°C). Addition of a surfactant, hexadecylamine (HDA) assists in the formation of the nanoparticles, due to its coordinating ability and low melting point which provides a molten flux like condition making this synthesis a solvent-less method. Decomposition of the carbonaceous precursors, HDA, TPA and $Fe(CO)_5$, also produces the carbonaceous shell coating the FeAs nanoparticles. The ~12 nm highly crystalline FeAs core was coated with a ~ 2 nm shell making these nanoparticles ~15 nm in size. Magnetic characterization of these nanoparticles revealed the superparamagnetic nature of these nanoparticles with a perfect anhysteretic nature of the isothermal magnetization above T_B. The T_B observed in this system was indeed high (240 K) when compared with other superparamagnetic systems conventionally utilized for magnetic storage devices. It could be further increased by decreasing the strength of the applied magnetic field. The narrow hysteresis with low magnitude of coercivity at 5K suggested soft ferromagnetic ordering in these nanoparticle ensemble. Mössbauer and XPS studies indicated that the Fe was present in +3 oxidation state and there was no signature of Fe(0) that could have been responsible for the increased magnetic moment and superparamagnetism. Typically for superparamagnetic nanoparticle ensemble, the need for isolation of the superparamagnetic domains (thereby inhibiting particle aggregation and enhancing the T_B) has been in constant limelight. Carbonaceous coating on these as-synthesized

nanoparticles formed in situ provided the physical non-magnetic barrier needed for such isolation. The high T_B and room temperature magnetic moment of these FeAs@C nanoparticles also make them potentially useful for applications in ferrofluids and magnetic refrigeration. In principle this method can be used as a general route towards synthesis of other arsenide nanostructures including the transition metal arsenide which show interesting magnetic and electronic properties (e.g. CoAs, MnAs) with finer control over morphology, composition and structure.

2. INTRODUCTION

The unexpected discovery of superconductivity in LaFePO by Hosono et al. in 2006[1] that led to identification of a new series of iron oxypnictide based superconductors, *Ln*Fe*Pn*O [*Ln* = La, Ce, Sm, Gd, Nd, Pr; *Pn* = P, As],[2-5] has made the iron pnictides a center of attraction to materials scientists. The iron pnictide based superconducting family was further enriched over the last couple of years with the discovery of new compositions, specifically the AFe$_2$As$_2$ (A = Ba, Sr etc.)[6] and the AFeAs (A = Li, Na)[7,8] which are generically referred to as [122] and the [111] series respectively, and the parent oxypnictide, LnFePnO is referred to as the [1111] series. The common structural motif in these layered superconductors is the anionic FeAs layer containing the edge shared FeAs$_4$ tetrahedra which is believed to be responsible for superconductivity.[9,10] The electronic and magnetic properties of these superconductors show a dependence on the geometry of the FeAs$_4$ tetrahedra.[11] While the [1111] series is built up by the alternate stacking of the anionic pnictide layer with the cationic Ln_2O_3 layer, the simpler ternary compositions

([111] and [122] series) contain the alkali or the alkaline earth cations placed between the FeAs layers.

In these pnictide superconductors, the magnetic exchange interactions between the Fe atoms within the pnictide layer plays a determining factor in defining the superconducting and electronic properties of these superconductors and the binary pnictides might serve as a proxy system to study these exchange interactions. More importantly, FeAs nanostructures will be an ideal starting point for the synthesis of nanostructures of these pnictide superconductors through simple sacrificial template approach.

Bulk FeAs is an interesting antiferromagnetic (T_N = 70 K) semiconductor material.[12] It crystallizes in the orthorhombic MnP structure type[13] and exhibits helimagnetism owing to the characteristic arrangement of the Fe^{3+} spins along the *c*-axis.[14] Recent work on FeAs using neutron diffraction studies insinuate the role of spin-density wave (SDW) filling the gaps in Fermi surface, as a possible explanation to the magnetic ordering below the T_N in this system.[15] Apart from being the backbone of the pnictide superconductors, these attributes also make FeAs very useful in spintronic applications and magnetic storage devices. However, it may be noted even though several transition metal pnictide, *TmPn* (*Tm* = Fe, Co, Ni, Mn; *Pn* = P, As) nanostructures are known in abundance,[16-22] reports of FeAs nanostructures are very limited till date. Lu *et. al.* have made FeAs nanoparticles sonochemically from transition metal chlorides and arsenic,[23] while Zhang and coworkers made FeAs nanocrystals from reductive recombination of $FeCl_3$ and $AsCl_3$ at 150 —180 °C.[24] However, these reports did not

provide any details about the magnetic nature of the FeAs nanoparticles, and also the morphology was very ill-defined.

While the high temperature solid state reactions form the most thermodynamically stable form of these pnictides, soft chemical synthesis routes and so called *chemie douce* methods relying on association at the molecular level might offer the much needed alternative to form the metastable nanostructured phases. Numerous phosphide and chalcogenide nanostructures[25] have been made by the solution based *hot-injection* method where the precursors are injected into a refluxing solution and the thermal gradient leads to spontaneous nucleation and nanostructure growth. Liquid phase reactions are especially lucrative since they offer better handle at morphology control and chemical composition of the resulting nanostructures. However, the suitable choice of the reactants and their relative reactivity's in the medium play a very definitive role towards the progress of the reaction. The dearth of synthetic strategies towards formation of arsenide nanostructures through solution chemistry is mainly due to the toxicity of many of the volatile As-precursors like $AsCl_3$, AsH_3 and even metallic As, which may be acting as an obstacle. However, recently triphenylarsine (TPA) has been used as As precursor for the growth of InAs and GaAs under solid-state conditions and refluxing in benzene respectively.[26,27] TPA as a precursor addresses the toxicity related issues and is a much more lucrative As precursor in lieu of its ease of handling, moderate reactivity and less toxicity.

In this paper we discuss a facile one step low-temperature method to synthesize FeAs nanoparticles in high yield by a simple surfactant-assisted arrested precipitation reaction between $Fe(CO)_5$ and triphenylarsine $((C_6H_5)_3As$, TPA) and reveal the

unprecedented superparamagnetic behavior of these nanoparticles with a high blocking temperature (240 K). At the initiation of the reaction, TPA attaches to the Fe-center through simple ligand exchange chemistry to form a probable intermediate which might act as the single source precursor, thereby facilitating the low-temperature growth in the absence of any catalyst. The method reported here does not require additional solvent medium thereby reducing by-products and simplifying the product purification steps.

3. EXPERIMENTAL

The synthesis of FeAs nanoparticles was carried out in a N_2 filled glove box containing less than 1 ppm of O_2. 1 mM of triphenylarsine and 5 mM of HDA was weighed and added to a three-neck round bottom flask equipped with a magnetic stir bar and air condenser. The mixture was slowly heated to 325° C during which the reactants slowly melted and the colorless mixture refluxed in its own vapors. 1 mM of $Fe(CO)_5$ maintained at room temperature was then injected using a syringe pump into the hot HDA + TPA mixture. Upon addition of $Fe(CO)_5$ the solution immediately turned black with rapid evolution of gases. After 5 min the gases subsided and the black solution was left to reflux for 3 hrs. After 3 hrs. the heating was stopped and the reaction was cooled down to room temperature. It should be noted here that the molar ratio for obtaining pure phase FeAs was 1 : 1 : 5 for Fe(CO)5 : TPA : HDA. If the As is taken in excess of 1 : 1 *wrt* Fe, the nanoparticle shows As-rich composition and the product contains a mixture of iron arsenide phases (e.g. $FeAs_2$ along with FeAs). The effect of varying the surfactant relative ratios has been discussed below (*vide infra*).

Purification: The as-synthesized product, by virtue of its attraction to a magnet, was purified through simple magnetic filtration. The isolated product was washed at least 3-4 times with ethanol and hexane using ultra-sonication to remove excess HDA and any unreacted precursors. After centrifugation the powder collected from the bottom of the tube was dried in air. The yield of the product was in excess of 90% *wrt* the amount of $Fe(CO)_5$ taken as the precursor. The product was characterized further through powder X-ray diffraction (pxrd), scanning and transmission electron microscopy (SEM and TEM respectively), Energy dispersive spectroscopy (EDS), X-ray photoelectron spectroscopy (XPS), Atomic Absorption spectroscopy (AAS), Raman analysis, Mössbauer and magnetic studies.

Characterization PXRD : The as-synthesized powder was finely ground and used for PXRD, which was carried out on a Philips Xpert diffractometer scanning from 5 to 90°. SEM, TEM & STEM: A Technai F20 microscope operating at 200 kV was used for TEM while a dual beam Helios FIB microscope was used for SEM and STEM studies. Samples for TEM and STEM were made by dispersing as- synthesized

FeAs nanoparticles in ethanol by ultra-sonication for 30 min and adding drops from the diluted dispersion on a carbon coated 200 mesh Cu grid followed by drying in air. XPS XPS analysis was performed with Kratos Axis 165, with a hemispherical 8 channel analyzer. Photoemission was stimulated with a monochromatic Al source for FeAs@C nanoparticles. The XPS spectra of Fe2p and As3d were collected at pass energy of 80 peV. Sputtering was performed for 5 min using argon gas.

Magnetic measurements: Magnetic moment and isothermal magnetization was collected from a SQUID magnetometer and the vibrating sample magnetization (VSM)

option of physical property measurement system (PPMS) respectively. The powdered

sample of known mass was loaded in a gel cap which was inserted into the magnetometer

with the help of standard sample loader. The diamagnetic signal from the gel cap was

collected separately and subtracted as a background from the signal obtained from the

sample. The ZFC data was obtained after cooling the sample down under zero magnetic

field and then measuring the magnetic susceptibility warming up data by applying a

magnetic field in the range of 100 – 1000 Oe. The FC data was collected as the sample

was cooled down under the same applied magnetic field. The isothermal magnetization

against applied field was collected at different temperatures ranging 5 K to 350 K by

applying magnetic fields from -20000 Oe to 20000 Oe.

Mossbauer: 57Fe Mössbauer experiments were performed in transmission

geometry at room temperature using a conventional constant acceleration spectrometer

and a gamma-ray source of 57Co in a Rh matrix. Velocity calibration and isomer shifts

are given with respect to alpha-Fe foil at room temperature. The Mossbauer data was

analyzed by Lorentzian line fitting using RECOIL software.[28]

Raman: The Raman spectroscopy was performed using the Horiba Jobin Yvon

Lab Raman ARAMIS model. The Laser used was He-Ne with a power of 17/4. An

average of 10 scans was collected.

AA Spectroscopy: The AAS was carried out on Perkin Elmer spectrometer (2800

model). The sample preparation involved digesting a known quantity of the sample in

measured volume of conc. HNO_3 and filtering to remove any undissolved residue. The

standard solutions were made in similar way by dissolving Fe wire in conc. HNO_3. The

Fe content in the sample was estimated by comparing with the standard.

4. RESULTS AND DISCUSSIONS.

The formation of the highly crystalline FeAs phase was confirmed by pxrd as shown in Figure 1, which revealed that the as-synthesized nanoparticles crystallized in the MnP structure-type (JCPDS file, card number (01—076—0458).[14] The diameter of the nanoparticles as calculated from Scherer equation was 13 nm.[29] No other phase of FeAs or any other impurity was detected. Size of the nanoparticles was dependent on the refluxing time.
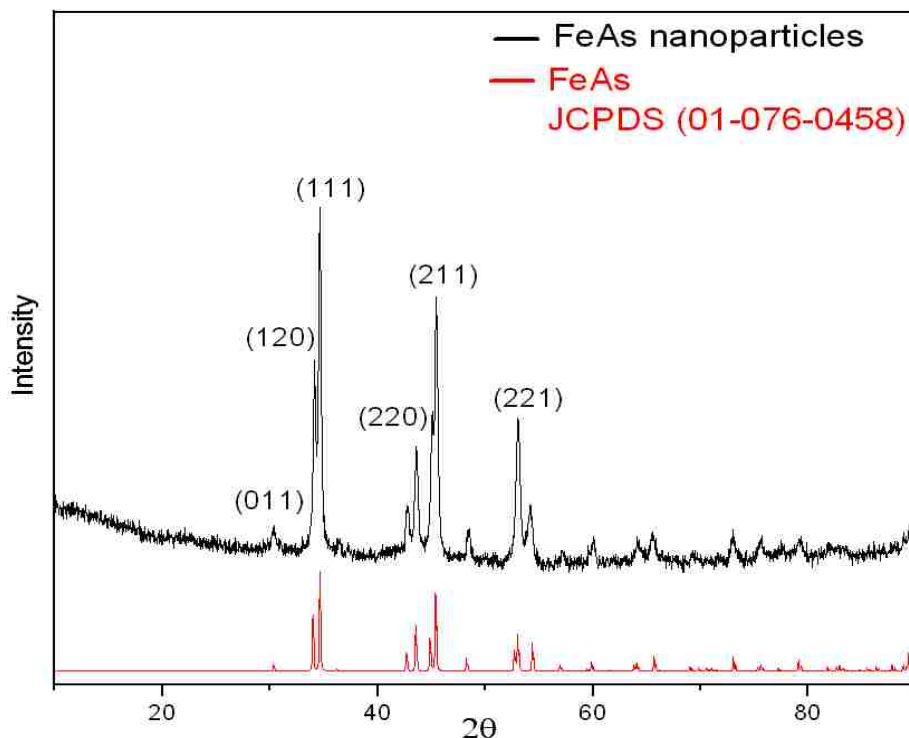
Figure 1: PXRD pattern of FeAs nanoparticles as synthesized at 300ºC

When the temperature of $Fe(CO)_5$ addition was reduced to 250°C a mixture of $FeAs_2$ and FeAs was obtained as seen from the pxrd pattern shown in supporting information Figure S1. Detailed investigations from the STEM and TEM images showed high yield of the nanoparticles in the product and also revealed high degree of

monodispersity in the nanoparticles ensemble. Furthermore, microscopic imaging

revealed that FeAs nanoparticles were core-shell type as seen in the low magnification

STEM image shown in Figures 2A and B.
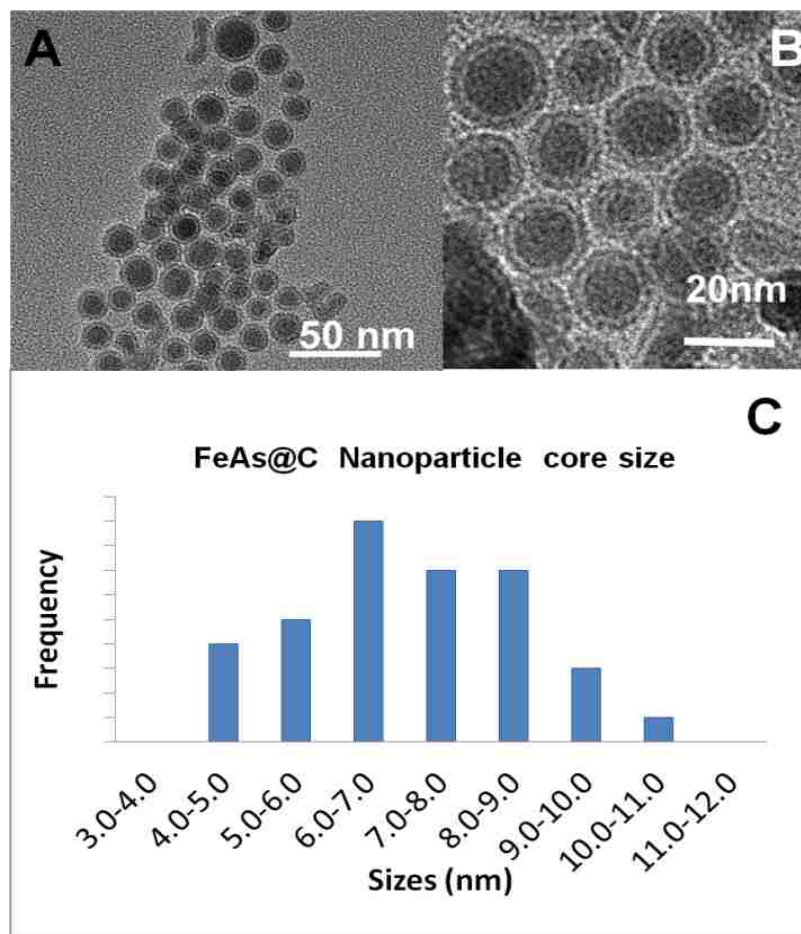
Figure 2: (A) - (B) STEM images of the nanoparticles showing core-shell nature and ordered arrangement. (C) Histogram analysis for the size distribution of the core in these nanoparticles

The average particle diameter was $10 - 15$ nm, the core size being $8 - 12$ nm. The

lighter contrast shell is approximately $2 - 4$ nm in thickness. Several wide area SEM

images were analyzed to obtain a statistical histogram for the particle size distribution.

The histogram showed that the mean size of the core falls well in the range of $8 - 10$ nm

as shown in Figure 2C while the particle size distribution was in the range of 10 – 15 nm

(Figure S2). The nanoparticles frequently exhibited a hexagonal arrangement on the

TEM grids as shown in Figure 2B. The presence of the surfactant was essential for

formation of the nanoparticles. HDA served both as a solvent and a capping agent.

Nitrogen containing coordinating polymers like copoly(styrene-4-vinylpyridine

and copoly(styrene–N-vinylpyrolidone) have long been known to act as nucleophiles and

brilliant capping agents.[30] In our opinion HDA also acts similar to these solvents. Other

experiments that involved changing the concentration of HDA indicated that

concentration of HDA alters the nanoparticle morphology. When the concentration of

HDA was reduced [1 : 1; HDA : Fe(CO)$_5$] nanoparticles did not form. An increase in

HDA concentration to [1 : 10; HDA : Fe(CO)$_5$] gave square shaped nanoparticles. Thus,

the role and optimal concentration of HDA was determined as an effective capping agent

at 5mM.The arsenic precursor, TPA, is very favorable in the sense that it is less volatile,

melts easily, decomposes at higher temperatures, and Therefore,, less hazardous.

Moreover, the handling of solid TPA does not require any complicated protocol.

However, to reduce the exposure towards As-precursors, the entire reaction was

performed in a N$_2$ filled dry box. The core in these nanoparticles was single crystalline

and exhibited lattice fringes corresponding to (110) spacing of FeAs as shown in the

HRTEM (Figure 3).The selected area electron diffraction (SAED) pattern was also

collected over an ensemble of nanoparticles which as expected, exhibited spotty ring

pattern typical for a random distribution of small crystallites. SAED could not be

performed on individual nanoparticles owing to the particle sizes being very small as

compared to the SAED aperture. The shell on the other hand, did not reveal any

crystalline ordering and was mostly amorphous.
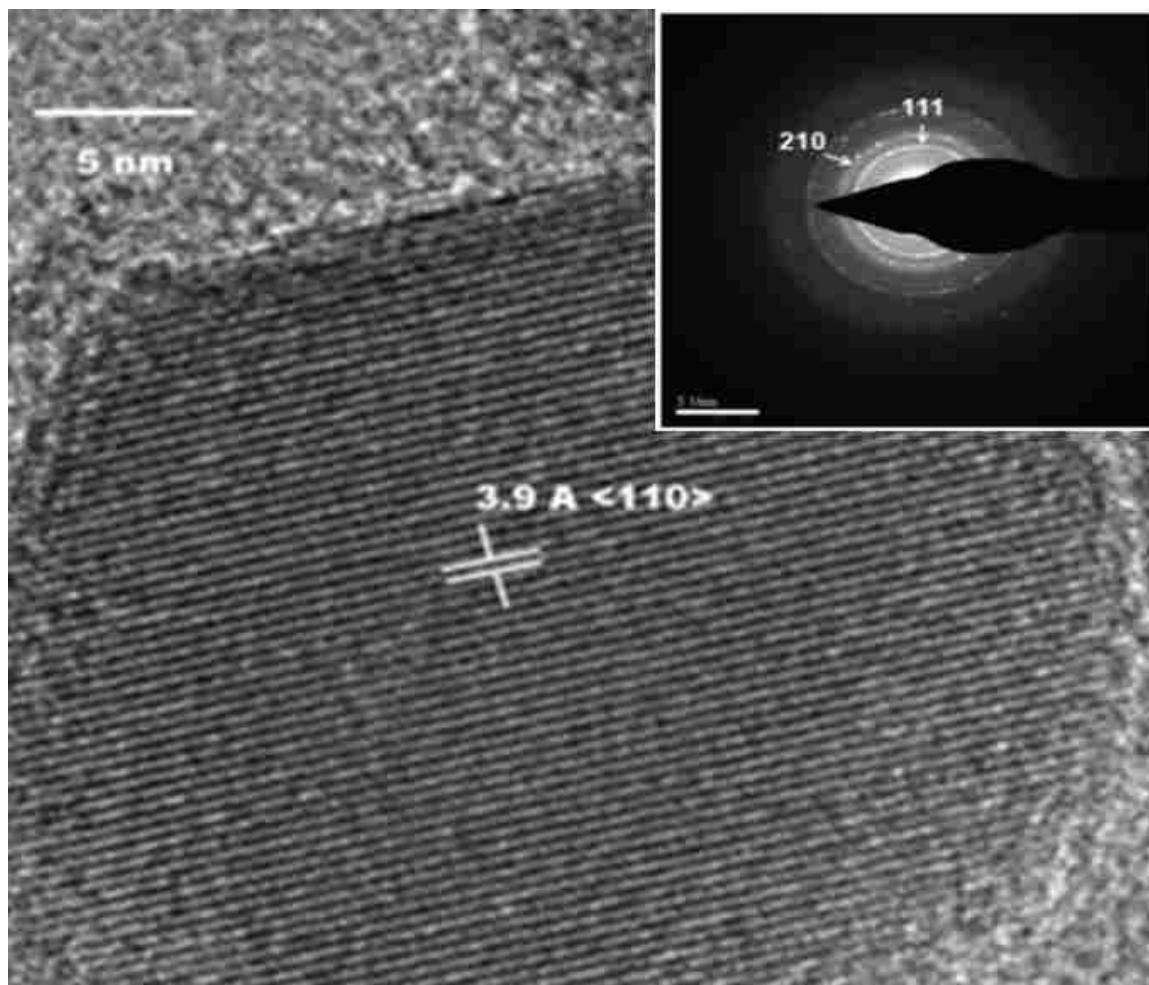
Figure 3: HRTEM image of a nanoparticle showing the crystalline nature of the core and lattice fringes corresponding to FeAs. Inset shows the SAED pattern collected from the core of the nanoparticle

Compositional analysis of the core and the shell was done through EDS line scan

analysis and XPS. The EDS spectrum as shown in Figure 4A verifies the presence of Fe

and As in the nanoparticles with an approximate ratio of 1 : 1.3. The XPS analysis

(Figure 4B) also confirms the presence of strong peaks at 767eV for Fe (2p) and 42 eV

for As (3d) respectively. The XPS and the EDS spectra collected from individual

nanoparticle also picked up significant amount of C.
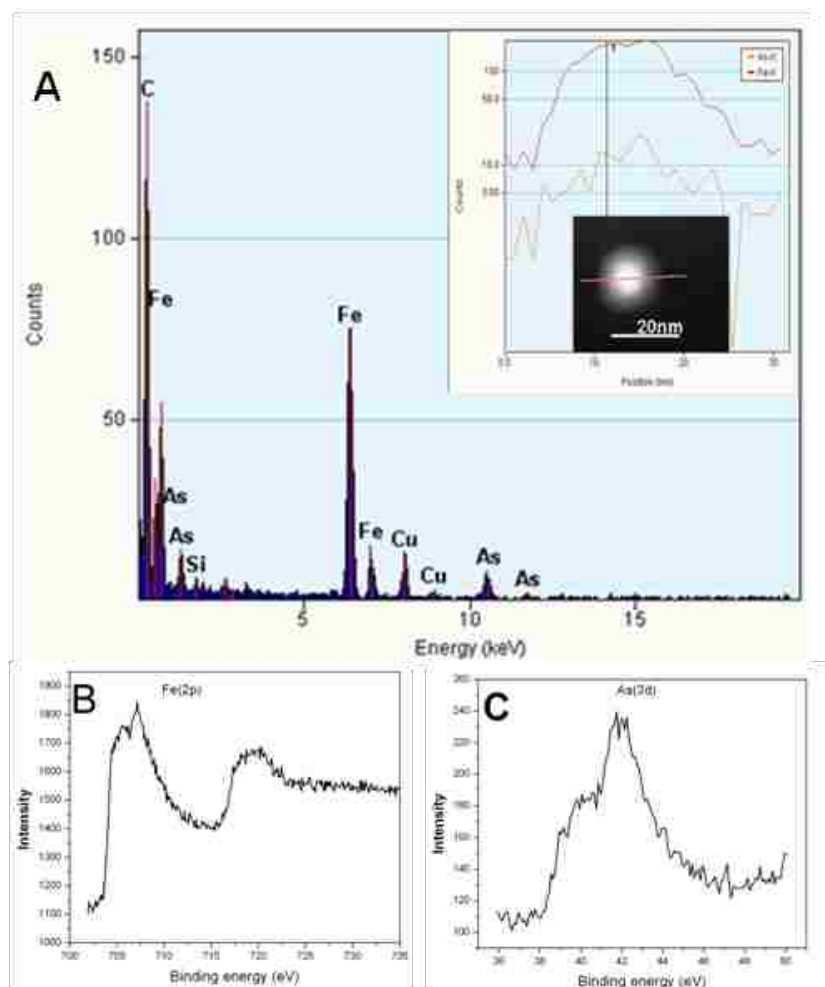
Figure 4 : (A) EDS spectrum from the nanoparticles. The inset shows EDS line scan across a single nanoparticle showing both Fe and As in the core. (B) – (C) XPS analysis of these nanoparticles showing the peaks corresponding to Fe(2p) at 767eV and As(3d) at 42eV

In order to get a better insight into the compositional analysis of the core and the

shell of these nanoparticles, detailed elemental mapping was carried out over a single

nanoparticle. A line scan performed on a single nanoparticle as shown in inset of Figure

4A showed that Fe and As peak intensities intensified at the same time in the nanoparticle core and diminished abruptly within the shell with the concentration of both Fe and As being maximum at the center. The carbon signal on the other hand is more concentrated near the shell and is minimal in the core of the nanoparticle (See Figure S3). These corroborated the fact that the FeAs nanoparticles were indeed covered with a carbonaceous shell resulting in the core-shell morphology Detailed XPS analysis also provided support of this proposed core-shell compositional variance, wherein the Fe (2p) and As (3d) signal increased considerably after sputtering for about 5 min which removed approximately 2 – 3 nm from the surface of the nanoparticles, thereby revealing the core. The core and shell composition of these nanoparticles were further studied through Raman spectroscopy. Raman spectra of the FeAs@C nanoparticles showed peaks at 223 cm^{-1}, 288 cm^{-1}, 406 cm^{-1}, and 605 cm^{-1} as seen in Figure 5. These bands correspond well with the Raman spectra obtained from bulk FeAs with a slight shift towards higher wavenumbers as expected for nanostructured morphology.[31]

The band at observed at 1314 cm^{-1} for the nanoparticle sample, however, was not prominent in bulk FeAs, but is rather a characteristic signature of the D-band on amorphous carbon.[32] It should be noted that the Raman spectra of the nanoparticles was distinctly different from the spectra obtained from pure HDA as shown in the inset of Figure 5. Hence the presence of HDA on the shell of these nanoparticles was ruled out and the shell was confirmed to be formed of amorphous carbon.
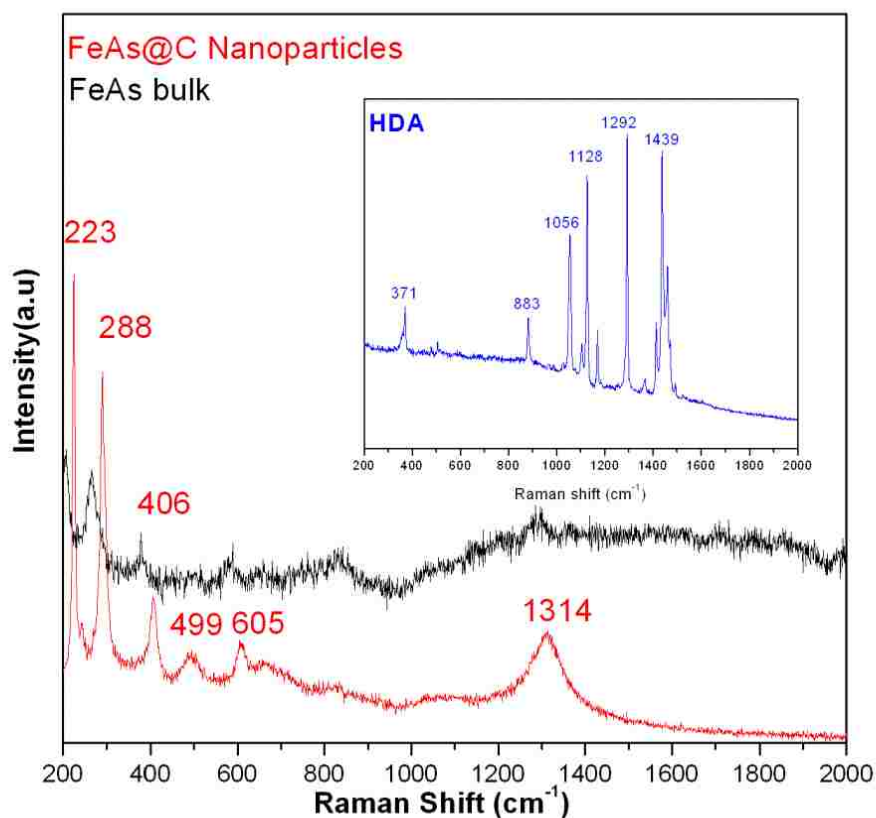
Figure 5: Raman spectra of FeAs@C nanoparticles and FeAs bulk. The inset shows the Raman spectra for HDA

Magnetic properties: FeAs has interesting magnetic properties in lieu of the characteristic arrangements of Fe atoms along the *c*-axis leading to helimagnetism.[14] Bulk FeAs is a double helical magnet below T_N = 77 K, (T_N is the Neel temperature), where the magnetic moments are at right angles to the spiral axis (common *c*-axis) in the absence of magnetic field.[14] However, unlike the other pnictides of similar structure type, FeAs exhibits a complex magnetic behavior in its bulk state. The magnetic susceptibility follows Curie-Weiss law in a narrow temperature range (350 - 600K), and deviation outside that range is believed to be due to some complex exchange interactions and the presence of Cooperative magnetism in the system.[14] To elucidate the magnetic behavior of these FeAs nanoparticles, magnetization as a function of temperature and applied field

was investigated. The magnetization behavior as a function of temperature was measured under zero-field cooled (ZFC) and field-cooled (FC) condition with an applied field of 100 -1000 Oe, and is plotted in Figure 5A – C. The absolute amount of Fe in these samples were obtained from AAS measurements (42.78 ppm) and all the magnetization data was normalized *wrt* the estimated amount of FeAs in the sample rather than the total sample mass used for magnetic studies. A typical divergence of the ZFC-FC curve was observed in the M *vs* T plots, which is characteristic of several magnetic phenomena like superparamagnetism[33] and spin-glass behavior. Previous researchers have observed such divergence in the ZFC-FC plots for the pnictide nanoparticles and ascribed them to the superparamagnetic nature of the nanoparticles.[34-37] In such cases, the maxima in the ZFC plot is considered to be the blocking temperature (T_B), which was representative of the minimum temperature above which spontaneous fluctuations of the particle moment was allowed leading to loss of magnetic ordering. Superparamagnetism is characteristic in ferro- or ferrimagnetic systems when the material size is reduced below a critical dimension, such that it shows single magnetic domain. The presence of superparamagnetism in nanoparticle ensemble is supported by two evidences. The first and foremost evidence is that the magnetization as a function of H/T (H = applied field, T = temperature) for non-interacting single domain particles can be fitted to the *Langevin equation* (Eq. 1) as shown below,[38]

$$M = M_0 \left[\coth\left(\frac{\mu H}{k_b T}\right) - \frac{1}{\left(\frac{\mu H}{k_b T}\right)} \right] \ \dots \ (1)$$

where, M = magnetization, M_0 = saturation magnetization, H = applied magnetic field, μ

= magnetic moment, T= temperature, and k_b = Boltzmann constant. For the FeAs

nanoparticles, the plot of M/M_0 vs H/T at different temperatures, converges into one

universal curve and could be fitted to the Langevin equation with a 99.98% accuracy as

shown in Figure 6D. The second condition for superparamagnetic behavior is

anhysteretic nature of the isothermal magnetization against applied field with zero

coercivity and remanence, which also must be temperature independent above T_B.[39,40] For

the FeAs nanoparticles magnetization as a function of applied magnetic field as(Figure

S4) respectively. The absence of coercivity and remanence (i.e. the anhysteretic nature)

in these plots was prominent above 77 K. Hence, from these magnetic characterizations it

was concluded that these FeAs nanoparticles are indeed superparamagnetic with a fairly

high T_B. There was no correspondence between the T_B and irreversibility temperature

T_{irr}, (T_{irr} = the temperature at which the ZFC and FC curves show divergence) (Figure 6A

– C) indicating considerable size dispersion among the nanoparticles.[12] Typically the

difference between the T_B and T_{irr} stems from the fact that all the nanoparticles in this

system do not have identical energy barriers of magnetic reversal owing to their different

sizes. This leads to a widening of the superparamagnetic transition over a temperature

range where the divergence of the ZFC-FC curves (T_{irr}) and maxima of the ZFC curve

(T_B) do not necessarily merge. As discussed previously from STEM and TEM studies

these FeAs nanoparticles indeed show narrow size dispersity (10 – 15 nm). At lower

temperatures, *viz* 5 and 10K, the magnetization plots show a very small coercivity (390

Oe) which might indicate very weak ferromagnetism in these particles or other short

range magnetic ordering like spin-glass.
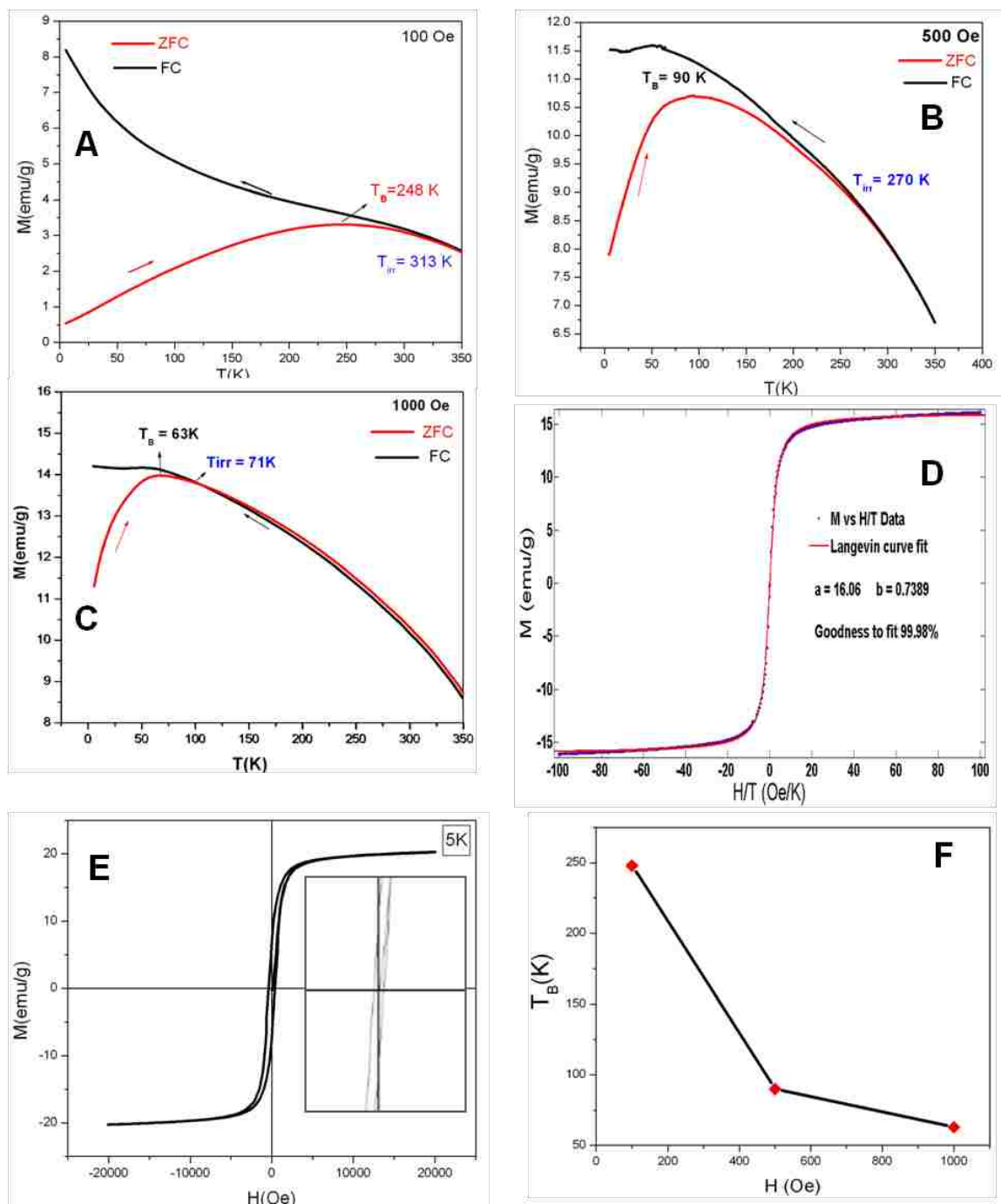
Figure 6 : (A) – (F) Magnetic measurement of the FeAs nanoparticles. The ZFC-FC plot of magnetic susceptibility against temperature under an applied field of (A) 100 Oe; (B) 500 Oe and (C) 1000 Oe. (D) The Langevin fit for M/Ms vs H/T plots (E) M vs H plot at 5 K showing a small coercivity. (F) Shows the dependence of T_B on the applied field

In accordance with other superparamagnetic systems,[23] the T_B was dependent on the field applied, and T_B decreased with increasing magnetic field as shown in Figure 6F. A fairly high saturation magnetization of ~15 emu/gm was observed with these nanoparticles at low temperatures. However it should be noted that at higher temperatures, the magnetization curve was still rising even above 20,000 Oe, indicating that the saturation magnetization will predictably be higher than that observed in the plots. In superparamagnetic nanoparticles, the T_B depends upon the size of the particles, the field applied and the experimental measuring time,[41] and is also influenced heavily by the extent of interparticle interactions. For the FeAs nanoparticles T_B as high as 240K was observed at the lowest field of 100 Oe. There are many outcomes and reasons of such a high T_B in our system. Magnetocrystalline anisotropy and the higher critical radius of the nanoparticles contribute to the high T_B. It also implies that superparamagnetism can be avoided up to 240 K which is a temperature closer to room temperature. Superparamagnets owing to their high magnetic moment are typically used in ferrofluids that may be used as magnetic inks, toners, and frictionless seals.[42] Magnetic refrigeration is another application that uses superparamagnetic materials by reduction of surrounding temperature by heat absorption through magnetocaloric effect.[43] For most of these applications, a T_B close to room temperature is desired for increasing the efficiency of the device. Typically higher T_Bs are observed in alloy nanoparticles like, Co@Au core shell nanoparticles (T_B = 290 K), Co@Cu (T_B = 235 K)[44] and Fe@Au core shell nanoparticles (170K),[45] and mostly elaborate measures are required to inhibit inter-particle interaction and increase the T_B to these values. Some of the measures include wrapping the nanoparticles with a spacer or non-magnetic shell or dispersing them in a polymer matrix

thereby diluting the interparticle interactions. Furthermore, it has been argued by Skumryev[46] that passivating such magnetic nanoparticles in an antiferromagnetic shell increases the T_B 30 fold, thereby beating the "superparamagnetic limit". In the present case, the as- synthesized FeAs nanoparticles being covered with a carbonaceous shell, by itself, presents a perfect assembly for decreasing the interparticle interactions thereby leading to inherently higher T_B. The carbonaceous shell around the magnetic FeAs nanoparticles also aids in pinning the magnetic moments within the nanoparticles. It also increases the chemical stability of FeAs@C nanoparticles towards surface oxidation. Size estimation of the FeAs nanoparticles from magnetic characterization:

For superparamagnetic nanoparticle ensembles above T_B, the *Langevin fit* can also be used for estimating the average particle volume by considering the following equations along with the *Langevin equation* (Eq. 1). Expressing experimental magnetization as a function of *H/T* reduces Eq. 1 to the following form:

$$y = a \left[\coth(bx) - \frac{1}{(bx)} \right] \qquad \dots (2)$$

$$where\ x = \frac{H}{T};\ y = M;\ a = M_0;\ and\ b = \frac{\mu}{k_b}$$

$$Particle\ moment, \mu = M_S < V > \cdots (3)$$

$$where\ M_S = Saturation\ moment\ of\ bulk\ FeAs\ and < V > =$$

$$average\ particle\ volume.$$

The theoretical saturation moment of bulk FeAs was calculated to be 93.9596 emu.gm^{-1} by considering 2.2 unpaired electrons per Fe(III) atom in FeAs.[12] From the

Langevin fit of the M *vs* H/T plot (Figure 6D), the parameters *a* and *b* could be obtained and Eq. 3 could be solved for <V> through proper substitution (the density of FeAs was taken as 7.721 gm.cc^{-1} corresponding to the crystalline phase observed in the pxrd pattern). The average particle diameter obtained through this approach was approximately 10 nm, which was close to the average core size seen in these superparamagnetic particles through extensive SEM and STEM studies.

Previously Brock at al. have investigated a series of iron pnictide nanoparticles and have reported that presence of trace amounts of Fe impurities in some of these nanoparticles interferes with the magnetic signal.[16] In our case however, we would like to underline the fact that at higher temperatures (above T_B) all the M *vs* H curves were anhysteretic in nature thereby ruling out the presence of any kind of bulk ferromagnetic impurities. Also, the nanoparticles obtained were mostly crystalline throughout as seen from the typical HRTEM image shown in Figure 3 thereby reducing the possibility of the presence of any unreacted Fe at the core. Careful elemental analysis through EDS and XPS failed to pick up any excess Fe and O signal from the edge of the nanoparticles, thereby minimizing the possibility of the presence of other Fe-containing impurities like Fe-oxide at the surface of the nanoparticles. From the normalized magnetization data, we estimated that the amount of Fe impurity needed to generate a saturation moment as high as that observed in the nanoparticle sample (~15 emu/g at 5 K) was approximately 8% by weight. This limit is well above the detection limit of Mössbauer spectroscopy which is considered to be the most sensitive technique for detection of Fe. Hence, Mössbauer spectroscopy was also performed on an ensemble of the FeAs@C nanoparticles to gain a

better insight into the various oxidation states of Fe present in these nanoparticles and also to determine the presence/absence of metallic Fe in them.

Mossbauer studies:

The Mössbauer spectra collected from an ensemble of FeAs nanoparticles at room temperature and at 90 K showed a doublet with isomer shift of 0.5385 mm/s and a quadruple splitting of 0.4572 mm/s, which corresponds well with that of bulk FeAs containing Fe in the +3 oxidation state **(**Figure 7 and S5 in supplementary information**).**[47] Fe in the zero oxidation state typically shows a sextet which was not observed with the FeAs@C nanoparticles, thereby ruling out the presence of unreacted Fe at the core of these nanoparticles and extraneous Fe impurity. The close similarity between the spectra obtained from the nanoparticles and the bulk FeAs ruled out the presence of any other oxidation states of Fe as impurity in the nanoparticle sample. The peaks showed some broadening mainly due to the reduced size and polydispersity of these nanoparticles.
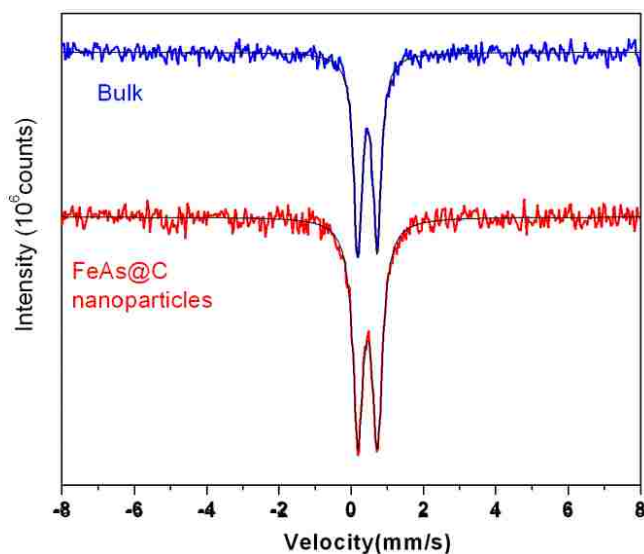
Figure 7 : Mossbauer spectra of FeAs@C nanoparticles collected at room temperature showing a doublet characteristic of Fe (III)

We are presently trying to collect the Mössbauer spectra from these nanoparticles at temperatures below the T_B, such that we can gain a better insight into the magnetically ordered state of these nanoparticles. Mechanism: To gain an insight into the formation mechanism of FeAs@C nanoparticles, aliquots were collected at various times during the reaction and detailed microscopy was carried out to analyze the particle size and composition. It was observed that a spherical nanoparticle-like morphology was formed within the first hour of the reaction. The aliquot collected ~30 min after adding the $Fe(CO)_5$ (t = 0), contained similar core-shell morphology as seen at t = 3 h. However, the size of these nanoparticles was slightly smaller and more importantly As was more concentrated near the edges of the nanoparticle, while the core was Fe-rich (see Figure S3 in supporting information).

From the EDAX analysis it was evident that As concentration in the nanoparticles increased with the reaction time and the concentration of As moved from near the periphery of the nanoparticles towards the core with progress of the reaction. The size of the nanoparticles between different aliquots collected at different stages of growth did not show a large variation indicating that spontaneous nucleation and diffusion controlled growth was predominant factors under the reaction conditions. On the basis of simple organometallic and coordination chemistry it can be expected that during initial stage of the reaction, ligand exchange takes place as soon as Fe(CO)5 is added into the mixture of TPA and HDA. The CO ligand is displaced by the $As(C_6H_5)_3$ to form an intermediate complex $[(C_6H_5)_3As-Fe(CO)_4]$ and free CO, generated according to the equation (4). This kind of ligand exchange with phosphines and arsines is very favorable since they act as electron donating Lewis base.[48] In principle, the intermediate

can behave as a single source precursor for both Fe and As. Single-source precursors which has all the elements of the product composition in one single molecule is very advantageous and has been widely used in nanomaterials synthesis.[49]

$$Fe(CO)_5 + As(C_6H_5)_3 \longrightarrow \left[\begin{array}{c} \text{Ph}_3As\text{-Fe(CO)}_4 \end{array} \right] + CO$$

$$FeAs + \text{Carbonaceous by-products} \qquad (4)$$
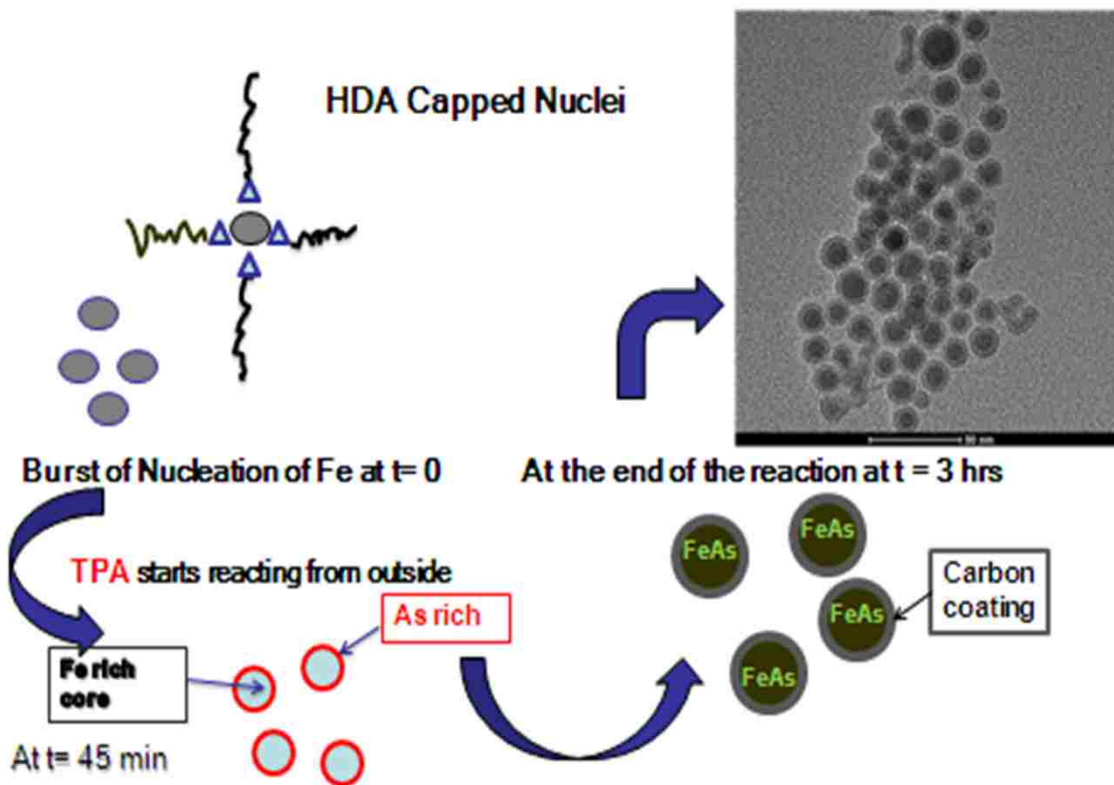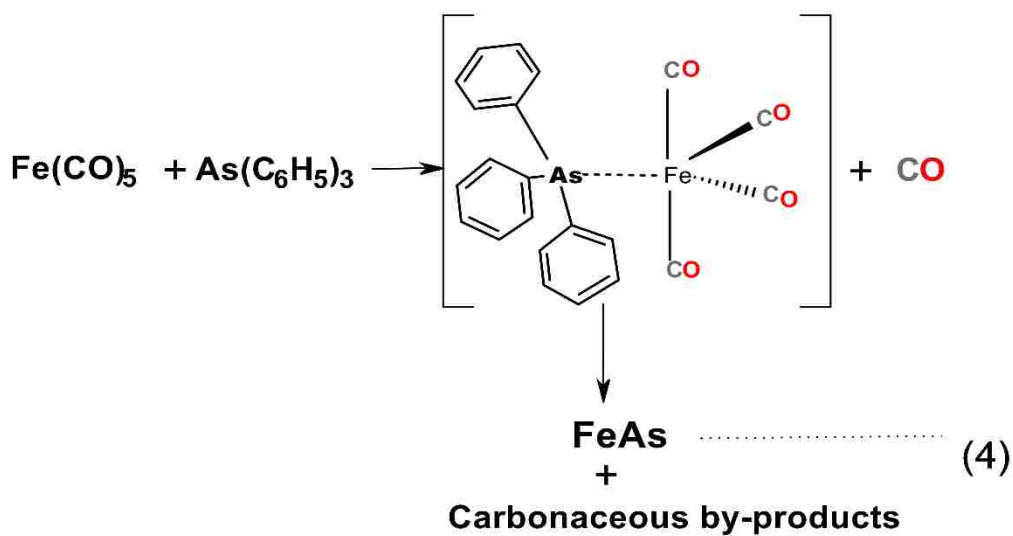
Figure 8: Proposed growth mechanism of the FeAs@C nanoparticles

In this case, the intermediate brings the As and Fe close enough as would be expected than the traditional solid state methods of FeAs synthesis. Proximity of As and Fe in this intermediate renders the possibility of an internal redox between As and Fe. The driving force is the difference in the reduction potentials of Fe^{3+}/Fe and As^{3+}/As^{3-} couples as shown in Eqs. 5 and 6 respectively. The presence of amine (HDA) in the mixture makes the reaction medium slightly basic, thereby decreasing the reducing ability of the arsine compound. Since the As^{3+}/As^{3-} has a more positive reduction potential, it acts as a stronger oxidizing agent thereby oxidizing Fe(0) to Fe^{3+} while itself being reduced to As^{3-}. The overall change in potential for this redox reaction is + 1.113 V as calculated by using equations 5 and 6.[50] The positive value of ΔE indicates that this reaction will be spontaneous since the change in internal free energy would be negative. Further importance of the basic medium was demonstrated by the use of oleic acid (5mM) as surfactant instead of HDA which failed to produce FeAs nanoparticles from $Fe(CO)_5$ and TPA. Temperature also plays a definitive role in this ligand exchange and internal redox, since it is observed that at low temperature, the product contains a mixture of FeAs and $FeAs_2$ (which contains Fe in the +2 oxidation state).

$$2Fe^{3+} \rightarrow 2Fe(0) + 6e^- \qquad E^0_{[Fe(3+)/Fe(0)]} = -0.768 \text{ V} \qquad ....(4)$$

$$As^{3+} + 6e^- \rightarrow As^{3-} \qquad E^0_{[As(3+)/As(3-)]} = + 0.345 \text{ V} \qquad ....(5)$$
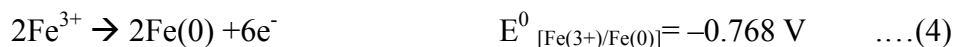
The following hypothesis is being made to explain the morphological conversion of the nanoparticles. At t = 0, there is a burst of nucleation due to addition of $Fe(CO)_5$ forming Fe-rich nuclei capped with HDA. TPA starts reacting at the surface of the nuclei

and the initial layers of FeAs formed coat the nuclei. At conditions of constant high

temperature (300°C) As diffuses deeper into the nuclei thereby promoting conversion of

the core to FeAs. The growth front of FeAs starts at the periphery of the nuclei and

moves inwards, somewhat similar to the *inside-out* growth mechanism seen in inorganic

fullerenes.[51] As time approaches t = 3 h, the entire core has been converted into FeAs. A

pictorial representation of this growth mechanism is shown in Figure 8. The

carbonaceous shell formation starts from the very preliminary stages of growth. The

presence of carbon rich species in the form of ligands and reactants (e.g. CO in $Fe(CO)_5$,

3 phenyl rings in TPA and the C_{16} chain in HDA) contributed to the formation of the

carbonaceous shell through decomposition of the molecular precursors. Previous

researchers working with TPA have also proposed that the pyrogenation of TPA generates

biphenyls, and the decomposition of these aromatic rings under the refluxing conditions

can lead to the formation of the carbonaceous shell. The enhanced catalytic activity of Fe

towards pyrolysis of the hydrocarbons has been well studied through the formation of

carbon nanotubes and nanofibers. In the present case it can be expected that the presence

of Fe-containing precursor facilitated the formation of the carbonaceous shell as has been

recently observed by the authors.[52]

5. CONCLUSIONS

We have successfully synthesized pure FeAs@C core—shell nanoparticles by a

simple, single step solution based method. These nanoparticles showed

superparamagnetism with a T_B as high as 240K and hence may find possible applications

as ferrofluids, magnetic recording materials and serve as model systems for

understanding helimagnetism at the nanoscale. The conversion of a helimagnet to a superparamagnet by reducing size provides us with a perfect practical example of a system where nanostructuring brings a change in the bulk properties. The magnetic exchange interactions in FeAs are complex and these kinds of findings might provide crucial tools for better understanding of the spin interactions in the pnictide layers in nano-structured geometry as well as the pnictide superconductors in the nanostructured geometry since their properties depend on the magnetic interactions of the pnictide layer.

These FeAs nanoparticles also bring us one step closer in synthesizing the novel iron arsenide based superconducting nanostructures like the LiFeAs. We are currently trying to incorporate Li into the FeAs nanoparticles through sacrificial template approach. The synthesis method reported here is a very simple, soft chemical approach which is facilitated by the ligand exchange capabilities of the arsine based ligands, and can be generalized for synthesizing nanostructures of other arsenides. In our preliminary research we have been able to make nanostructures of other arsenides like CoAs, CrAs, MnAs and InAs by employing the above methodology. The solution based approach also makes provides opportunities for introducing dopants in the nanostructure and also induce anisotropic growth by using suitable catalysts through *SLS* growth techniques.

6. ASSOCIATED CONTENT

Supporting Information. PXRD, M vs H (Hysteresis curves) and line scan with EDS data are available free of charge via the Internet at http://pubs.acs.org."

7. AUTHOR INFORMATION

Corresponding Author

* nathm@mst.edu

Author Contributions

The manuscript was written through contributions of all authors. All authors have given approval to the final version of the manuscript. ‡These authors contributed equally.

9. REFERENCES

(1)   Kamihara, Y.; Hiramatsu, H.; Hirano, M.; Kawamura, R.; Yanagi, H.; Kamiya, T.; Hosono, H. *J. Am. Chem. Soc*. **2006**, *128*, 10012.

(2)   Matsuishi, S.; Hosono, H. *Mater. Integr*. **2011**, 24, 42.

(3)   Kamihara, Y.; Watanabe, T.; Hirano, M.; Hosono, H. *J. Am. Chem. Soc.* **2008**, *130*, 3296.

(4)   Johrendt, D.; Pottgen, R. *Angew. Chem., Int. Ed*. **2008**, *47*, 4782 and references therein.

(5)   Chen, X. H.; Wu, T.; Wu, G.; Liu, R. H.; Chen, H.; Fang, D. F. *Nature* **2008**, *453*, 761.

(6)   Torikachvili, M. S.; Bud'ko, S. L.; Ni, N.; Canfield, P. C. *Phys. Rev. Lett*. **2008**, *101*, 057006(4).

(7)   Rotter, M.; Tegel, M.; Johrendt, D.; Schellenberg, I.; Hermes, W.; Pöttgen, R. *Phys. Rev. B* **2008**, *78*, 020503/1.

(8)   Zhang, S. J.; Wang, X. C.; Sammynaiken, R.; Tse, J. S.; Yang, L. X.; Li, Z.; Liu, Q. Q.; Desgreniers, S.; Yao, Y.; Liu, H. Z.; Jin, C. Q. *Phys. Rev. B* **2009**, *80*, 014506(1).

(9)   Alireza, P. L.; Ko, Y. T. C.; Gillett, J.; Petrone, C. M.; Cole, J. M.; Lonzarich, G. G.; Sebastian, S. E. *J. Phys.: Condens. Matter* **2009**, *21*, 012208.

(10)   Hosono, H. *J. Phys. Soc.* Jpn. **2008**, *77 (Suppl. C)*, 1.

(11)   Hase, I.; Yanagisawa, T. *Phys. C (Amsterdam, Neth.)* **2010**, *470*, 538.

(12)   Shirai, M. *Phys. E (Amsterdam, Neth.)* **2001**, 10, 143. Segawa, K.; Ando, Y. J. Phys. Soc. Jpn. 2009, *78*, 104720.

(13)   Selte, K.; Kjekshus, A. *Acta Chem. Scand.* **1969**, *23*, 204.

(14)   Selte, K.; Kjekshus, A.; Andresen, A. F. *Acta Chem. Scand*. **1972**, *26*, 3101.

(15)   Jeffries, J. R.; Butch, N. P.; Cynn, H.; Saha, S. R.; Kirshenbaum, K.; Weir, S. T.; Vohra, Y. K.; Paglione, *J. Phys. Rev. B: Condens. Matter Mater. Phys*. **2011**, *83*, 134520/1.

(16)   Muthuswamy, E.; Kharel, P. R.; Lawes, G.; Brock, S. L. *ACS Nano* **2009**, *3*, 238.

(17)   Park, J.; Koo, B.; Yoon, K. Y.; Hwang, Y.; Kang, M.; Park, J. G.; Hyeon, T. *J. Am. Chem. Soc.* **2005**, *127*, 8433.

(18)   Yang, Li; Malik, A. M.; O'Brien, P. *J. Am. Chem. Soc*. **2005**, *127*, 16020.

(19)   Qian, C.; Franklin, K.; Ma, L.; Tsui, F.; Yang, P.; Liu, J. *J. Am. Chem. Soc.* **2004**, *126*, 1195.

(20)   Muthuswamy, E.; Savithra, G. H. L.; Brock, S. L. *ACS Nano* **2011**, *5*, 2402.

(21)   Perera, S. C.; Tsoi, G.; Wegner, L. E.; Brock, S. L. *J. Am. Chem. Soc*. **2003**, *125*, 13960.

(22)   Tian, P.; Zhang, Y.; Senevirathne, K.; Brock, S. L.; Dixit, A.; Lawes, G.; Billinge, S. J. L. *ACS Nano* **2011**, *5*, 2970.

(23) Lu, J.; Xie, Y.; Jiang, X.; He, W.; Du, G. *J. Mater. Chem.* **2001**, *11*, 3281.

(24) Zhang, X. M.; Wang, C.; Qian, X. F.; Xie, Y.; Qian, Y. T. *J. Solid State Chem.* **1999**, *144*, 237.

(25) Afzaal, M.; Malik, A. M.; O'Brien, *P. Chem. Rev.* **2010**, *110*, 4417.

(26) Wang, J.; Yang, Q. *Dalton Trans.* **2008**, 6060.

(27) Wang, J.; Yang, Q. *Chem. Lett.* **2008**, *37*, 306.

(28) Recoil software: Lagarec, K.; Rancourt, D. G. *Nucl. Instrum. Methods Phys. Res., Sect. B* **1997**, *129*, 266.

(29) Patterson, A. L. *Phys. Rev.* **1939**, *56*, 978.

(30) Schaufelberger, F. A. *J. Met.* **1956**, *8*, 695.

(31) Choi, H. C.; Jung, Y. M.; Kim, S. B. *Vib. Spectrosc.* **2005**, *37*, 33.

(32) Ferarri, A. C.; Robertson, *J. Phys Rev. B* **2000**, *61*, 14095.

(33) Rondinone, A. J.; Samia, A. C. S.; Zhang, Z. J. *J. Phys. Chem. B* **1999**, *103*, 6876.

(34) Mikhaylova, M.; Kim, D. K.; Bobrysheva, N.; Osmolowsky, M.; Semenov, V.; Tsakalakos, T.; Muhammed, M. *Langmuir* **2004**, *20*, 2472.

(35) Yun-Hao, X.; Jian-Ping, W. *IEEE Trans. Magn.* **2007**, *43*, 3109.

(36) Bala, T.; Bhame, S. D.; Joy, P. A.; Prasad, B. L. V.; Sastry, M. *J. Mater. Chem.* **2004**, *14*, 2941−2945.

(37) Zelenakova, A.; Zelenak, V.; Degmova, J.; Kovac, J.; Sedlackova, K.; Kusy, M.; Sitek, J. Rev. Adv. Mater. *Sci.* **2008**, *18*, 501−504.

(38) Knobel, M. N.; W.C.; Socolovsky, L. M.; De Biasi, E.; Vargas, J. M.; Denardin, J. C. *J. Nanosci. Nanotechnol.* **2008**, *8*, 2836−2857.

(39) Unruh, K.; Chien, C. Nanomaterials; Synthesis, Properties and Applications; Edelstien, A., Cammarata, C., Eds.; Taylor and Francis: New York, **1996**; pp 352−359.

(40) Lu, A. H.; Salabas, E. L.; Schuth, F. *Angew. Chem., Int. Ed.* **2007**, *46*, 1222−1244.

(41)   Opel, M.; Nielsen, K. W.; Bauer, S.; Goennenwein, S. T. B.; Cezar, J. C.; Schmeisser, D.; Simon, J.; Mader, W.; Gross, R. Eur. *Phys. J. B* **2008**, *63*, 437.

(42)   Lee, W. R.; Kim, M. G.; Choi, J.-R.; Park, J.-I.; Ko, S. J.; Oh, S. J.; Cheon, J. *J. Am. Chem. Soc.* **2005**, *127*, 16090.

(43)   Raj, K.; Moskowqitz, R. *J. Magn. Magn. Mater.* **1990**, *85*, 233.

(44)   McMichael, R. D.; Shull, R. D.; Swartzendruber, L. J.; Bennett, L. H.; Watson, R. E. *J. Magn. Magn. Mater*. **1992**, *111*, 29.

(45)   Zhang, J.; Post, M.; Veres, T.; Jakubek, Z. J.; Guan, J.; Wang, D.; Normandin, F.; Deslandes, Y.; Simard, B. *J. Phys. Chem. B* **2006**, *110*, 7122.

(46)   Skumryev, V.; Stoyanov, S.; Zhang, Y.; Hadjipanayis, G.; Givord, D.; Nogues, J. *Nature* **2003**, *423*, 850.

(47)   Kulshreshtha, S. K.; Raj, P.; Rao, U. R. K. *Proc. Nucl. Phys. Solid State Phys. Symp*. **1973**, *16*, 316.

(48)   Crabtree, R. H. The Organometallic Chemistry of the Transition Metals; Wiley: **2001**; p 96.

(49)   Smith, K. D; Luther, M. J; Semonin, E. O; Nozik, J. A; Matthew C. Beard, C. B. *ACS Nano* **2011**, *5*, 183.

(50)   Bard, A. J.; Parsons, R.; Jordan, *J. Standard Potentials in Aqueous Solutions*; IUPAC (Marcel Dekker): New York, **1985**.

(51)   Feldman, Y. W., E.; Srolovitz, D. J.; Tenne, R. *Science* **1995**, *267*, 222.

(52)   Dü ndar-Tekkaya, E.; Karatepe, N. *World Acad. Sci., Eng. Technol*. **2011**, *No. 55*, 225−231.

(53)   Mishra, S.; Song, K.; Koza, J. A.; Nath, M. *ACS Nano* **2013**, *7*, 1045.

10. SUPPORTING INFORMATION
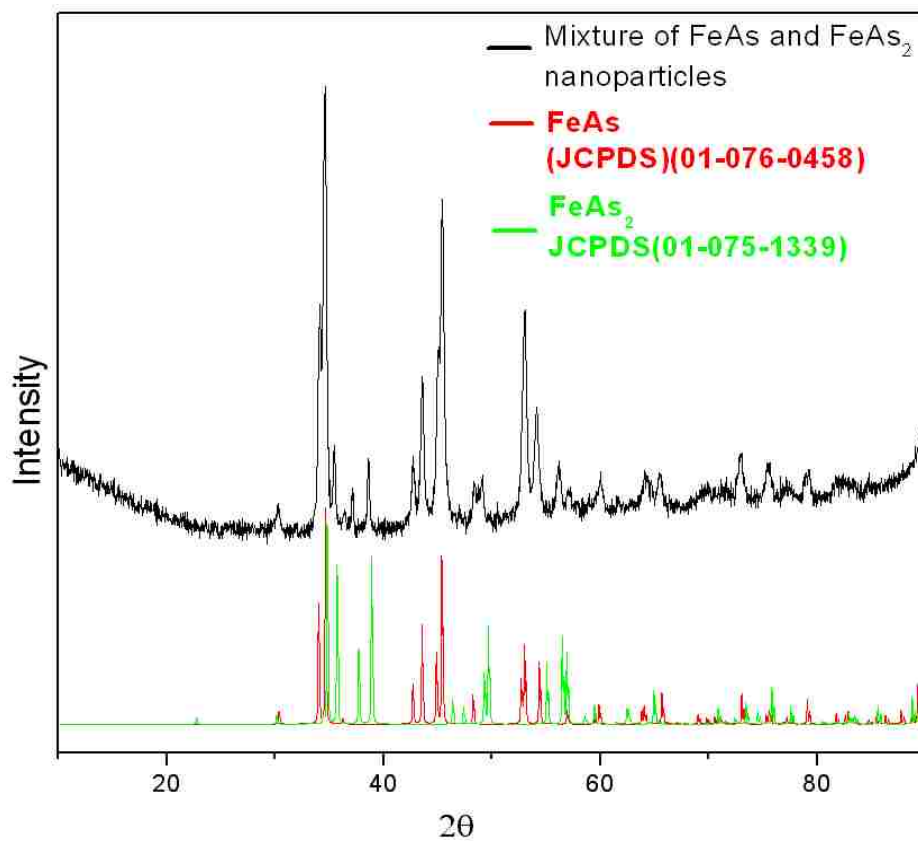
Figure S1: PXRD pattern of nanoparticles synthesized at 250°C
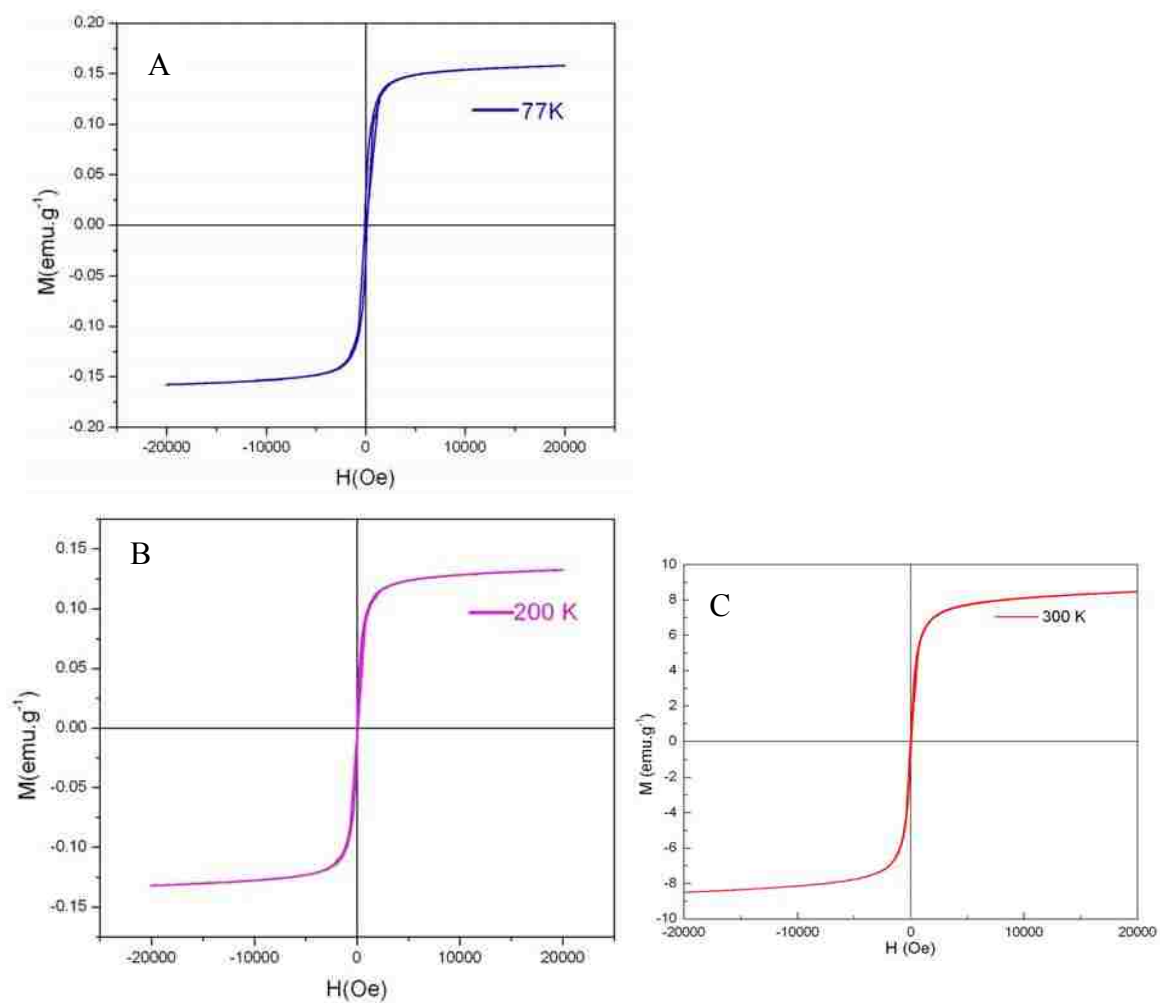
Figure S2: (A), (B), (C) show hysteresis curves at 77 K, 200 K, 300 K respectively showing the anhysteretic nature
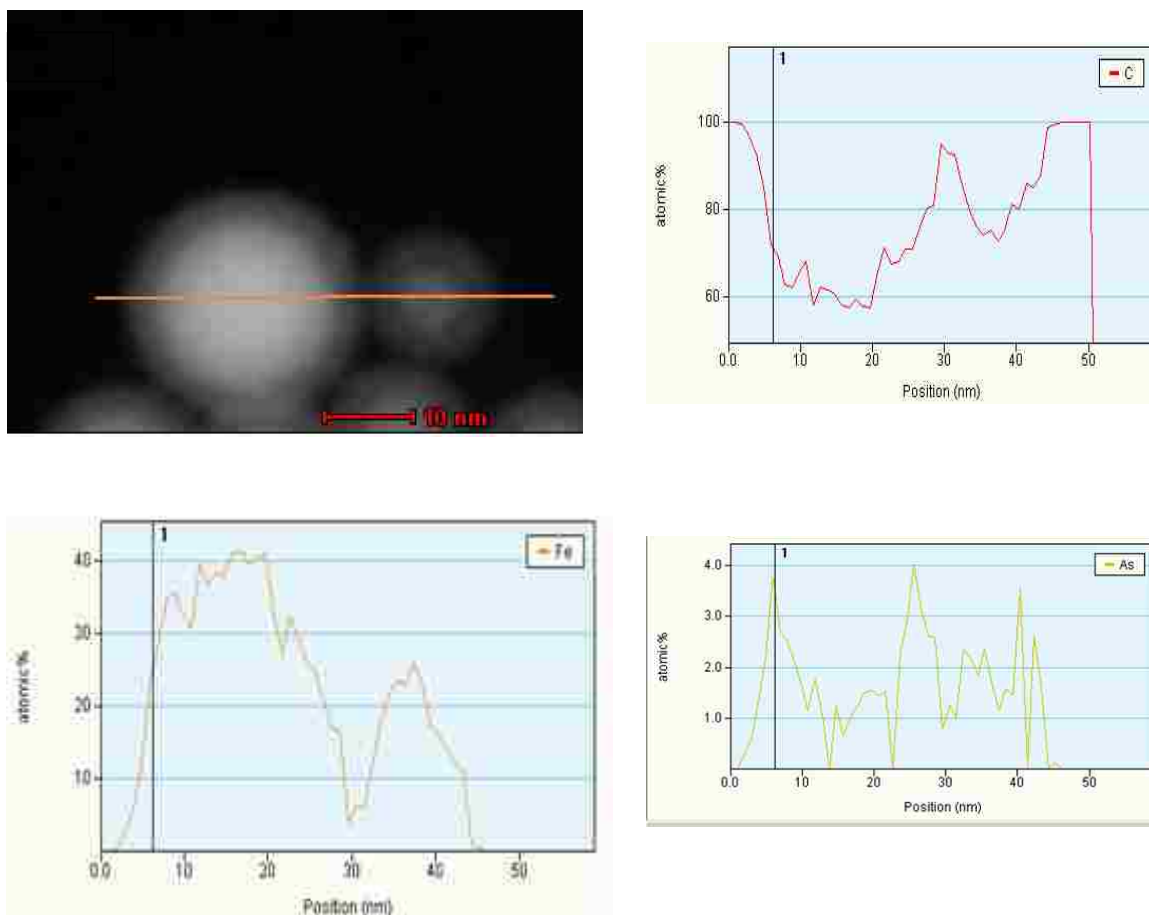
Figure S3: Line scan across the nanoparticles collected after 45min of the reaction

II. SYNTHESIS AND MAGNETIC PROPERTIES OF SUPERPARAMAGNETIC CoAs NANOSTRUCTURES

.

Synthesis and Magnetic Properties of Superparamagnetic CoAs Nanostructures.

Prachi Desai, Akshay Pariti, Manashi Nath*

Missouri University of Science and Technology, USA
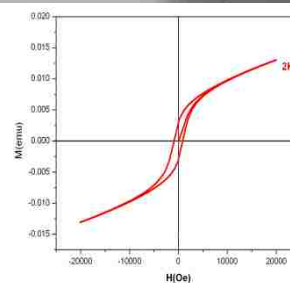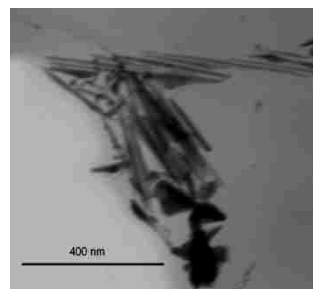
CoAs nanowires showing ferromagnetic response.

http://web.mst.edu/~nathm/Manashi-home-page.html

1. ABSTRACT

This article provides a comprehensive guide on the synthesis and characterization of superparamagnetic CoAs nanoparticles and elongated nanostructures with high blocking temperature, T_B, *via* hot –injection precipitation and solvothermal methods. Cobalt arsenides constitute an important family of magnetically active solids that find variety of applications ranging from magnetic semiconductors to biomedical imaging. While the higher temperature hot-injection precipitation technique (300 °C) yields pure CoAs nanostructures, the lower temperature solvothermal method (200°C) yields a mixture of CoAs nanoparticles along with other Co-based impure phases. The synthesis in all these cases involved usage of triphenylarsine $((C_6H_5)_3As)$ as the As precursor which reacts with solid $Co_2(CO)_8$ by ligand displacement to yield a single source precursor. The surfactant, hexadecylamine (HDA) further assists in controlling the morphology of the nanostructures. HDA also provides basic medium and molten flux like conditions for the redox chemistry to occur between Co and As at elevated temperatures. The influence of the length of reaction time was investigated by studying the evolution of product morphology over time. It was observed that while spontaneous nucleation at higher temperature followed by controlled growth led to the predominant formation of short nanorods, with longer reaction time, the nanorods were further converted to nanoparticles. The size of the nanoparticles obtained, were mostly in the range of 10 – 15 nm. The key finding of this work is exceptionally high coercivity in CoAs nanostructures for the first time. Coercivity observed was as high as 0.1T (1000 Oe) at 2K. These kind of magnetic nanostructures find multiple applications in spintronics whereas the

superparamagnetic nanoparticles are viable for use in magnetic storage, ferrofluids and as contrast enhancing agents in MRI.

2. KEYWORDS

CoAs, Cobalt monoarsenide, Superparamagnetic nanoparticles, Arsenide nanostructures, Hexadecylamine

3. INTRODUCTION

Transition metal pnictides have constituted an important family of compounds in materials chemistry and have gained importance in photovoltaic,[1] spin-dependent transport,[2] optoelectronics,[3] and ferromagnetic semiconductors.[4] The extensive interest in transition metal pnictides was further enhanced by the superior catalytic properties of transition metal phosphides, e.g. unsupported Ni2P particles were shown to have enhanced catalytic activity towards hydrodesulfurization (HDS) of organic chemicals.[5] The discovery of high temperature superconductivity in Fe-based pnictide superconductors, have also rejuvenated interest towards these materials.[6-8] Experimental and computational studies of Li^+ extraction/insertion mechanisms in cubic-transition metal pnictides, Li_xMPn_4 (MPn = TiP, VP, VAs) have also suggested that these materials have high specific capacities, and are promising anode materials for Li-ion batteries.[9] With these attributes transition metal pnictides have emerged as worthy successors to main group pnictides like GaAs, InAs, InP etc. which have applications of their own in optoelectronics.[10] In addition to interesting electronic properties, FeAs,

FeP, Fe_2P and MnP nanoparticles and nanorods also exhibit novel magnetic properties.[11,12]

The novel magnetic properties of transition metal pnictides make them promising for futuristic applications like quantum computing.[13] Cobalt monoarsenide, CoAs, belonging to the transition metal pnictide family constitutes an important member of the group. It has a MnP-type crystal structure with orthorhombic space group *Pmcn* at room temperature.[14] A continuous phase transition between the MnP and NiAs structure-types occurs at 1248 ± 20 K.[14] Pnictide rich phases of Co*Pn* are semiconducting (in CoP2/CoP3) whereas Co rich phases show metallic behavior.[15] Metallic nature of such nanoparticles may be exploited in nanofluids and nanoinks for contact metallization.[16] This metallic nature was also reported in diffuse reflectance data for CoAs by Selte et al.[14] For bulk CoAs, no long range magnetic order is observed. Previous research conducted by other groups indicate that the magnetic susceptibility shows a broad minimum at ~ 225 K, with Curie-Weiss behavior above 490 K giving $\theta \approx -230$ K and a paramagnetic moment of 1.15 μB/Co.[17] The anomalous temperature dependence below 490K is attributed to thermal distribution of electrons between magnetic states. CoAs nano-islands are very predominant in the III-V semiconductors, and affect their properties to a certain extent. Whenever Co metal has been used for purpose of contact metallization, CoAs nanostructures were found within GaAs substrates.[18] These CoAs nano-islands affect the properties of the parent semiconductors. However, reports of CoAs nanostructures by themselves and a systematic study of their magnetic properties are still very rare to date. The rich variety of magnetic properties exhibited by Co-salts,

warrants detailed investigation of this interesting class of Co-pnictide based magnetic nanostructures.

Magnetic nanoparticles and nanowires have been found to have great importance in both fundamental research and technical applications such as in ferrofluids, permanent magnets, recording media, drug carriers and catalysts.[19- 21] Based on their novel nanoscale magnetism, roles of these magnetic nanostructures in areas of biology, medicine, geology and materials science are fast expanding. Magnetism at the nanoscale can be controlled by single magnetic domain and magnetic anisotropy (due to increased surface area). For instance when the particle size/grain size matches the magnetic domain size, effects like superparamagnetism dominate and the bulk magnetic properties might be altered.[22] Also for nanoparticles/nanowires with small sizes it has been observed that at low temperature ordering effects like ferromagnetism comes into play.[23] Ferromagnetic nanostructures can act as spin–injection systems in spintronic devices when used in conjunction with semiconductors.[24]

Traditionally, bulk CoAs is prepared by solid state metathesis routes, reduction of arsenate precursors and liquid ammonia reduction techniques respectively.[25,26] Other methods of synthesis include physical deposition and MOCVD using complexes that may be toxic and require high processing temperatures.[27] Mesh like nanostructured CoAs has also been synthesized by Lu and Xie et al.[28] Thin films of CoAs by using metal-organic complex 1,3-bis(tert-butyl)-2-[tetracarbonyl-cobalt(-1)]-1,3,2-diazarsolidine were also synthesized by Klingan et al. in 1995 using the CVD method.[29] However, these conventional methods, even though yields compositionally pure samples, are not very

amenable to morphology control. On the other hand, research incorporating nanostructures of the transition metal pnictides received a major boost following the identification of simple coordination complexes like trioctylphosphine (TOP), trioctylphosphine oxide (TOPO) tris(trimethylsilyl)phosphine (TMSP) and triphenylarsine (TPA) as facile precursors for generating the phosphides and arsenide through *chemie douche* method.[30,12] Soft chemical synthesis methods offers controlled growth and provides more opportunity for tuning the morphology of the product through subtle variation of precursor, experimental conditions like temperatures, solvents etc., and by introducing additional morphology-directing agents like surfactants. Herein, we report a low temperature solvothermal and hot-injection precipitation methods for the synthesis of CoAs nanoparticles and ultrathin nanowires. Detailed characterization has been carried out to elucidate the composition, morphology and phase purity of the nano-structured products. We have also investigated the formation mechanism of the nanostructures through exploring variable reaction parameters. The nanostructures were ferromagnetic at low temperatures and superparamagnetic at high temperatures making them suitable for spintronics. These nanostructures of CoAs also exhibited high coercivity and saturation magnetization. This is the first report of one-dimensional CoAs nanostructures that have ferromagnetic properties. Nanostructured induced ferromagnetism has been explored in the past by Stamplecoskie in Mn doped GaN nanowires,[31] and in *TmPn* (where *Tm*=Transition metals, *Pn* = Pnictogen) systems previously by Wang et al. in Fe_2P/ FeP nanocables.[11] Recently, authors of this manuscript have also found similar results in FeAs@C nanoparticles which displayed superparamagnetism at 247K.[12]

4. EXPERIMENTAL METHODS

Chemicals. The chemicals used in these syntheses were of analytical purity. Tripheynlarsine (99%) was purchased from Alfa Aeser, hexadecylamine (HDA) (90%) and $Co_2(CO)_8$ from Strem chemicals. These chemicals were used as purchased without further purification.

Synthesis. All the reactions were performed inside a N_2-filled glove box with less than 1 ppm of O_2. This ensured minimal exposure to the As-precursors.

Method (IA) – Hot-injection. 1 mM of triphenylarsine (TPA) and 5 mM of HDA were taken in a 3-neck round bottom flask equipped with a condenser. The mixture was heated till 300 °C. At that temperature, 1mM of solid $Co_2(CO)_8$ was added to the hot mixture. After addition the reaction mixture was refluxed for variable times (typically 45 min – 3 h). Upon completion, heating was stopped and the mixture was cooled down to room temperature. It was observed that the blackish product was attracted to a laboratory magnet. Hence, the product was purified using combination of magnetic filtration and ultracentrifugation (in ethanol and hexane successively). It should be noted here that use of HDA was very crucial to formation of these nanoparticles and using other surfactants did not lead to similar results.

Method (IB) Hot-injection. A minor modification to the method IA was made by adding oleylamine (OA) to $Co_2(CO)_8$ thereby increasing the solubility of the solid carbonyl precursor and making it liquid and easier to inject into the hot reaction mixture. In this method 1mM of $Co_2(CO)_8$ was dissolved in 3 mL of oleylamine by magnetic stirring. The resulting pink frothy solution was added in a single step to the hot mixture of 1mM TPA and 5mM HDA (at 300 °C). After 45 min the temperature had dropped to

260 °C, and the black magnetic product was well separated. The heating was stopped after one hour. The reaction was cooled and purified by magnetic filtration in ethanol. The additional advantage of this method was the use of mixed surfactants (HDA and oleylamine in the reaction mixture).

Method (II) Solvothermal. 1 mM of TPA, 1mM of $Co_2(CO)_8$ and 5 mM of HDA were weighed and added to a 23ml Teflon lined autoclave inside a N2 filled glove box with less than 1ppm of O_2. The Teflon liner was then sealed inside an autoclave and heated to 200° C in an oven maintained at constant temperature. The duration of the heating cycle varied from 3 – 24 h where the products from lesser heating times were used to elucidate the formation mechanism of the nanostructures. After the desired heating period, the autoclaves were allowed to cool down and the product was purified by as described above.

Characterizations. PXRD The as-synthesized powder was finely ground and used for powder X-ray diffraction (PXRD), which was carried out on a Philips Xpert diffractometer scanning from 5° to 90° (2θ).

TEM, STEM. Samples for transmission electron microscopy (TEM) and scanning transmission electron microscopy (STEM) were performed in a Technai TEM operating at 200 kV and a Dual-beam FEI Helios microscope, respectively. The samples were prepared by dispersing as-synthesized CoAs nanoparticles in ethanol by ultra-sonication for 30 min. Drops of the diluted dispersion were taken on a holey carbon coated 200 mesh Cu grid followed by drying in air.

Magnetic measurements. Magnetic moment and isothermal magnetization was collected from a SQUID magnetometer and the VSM option of PPMS respectively. The

powdered sample was loaded in a gel cap and was inserted into the magnetometer with

the help of standard sample loader. The diamagnetic signal from the gel cap was

collected separately and subtracted as a background from the signal obtained from the

sample. The zero field cooled (ZFC) data was obtained after cooling the sample from 300

to 5 K under 0 magnetic field and then by measuring the magnetic susceptibility while

warming up the sample from 5K. The field cooled (FC) data was collected

simultaneously as the sample was being cooled down under an applied magnetic field of

100-1000 Oe. The isothermal magnetization against applied field was collected at

different temperatures ranging 2Kto 350K by varying the applied magnetic fields from -

20,000 Oe to 20,000 Oe.

5. RESULTS AND DISCUSSIONS

Figure 1 shows the PXRD pattern obtained from an ensemble of the nanowires

and nanoparticles. The nanostructures obtained through hot-injection based methods (i.e.

IA and IB) both exhibited pattern similar to pure CoAs (JCPDS no 01-077-1351) which

crystallizes in the MnP-type structure. The solvothermal method (method II) on the other

hand, showed the presence of trace impurities in addition to CoAs in the pxrd pattern.

The impurities were identified as due to hydrated cobalt hydroxycarbonate

($[Co(CO_3)_{0.5}(OH)]0.11H_2O$) cobalt carbonate and cobalt oxide (Co3O4). During a series

of reaction with HDA and Co-salts under hydrothermal conditions, the authors have

observed that these are ideal reaction conditions to form nanowires of $Co(CO_3)_{0.5}(OH)$,

which could be further heat-treated to yield Co_3O_4. Hence, the presence of these

compounds as impurities in the product of the hydrothermal reaction (method II) in the
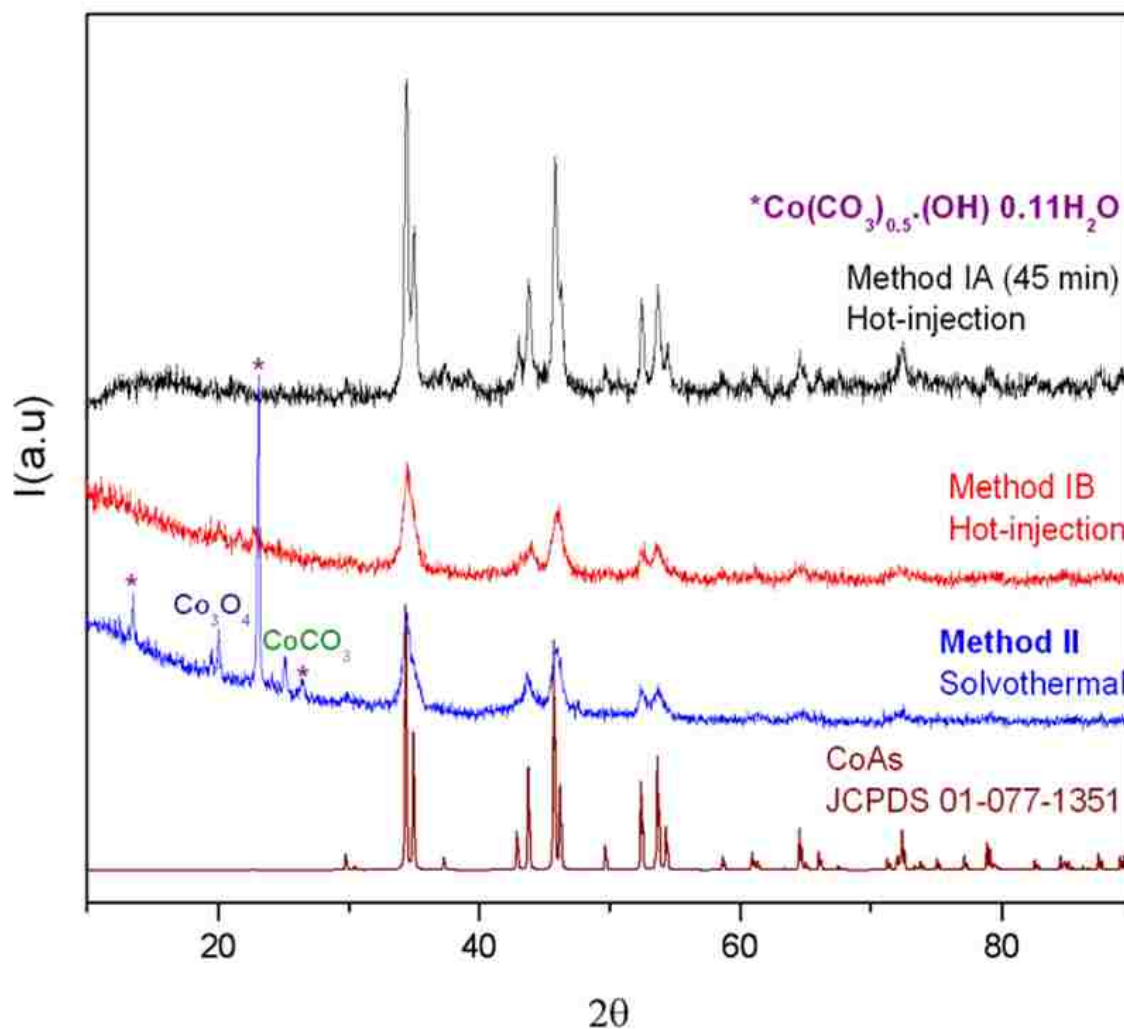
Figure1: PXRD pattern of CoAs nanostructures obtained by methods IA, IB and II. The plot at the bottom refers to standard CoAs as reported in the literature

present case may be traced back to the competing reaction pathways and incomplete conversion of the Co-based precursors. However, these impurity peaks were markedly absent in the product from methods IA and IB indicating that at high temperatures most of the carbonyl precursor gets consumed in formation of nanostructured CoAs. In the low-temperature solvothermal reaction, on the other hand, the reaction proceeds *via* the "slow decomposition" of $Co_2(CO)_8$ thereby leading to competing reaction pathways, incomplete decomposition and product impurities. The particle sizes of the CoAs

nanoparticles as determined from Scherer equation was 15 nm in accordance with the

size obtained from the electron microscopic image analysis for methods **IA** and **IB**. The

morphology of the CoAs obtained was studied through detailed microscopy techniques,

namely, SEM, TEM, and STEM. It was observed that the morphology of the products

obtained from the different synthesis methods were dissimilar. While the solution-based,

surfactant-assisted, hot-injection method produced anisotropic nanostructures (elongated

nanoparticles and short nanorods), the solvothermal method yields very uniform

nanoparticle morphology *albeit* of non-uniform composition. The evolution of

morphology of the product from method **IA** was studied by taking aliquots of the reaction

mixture at various times after injecting the Co-precursor. It was observed that within the

first 10 minutes, the product morphology was dominated by anisotropic nanorods (Figure

2A) which grew out to form short ultrathin nanowires of CoAs around 20 minute of

reaction time (Figure 2B). The nanowires formed were found to be highly crystalline

exhibiting lattice fringes corresponding to the <121> planes of CoAs which were at an

inclination (~15 degrees) to the direction of wire growth. Prolonged reaction at and after

45 min resulted in agglomeration of these nanowires and at the end of 3 hrs. the shape

deformation takes place forming huge agglomerates as shown in supplementary Fig. S-1

in the Electronic Supplementary Material (ESM). It must be noted that in spite of this

agglomeration the nanowire structure remained intact under these conditions. Previously

it was observed by the authors that using similar precursors with high carbon content as

the $Fe(CO)_5$ along with the C-rich amine resulted in core-shell nanostructures with a

carbonaceous shell.[31] In the current case however, absence of a conformal and well

defined carbon shell (Figure 2C), is presumably due to low catalytic activity of Co in

comparison to Fe. Co is less aggressive and it does not pyrolyze the carbonaceous

precursors as would be expected in the case of Fe precursor. This low reactivity of the

cobalt precursor also aids in formation of one dimensional nanostructure by controlling

the growth through limited, but steady supply of growth species in solution, allowing for
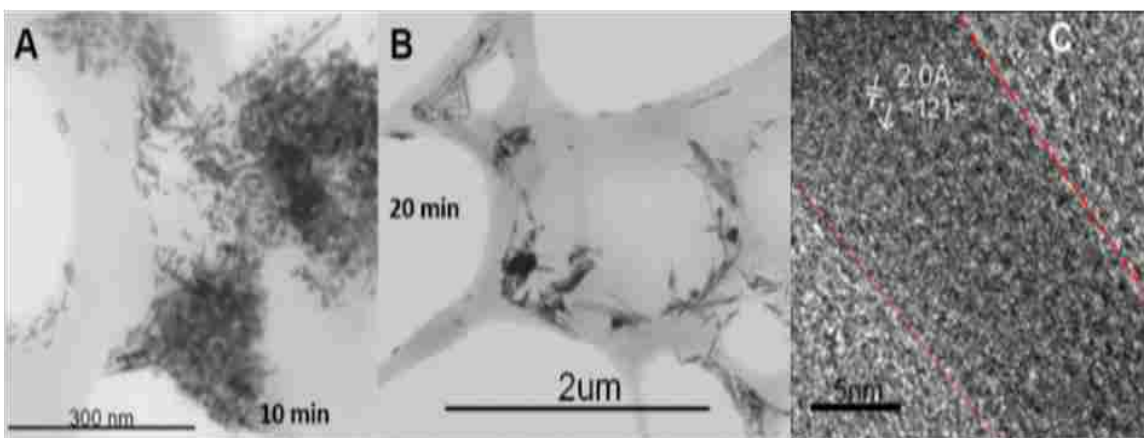
the formation of nanowires.

Figure 2. Bright Field TEM images of CoAs nanostructures obtained after (A) 10 min; (B) 20 min of reaction time by method I. (C) HRTEM image of a nanowire after 20 min reaction time

In method **IB** mixed surfactants were used in the reaction mixture where

$Co_2(CO)_8$ was dissolved in oleylamine and later injected into the hot HDA and TPA

mixture. It was noted that this method with mixed surfactants resulted in a change in

morphology of the CoAs nanostructures.

Anisotropic and elongated nanoparticles along with the spherical particles can be

seen in the products from method **IB**, (Figure 3A and inset). The nanoparticles obtained

were single crystalline exhibiting a lattice fringes corresponding to (110) spacing in

nanoparticles as shown in Figure 3B. These nanoparticles were further used for magnetic

characterizations. The lattice spacing observed for both the nanoparticle (method **IB**) and

nanorods (method **IA**) were consistent with the d spacing corresponding to the CoAs

structure as reported in JCPDS file, card number 01-077-1351. In some of these

nanostructures, a thin shell, not quite crystalline was observed.
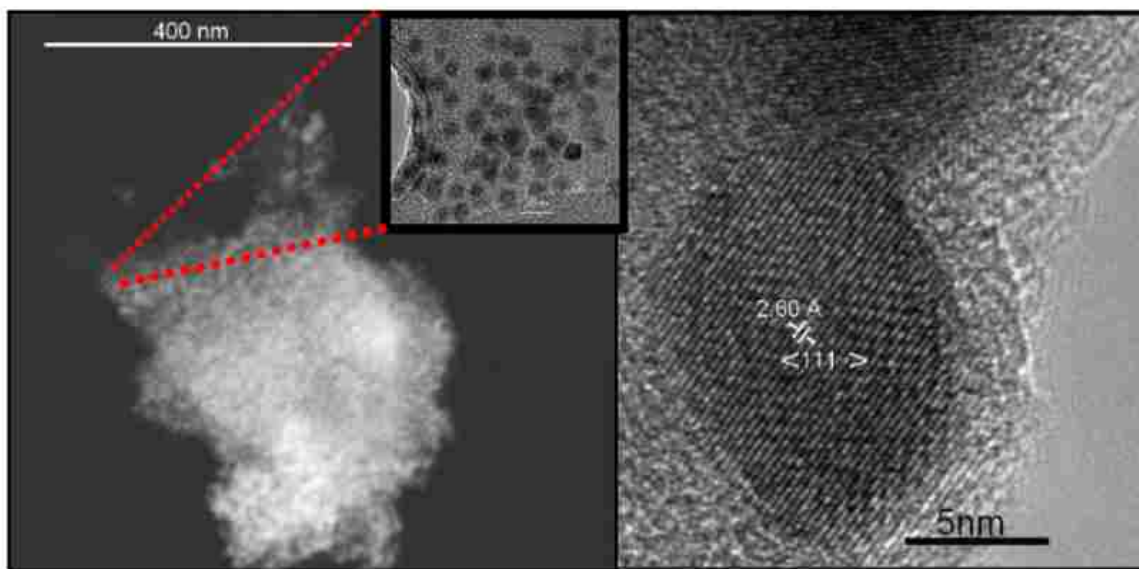
Figure 3 (A) Low magnification HAADF STEM image of CoAs nanoparticles generated by the mixed surfactant system (method IB). Inset shows the low magnification TEM. (B) HRTEM of the same nanoparticle showing crystalline nature.

The authors have also tried to make CoAs nanostructures through solvothermal

techniques, which is very amenable, low-temperature solution-based technique to make

nanostructures.[34] In addition, the solvothermal technique also provides some insights

into the evolution of product morphology with time and hence can be used as a tool for

elucidating the mechanism of growth of CoAs nanostructures under conditions of

prolonged time and relatively low temperatures. Thus, the solvothermal reaction under

method **II** provided a window for a "peek" into the evolution of CoAs nanostructures

with time. This progress is visualized in Figure 4.

In the low temperature, solvothermal method **II** the decomposition of the Co$_2$(CO)$_8$ was less drastic. Based on the elemental analysis at the end of 3 hrs. cubic nanocrystals completely composed of metallic Co were formed (see Figure 4A).
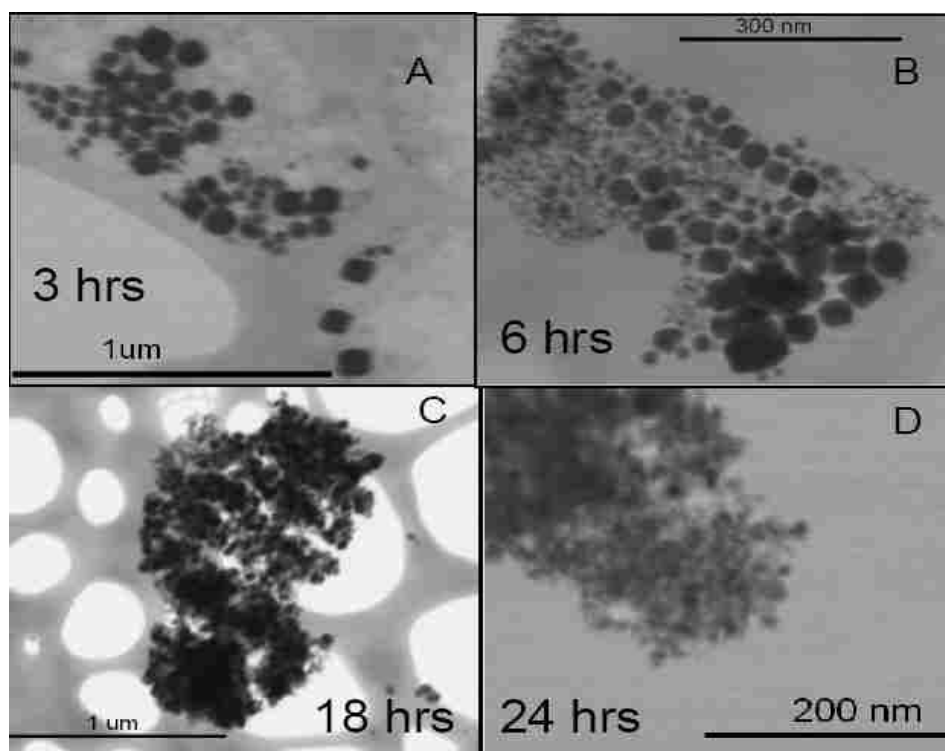
Figure 4: Morphology evolution of CoAs nanoparticles in solvothermal method II. STEM image of nanoparticles obtained at (A) 3hrs; (B) 6 hrs.; (C) 18 hrs. and 24 hrs

The nanocrystals were nearly monodisperse and well faceted. The reactivity of TPA and inclusion of As into the reactant system was very minimal at this point and EDS analysis of the product confirmed that there was almost no sign of As in the nanostructures after 3h of reaction. As the reaction proceeded further the TPA starts reacting with the metallic cobalt and started forming the smaller nanoparticles as seen is STEM image (Figure 4B) taken after 6 hrs. reaction.

Two contrasting phases appear at this point in the product. The dark contrast Co nanocrystals, also confirmed by point EDS scan, are visible along with the much small

sized CoAs nanostructures with lighter contrast. After 24 hrs. the sample exclusively

consisted of a network of ultra-small CoAs nanoparticles. It was further observed that

some of these nanoparticles had oriented to form ultra-thin one dimensional

nanostructures in several regions. However, the amounts of As in the 1-dimensional

nanostructures were lesser that that in the particles, and some of the 1-dimensional

structures were devoid of As and contained only Co and O as per the EDS analysis. This

observation was converged with the pxrd analysis and it was inferred that the

nanoparticles uniformly containing Co and As, were mostly made up of CoAs while the

1-dimensional structures were formed by the cobalt hydroxycarbonate phases. This was

in corroboration of a separate study carried out by the authors where cobalt

hydroxycarbonate nanowires were formed through solvothermal decomposition of cobalt

carbonyl in presence of an amine.[32] Based on these observations the appropriate time

for reaction was established to be in between 18-24 hrs. via the solvothermal method

(method **II**).

The elemental compositions of the nanostructures obtained from all the methods

IA, IB and **II** (after 24 h) were further estimated by EDS analysis which confirmed the

presence Co and As exclusively in 1:1 ratio. A typical EDS analysis of an ensemble of

nanoparticles and one dimensional nanostructures obtained under area scan is shown in

Figure 5A.

XPS analysis was also performed to confirm the presence of Co and As in all of

these samples. Strong peaks were observed at 778eV and 40eV for Co(2p) for As(3d),

respectively, indicating the presence of Co and As in these nanostructures (Figure 5B and

C). Based on the high purity and morphological uniformity of the nanostructures, the products from methods **IA** and **IB** were further characterized through magnetic property measurements. The magnetization (M) as a function of temperature (T) and applied magnetic field (H) were obtained for an ensemble of CoAs nanostructures loaded inside a gel cap sample holder.All the magnetization data were normalized with respect to actual Co content in the sample as estimated from atomic absorption spectroscopy (AAS) studies.
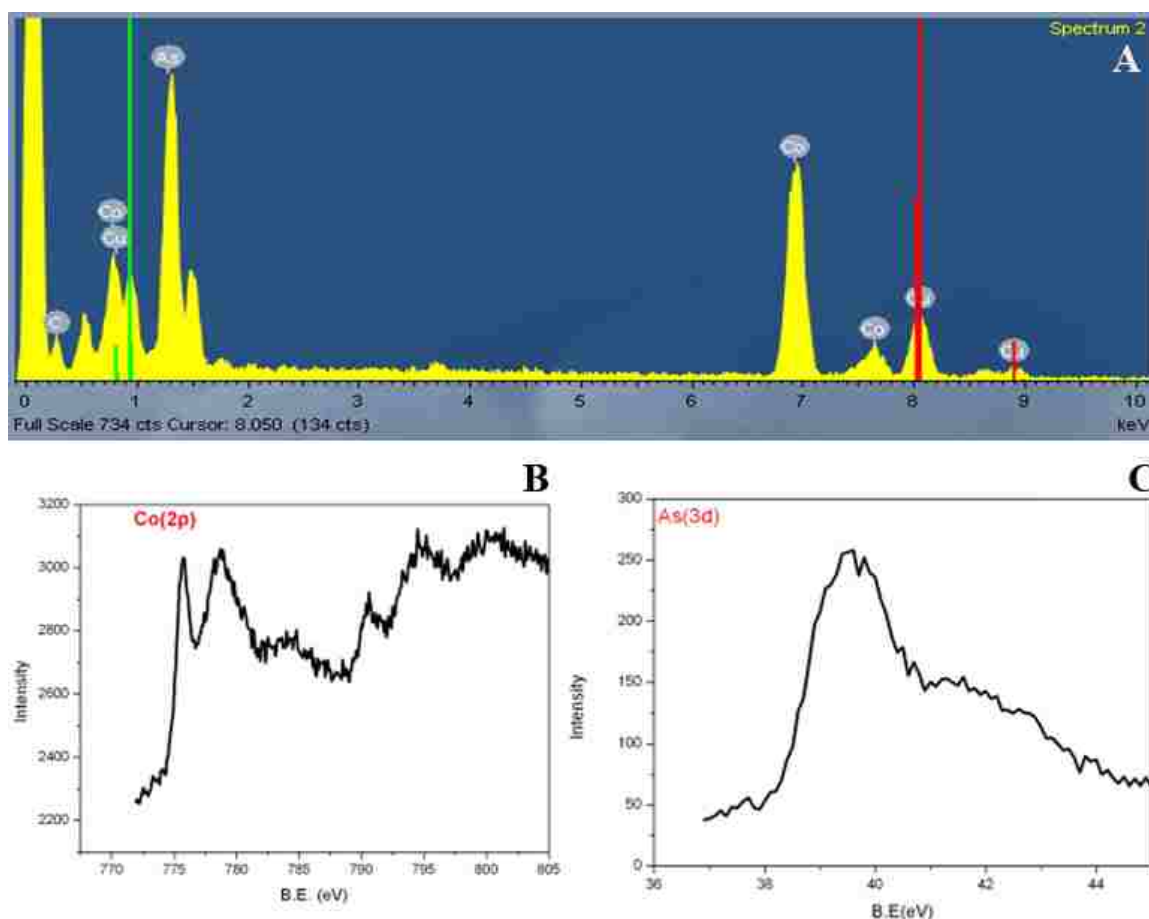

Figure 5: (A) Typical EDS spectrum of an ensemble of CoAs nanoparticles (methods IA & IB). (B), (C) XPS spectra of the nanoparticles showing peaks at 778eV and 40 eV observed for Co(2p) and As(3d), respectively

It was seen that under the influence of magnetic field of 100 Oe there was an early onset of divergence in the ZFC and FC plots for *M vs. T* curves. This is suggestive of some form of magnetic interactions within these nanoparticles including superparamagnetism. In such cases, the maxima in the ZFC plot is taken as the bloc king temperature, T_B, which represents the minimum temperature above which spontaneous fluctuation of the particle moment occurred, leading to loss of magnetic ordering.

As shown in Figure 6A the superparamagnetic T_B, was estimated to be 167 K for the CoAs nanoparticles obtained from method **IB**, which lies close to the ZFC-FC divergence temperature. The isothermal magnetization against applied field (*M vs H* hysteresis loops) as shown in Figure 6B, further outlined the superparamagnetic nature of the nanoparticles. The anhysteretic nature of isothermal magnetization against the applied field with zero coercivity and zero remanence at temperatures close to room temperature (300 K) indicates that these CoAs nanoparticles are superparamagnetic at ambient temperature. In the low temperature region, on the other hand, narrow coercivity and nature of the curves indicates that there exist signs of a ferromagnetic ordering. Thus it can be inferred that these nanoparticles are superparamagnetic above 170 K while at low temperature they exhibit ferromagnet-like ordering of the magnetic moments. At 2K the coercivity and saturation magnetization are 917 Oe and 0.0035 emu/g, respectively. The isothermal magnetization curve above the blocking temperature, T_B could be fitted with the *Langevin* equation (1) as shown in Figure 6C.

$$M = M_0 \left[\coth\left(\frac{\mu H}{k_b T}\right) - \frac{1}{\left(\frac{\mu H}{k_b T}\right)} \right] \qquad \ldots(1)$$

where M= Magnetization, M_0= saturation magnetization, H = applied magnetic field, μ=

Particle magnetic moment, T= temperature and kb = Boltzmann constant

For curve fitting purposes the isothermal magnetization *M* is plotted against *H/T* and the

Langevin equation, expressed as:

$$y = a \left[\coth(bx) - \frac{1}{(bx)} \right] \qquad \ldots (2)$$

For superparamagnetic particles, the parameters (*a* and *b*) derived from the

Langevin fit (eqs. 1 & 2) can be also used to estimate the average particle volume using

the relation (3) below, where <V> is the average particle volume, *MS* is the saturation

magnetization of bulk CoAs, and *μ* is the particle moment. (3) The parameter *b* derived

from the *Langevin* fit can be used to estimate *μ* (eq. 2). The theoretical saturation

magnetization *Ms* for CoAs is 140.25 emu/g considering 0.5 unpaired electrons per Co

(III) atom in CoAs with density 6.73 g/cc. The average particle size for CoAs

nanoparticles from method **IB** was thus calculated to be ~11 nm in diameter which is

close to the size observed in extensive HRTEM studies. The anisotropic CoAs

nanostructures obtained from method **IA** after 20 min reaction time, showed a slightly

different magnetic behavior. The isothermal magnetization curves showed a small

coercivity even at 300 K indicating some soft ferromagnetic behavior in these

nanostructures. The coercivity increases with decreasing temperature, thus at 300 K the

coercivity is in the order of 441 Oe while at 2K the coercivity is increased to 1124 Oe

(Figure 6D). It must also be noted that in both the cases (at 2K and 300K) the saturation
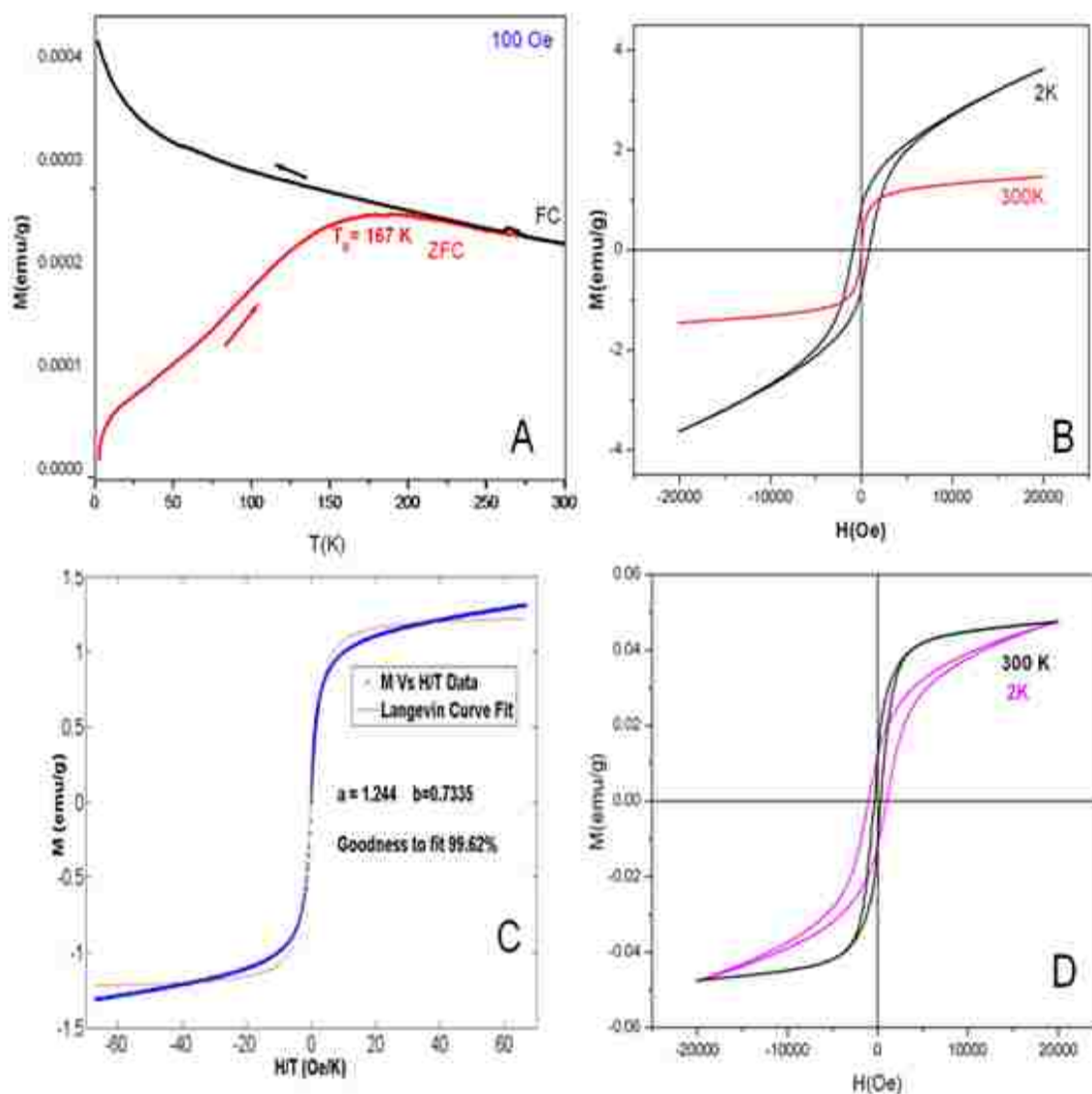
Figure 6. (A) M vs T curve at 100 Oe. (B) M vs H hysteresis loops at 2K and 300K showing ferromagnetism and superparamagnetism in sample containing CoAs nanoparticles (from Method IB). (C) Langevin fit of the anhysteretic isothermal magnetization plot at 300 K, illustrating the superparamagnetic behavior of the CoAs nanostructures obtained from method IB. (D) Isothermal magnetization plot of CoAs nanostructures obtained by method IA
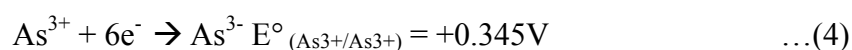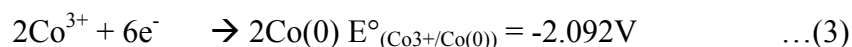
magnetization Ms was as high as 0.047emu.g-1. The *M vs T* plot for these nanostructures

shows divergence even at 300 K, and while the FC plot was featureless, the ZFC curve

showed deviation from linearity (Fig. S-2 in the Electronic Supplementary Material

(ESM)). This kind of deviation has also been observed in bulk CoAs[14] and has been attributed to thermal fluctuation leading to alteration in the spin states. In the present case, the divergence of the ZFC-FC plot along with the nature of the hysteresis loops indicate that the anisotropic CoAs nanostructures might still be superparamagnetic. However, the T_B in this case is much higher, such that at room temperature the nanostructures are already in the vicinity of an ordered state. Since the T_B in superparamagnetic particles depend on the magnetic anisotropic constant which in turn depends on the particle shape,[35,36] it has been observed previously that T_B can be increased in 1-dimensional nanorods.[37] In the present case as the anisotropy and size of the CoAs nanostructures increase, it will lead to higher magnetic anisotropy constant thereby, yielding a higher T_B. Higher T_B along with larger coercivity increases the applicability of these nanostructures making them suitable for magnetic memory storage and related devices. This is another piece of evidence that supports the conclusion that the magnetic properties of these nanostructures can be markedly different from those of the bulk CoAs.

Mechanism:

Aliquots of CoAs solution were taken out at various times to study the mechanism of formation and morphology evolution of these nanoparticles. It was hypothesized that in method **IA** cobalt carbonyl nuclei acted as seeds that are generated at high temperatures. Growth of these seeds as time progresses forms the nanorods within the first 10 min, however after 20 min they grow into elongated ultrathin nanowires with small diameters as seen in Figures 2A & B. In Method **IB**, the mixed surfactant yields more isotropic particles as has also been observed by Yang et al. when synthesizing CoP

nanoparticles.[38] Mechanistically speaking, the formation of the CoAs is similar to what we had proposed earlier for FeAs.[12] The CO ligand in the $Co_2(CO)_8$ gets displaced by the $As(C_6H_5)_3$ ligand, forming an intermediate which can be viewed as a single source precursor having Co and As in close proximity. Even though there is no direct evidence of formation of the single source precursor, its creation can be understood from basic chemistry principles of ligand exchange and HSAB theory. This type of ligand exchange is very well-known in organometallic chemistry and is guided by the Lewis basicity of the arsine ligands. The proximity of Co and As in this intermediate facilitates an internal redox reaction between the Co^{3+}/Co^0 and As^{3+}/As^{3-} couples as shown in equations (4) and (5) below. The amine in the system which is used in excess serves both as a solvation and nucleation medium and also provides a very basic medium thereby decreasing the reducing ability of the arsine compound. The importance of the basic medium is further corroborated by the fact that using an acidic surfactant like oleic acid fails to produce the CoAs nanostructures. The overall redox potential change for this reaction is +2.437 V. The positive ΔE indicates that the ΔG will be negative and this reaction is spontaneous. However, in contrast to the FeAs nanoparticles obtained by the authors, the pyrolytic properties of Co towards carbon sources is not high as compared to Fe, therefore, little to no carbon content is present in these nanoparticles.

$$2Co^{3+} + 6e^- \rightarrow 2Co(0) \; E°_{(Co3+/Co(0))} = -2.092V \qquad \ldots(3)$$

$$As^{3+} + 6e^- \rightarrow As^{3-} \; E°_{(As3+/As3+)} = +0.345V \qquad \ldots(4)$$

For the evolution of nanostructure morphology, it can be deciphered that, two antagonistic reaction mechanisms are in operation here. The reactivity of the precursors, which in turn is tuned by the choice of reaction temperature, clearly affects the morphology of the product. In the high temperature solution-based *hot injection* route, *a.k.a.* methods **IA** and **IB** nucleation occurs at high temperatures being followed by ripening and agglomeration at longer times. In the low temperature solvothermal based synthesis, on the other hand, differential dissolution and decomposition rates for both precursors have a handle on the morphology of the products at various times. As the involvement of TPA increases with the progress of the reaction under solvothermal conditions, the CoAs nanoparticles formed at lower temperature are more uniform in terms of size distribution (controlled growth). However, due to the variable involvement of TPA, it also leads to a competing reaction mechanisms, where, the cobalt carbonyl precursor under goes decomposition by itself in presence of HDA forming the cobalt hydroxycarbonate nanostructures. Hence the solvothermal route although produces better CoAs nanoparticles, yields an impure overall product composition.

6. CONCLUSION

In summary, we have successfully synthesized CoAs nanostructures through simple solution based techniques. These nanostructures were found to be superparamagnetic with fairly high T_{BS} (>167 K) and exhibit ferromagnet-like behavior below the superparamagnetic regime The coercivity observed for some of these nanoparticles are moderately high. The conversion of a Pauli paramagnet to a superparamagnet in the nanoscale is noteworthy. The rich variety of magnetic properties

exhibited by the cobalt-based systems have made these solids very captivating for the materials research community since they offer valuable insight into understanding the structure-property correlation. Through this study the authors have provided a comprehensive guide on controlling the product morphology and composition by subtle variation of the reaction parameters. While higher temperature gives pure phase CoAs, the product morphology can be varied from nanorods to nanoparticles by using either simple amine surfactant or co-surfactant respectively. The lower temperature solvothermal method on the other hand yields smaller uniformly sized nanoparticles and thin nanowires, however, the product composition is compromised yielding mixture of cobalt arsenide and carbonate based nanostructures. From these observations it is apparent that even with the same precursors and under similar reaction conditions, it is possible to tune the product morphology through subtle variation of the experimental parameters. This kind of morphology control can be potentially useful for the magnetic nanostructures which have possible applications as spin injection systems in nano-semiconductors for facilitating spintronics.

7. REFERENCES

[1]   Tablero, C.; Garcia, A. J.; Fernandez, J. J.; Palacios, P.; Wahnon, P., First Principles Characterization of Direct Transitions for High Efficiency New Photovoltaic Materials. *Comput. Mater. Sci.* **2003,** *27*, 58-64.

[2]   Brandt, M. S.; Goennenwein, S. T. B.; Graf, T.; Huebl, H.; Lauterbach, S.; Stutzmann, M., Spin-Dependent Transport in Elemental and Compound Semiconductors and Nanostructures. *Phys. Status Solidi C* **2004,** *1*, 2056-2078.

[3]   Mohney, S. E., Condensed Phase Equilibria in the Metal-In-P systems. *J. Electron. Mater.* **1998,** *27*, 24-29.

[4]   Dobrowolski, W.; Kossut, J.; Story, T., II-VI and IV-VI Diluted Magnetic Semiconductors-New Bulk Materials and Low-Dimensional Quantum Structures. *Handbook. Magn. Mater.* **2003,** *15*, 289-377.

[5]   Oyama, S. T., Novel Catalysts for Advanced Hydroprocessing: Transition Metal Phosphides. *J. Catal.* **2003,** *216*, 343-352.

[6]   Wang, X. C.; Liu, Q. Q.; Lv, Y. X.; Gao, W. B.; Yang, L. X.; Yu, R. C.; Li, F. Y.; Jin, C. Q., The Superconductivity at 18 K in LiFeAs system. *Solid State commun.* **2008,** *148*, 538-540.

[7]   Kohama, Y.; Kamihara, Y.; Kawaji, H.; Atake, T.; Hirano, M.; Hosono, H., Possible Unconventional Superconductivity in Iron-based Layered Compound LaFePO: study of heat capacity. *J. Phys. Soc. Jpn.* **2008,** *77*, 094715/1-094715/4.

[8]   Johrendt, D.; Hosono, H.; Hoffmann, R.-D.; Pöttgen, R., Structural Chemistry of Superconducting Pnictides and Pnictide Oxides with Layered Sructures. *Z. Kristallogr.* **2011,** *226*, 435-446.

[9]   Bichat, M. P.; Gillot, F.; Monconduit, L.; Favier, F.; Morcrette, M.; Lemoigno, F.; Doublet, M. L., Redox-Induced Structural Change in Anode Materials Based on Tetrahedral (MPn4)x- Transition Metal Pnictides. *Chem. Mater.* **2004,** *16*, 1002-1013.

[10]   Craford, G. M. Properties and electroluminescence of the gallium arsenide phosphide (GaAs1-xPx) ternary system. *Progr. Solid State Chem.* **1973**, *8*, 127-165.

[11]   Queisser, H. J. Optical evaluation of radiative recombination in II-V compound semiconductors. *Czech. J. Phys. B* **1980**, *30*, 365-374.

[12] Wang, J.-L.; Yang, Q.; Zhou, J.; Sun, K.-W.; Zhang, Z.-D.; Feng, X.-M.; Li, T.-W., Magnetic Fe2P nanowires and Fe2P@C core@shell nanocables. *Nano Res.* **2010,** *3*, 211-221. Susanthri C. Perera, G. T., Lowell E. Wenger, Stephanie L.Brock, Synthesis of MnP Nanocrystals by Treatment of Metal Carbonyl Complexes. *J. Am. Chem. Soc.* **2003,** *125,* 13960-13961.

[13] Desai, P.; Song, K.; Koza, J.; Pariti, A.; Nath, M., Soft-Chemical Synthetic Route to Superparamagnetic FeAs@C Core-Shell Nanoparticles Exhibiting High Blocking Temperature. *Chem. Mater.* **2013,** *25*, 1510-1518.

[14] Khosravizadeh, S.; Hashemifar, S. J.; Akbarzadeh, H. Novel description of bonding and magnetism in 3d transition metal arsenides. *J. Appl. Phys.* **2013**, *114*, 113906/1 – 113906/4.

[15] Selte, K.; Kjekshus, A., Structural and Magnetic Properties of CoAs. *Acta. Chem. Scand.* **1971,** (25). 14.

[16] Siegrist, T.; Hulliger, F., High-temperature Behavior of Cobalt Arsenide (CoAs2) and Cobalt antimonide (CoSb2). *J. Solid State Chem.* **1986,** *63*, 23-30.

[17] Kim, S. H.; Lee, J. T.; Kim, M. S.; Heo, S. Y. Dispersion Adjuvant for Metal Nanoparticles and Metal Nanoink comprising the Dispersed Metal Nanoparticles. US20070244220A1, 2007.

[18] Selte, K.; Kjekshus, A., Phase Transitions between Manganese Phosphide and Nickel Arsenide type structures. *Acta Chem. Scand.* **1973,** *27*, 3195-206.

[19] Ludge, K.; Vogt, P.; Richter, W.; Fimland, B.-O.; Braun, W.; Esser, N. Metallic nanostructures on Co/GaAs(001) (4x2) surfaces. *J. Vac. Sci. Technol. B* **2004**, *22*, 2008. Farrell, H. H.; LaViolette, R. A.; Schultz, B. D.; Ludge, K.; Palmstrom, C. J., Self-assembled CoAs nanostructures. *J. Vac. Sci. Technol., B* **2003,** *21*, 1760-1764.

[20] Raj, K.; Moskowitz, R., Commercial Applications of Ferrofluids. *J. Magn. Magn. Mater.* **1990,** *85*, 233-45.

[21] Kharisov, B. I.; Dias, H. V. R.; Kharissova, O. V.; Jimenez-Perez, V. M.; Olvera, P. B.; Munoz, F. B., Iron-containing Nanomaterials: Synthesis, Properties, and Environmental applications. *RSC Adv.* **2012,** *2*, 9325-9358.

[22] Zhang, L.; Webster, T. J., Nanotechnology and Nanomaterials: Promises for Improved Tissue Regeneration. *Nano Today* **2009**, *4*, 66-80.

[23]   Jun, Y.-w.; Seo, J.-w.; Cheon, J., Nanoscaling Laws of Magnetic Nanoparticles and Their Applicabilities in Biomedical Sciences. *Acc. Chem. Res.* **2008,** *41*, 179-189.

[24]   Teng, X.; Han, W.-Q.; Ku, W.; Hucker, M., Synthesis of Ultrathin Palladium and Platinum Nanowires and a Study of their Magnetic Properties. *Angew. Chem., Int. Ed.* **2008,** *47*, 2055-2058.

[25]   Schmidt, G.; Ferrand, D.; Molenkamp, L. W.; Filip, A. T.; van, W. B. J., Fundamental Obstacle for Electrical Spin injection from a Ferromagnetic Metal into a Diffusive Semiconductor. *Phys. Rev. B: Condens. Matter Mater. Phys.* **2000,** *62*, R4790-R4793.

[26]   Parkin, I. P., Solid State Metathesis Reaction for Metal Borides, Silicides, Pnictides and Chalcogenides: Ionic or Elemental Pathways. *Chem. Soc. Rev.* **1996,** *25*, 199-207.

[27]   Remen, T. F.; Nemoitin, M. A.; Vaisburd, S. E., Synthesis of Iron, Cobalt, and Nickel Monoarsenides. *Tr. Proekt. Nauch.-Issled. Inst. Gipronikel (Gos. Inst. Proekt. Predpr. Nikelevoi Prom.)* **1968,** *No. 38*, 60-2.

[28]   Hsu, C. C.; Jin, G. L.; Ho, J.; Chen, W. D., Interfacial Reactions in the Cobalt/silicon/gallium arsenide and Si/Co/GaAs systems. *J. Vac. Sci. Technol., A.* **1992,** *10*, 1020-1028.

[29]   Lu, J.; Xie, Y.; Jiang, X.; He, W.; Du, G., A Safe Sonochemical Route to Iron, Cobalt and Nickel Monoarsenides. *J. Mater. Chem.* **2001,** *11*, 3281-3284.

[30]   Klingan, F.-R.; Miehr, A.; Fischer, R. A.; Herrmann, W. A., Thin Films of CoAs from Low-Temperature Metalorganic Chemical Vapor Deposition of a Novel Single-Source Precursor compound. *Appl. Phys. Lett.* **1995,** *67*, 822-4.

[31]   Henkes, A. E.; Schaak, R. E., Trioctylphosphine: A General Phosphorus Source for the Low-Temperature Conversion of Metals into Metal Phosphides. *Chem. Mater.* **2007,** *19*, 4234-4242.

[32]   Wang, Q.; Sun, Q.; Jena, P., Ferromagnetism in Mn-Doped GaN Nanowires. *Phys. Rev. Lett.* **2005,** *95*, 167202.

[33]   Desai P, Nath. M., Hydrothermal Synthesis of Co(CO3)0.5. (OH) 0.11 H2O Nanowires and conversion to Anti-Ferromagnetic Co3O4 Nanowires. (Unpublished results)

[34]   Patterson, A. L., The Scherrer Formula for X-Ray Particle Size Determination. *Phys. Rev.* **1939,** *56*, 978-982.

[35]   Cushing, B. L.; Kolesnichenko, V. L.;O'Connor, C. J.,Recent Advances in the Liquid-Phase Syntheses of Inorganic Nanoparticles, *Chem. Rev.* **2004**, *104*, 3893−3946.

[36]   Antoniak, C.; Lindner, J.; Farle, M., Magnetic Anisotropy and its Temperature Dependence in iron-rich FexPt1-x Nanoparticles. *Europhys. Lett.* **2005,** *70.* 10485-10489.

[37]   Cowburn, R.P., Property Variation with Shape in Magnetic Nanoelements *J. Phys. D: Appl. Phys.* **2000,** *33,* R1-R16.

[38]   Liying, Z.; Yafei, Z. , Fabrication and Magnetic Properties of Fe3O4 nanowire Arrays in Different Diameters. *J. Magn. Magn. Mater.***2009***,321,*L15-L20

[39]   Yang Li; Malik, M. A.; O'Brien, P., Synthesis of Single-Crystalline CoP Nanowires by a One-Pot Metal-Organic. *J. Am. Chem. Soc.* **2005,** *127*,16020-16021

8. ELECTRONIC SUPPLEMENTRY MATERIAL

Synthesis and Magnetic Properties of Superparamagnetic CoAs Nanostructures

Prachi Desai [1], Akshay Pariti [2], and Manashi Nath[1](✉)

[1]Department of Chemistry, Missouri University of Science & Technology, Rolla, MO 65409

[2] Department of Chemical and Biochemical Engineering, Missouri University of Science & Technology, Rolla, MO 65409
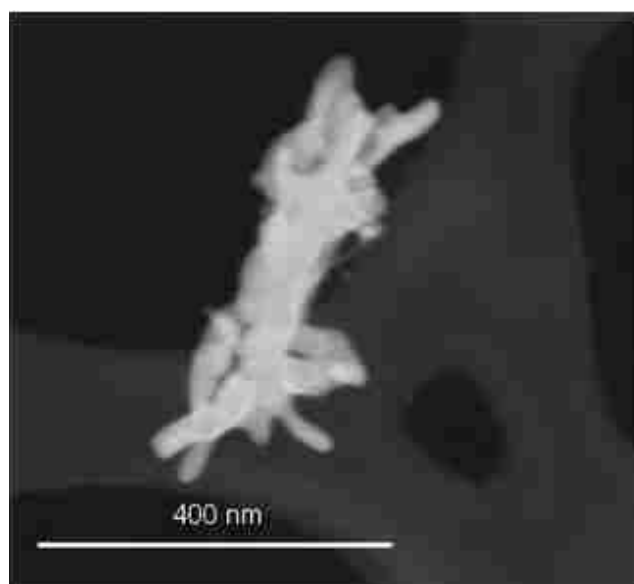
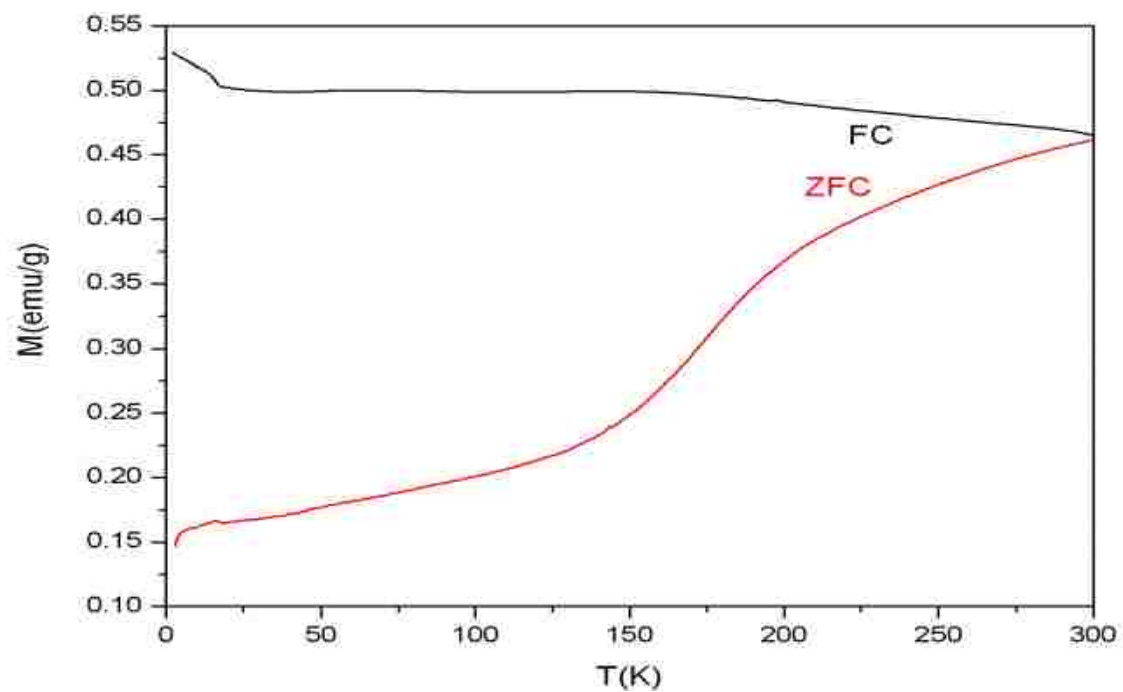Fig S-1: Agglomerated Nanowires after 180 min by method IA

Fig S2: Magnetization against temperature plot for CoAs nanowires obtained by method IA

III. A GENERALIZED PROTOCOL FOR SYNTHESIS OF NANOSTRUCTURED TRANSITION METAL ARSENIDES

P. Desai, M. Nath[*]

Department of Chemistry, Missouri university of Science and Technology, Rolla, MO 65409.

Email: nathm@mst.edu

This article illustrates a novel route for the synthesis of nanostructured transition metal arsenides including those of FeAs, CoAs, MnAs and CrAs through a generalized protocol. The key feature of the method is the use of one step *hot –injection* and the clever use of a combination of precursors which are low melting and highly reactive such as metal carbonyls and triphenylarsine in a solvent-less setup. This method also facilitates the formation of one dimensional nanostructures as we move across the periodic table from CrAs to CoAs. The chemical basis of this reaction is a simple redox chemistry between the transition metal [oxidized from elemental state to Tm^{3+}] in lieu reduction of As^{3+} to As^{3-}. The nanostructures can serve as model systems for the exploration of various magnetic properties, their applications and can also function as starting materials for the pnictide based nano-superconductors.

Keywords: Transition metal arsenides, nanoparticles, hexadecylamine, Triphenylarsine.

INTRODUCTION

Metal pnictides are an important class of compounds exhibiting interesting electronic, semiconducting, optical and magnetic properties.[1] For the last decade a major emphasis for pnictides was laid on main groups metal phosphides and arsenides like InP, GaAs, InAs etc. These have taken a center stage as a potential replacement to Si in applications related to electronics, optoelectronics and photovoltaics. Much recently, as a subgroup binary transition metal-pnictides owing to their structures and magnetic properties have gained importance as semiconductors,[2, 3], anode materials for Li-ion batteries [4] and novel magnetic materials [5]. Amongst the arsenides, CrAs is a half metallic ferromagnet with a band gap of 1.8 eV [6] while MnAs also shows ferromagnetic interactions [7] Such ferromagnetic semiconductors are important in the field of spintronics. MnAs is also known to have a large electromotive force that can be used to convert magnetic energy to electrical energy when used as components of circuits.[7] FeAs is a helimagnet [8] with helical arrangement of spins associated with Fe atoms which has an overall anti-ferromagnetic ordering below 77K. It was found that the ferromagnetic order is more stable than the anti-ferromagnetic state for VAs, CrAs, and MnAs, the greatest energy gain being predicted for CrAs[9]The mixed arsenides like MnAs$_{(1-x)}$P$_x$, [10] are also useful as thermoelectrics. Apart from the binaries, other mixed metal phosphides containing two or more transition metals have been used to improve the fire safety properties of polypropylene.[11] Other applications also include their usage as important catalysts for hydrodenitrogenation (HDN) [12] hydrodesulfurization(HDS)[13 and hydroprocessing [14] of specialty chemicals [12, 13, 14, 15] especially with transition metal phosphides. Metal phosphides nanoparticles (Ni$_2$P) have been used as

electrocatalysts for hydrogen evolution reactions.[16] The role of enhanced surface area with nanostructuring, and exposed crystal faces has increased their effectiveness in catalysis. In spite of the plethora useful applications, there has been a lack of lacking a rationalized synthesis protocol for the transition metal arsenides. We have attempted to design a generalized facile synthesis route to the transition metal arsenide based on our previous report on the synthesis of superparamagnetic FeAs nanoparticles.[17] The work done in the area of 3d phosphides has provided the motivation for this work on transition metal arsenides.[18, 19,20] The crystal structures of binary transition metal arsenides are 3D networks containing the EAs_6 [E = transition metal] octahedra or trigonal prisms. They crystallize in 5 structure types: face-centered cubic NaCl-type (for ScAs)[21]; hexagonal TiP-type (for TiAs[21] and HfAs[22]); orthorhombic MnP-type (for VAs[23], CrAs,[24] FeAs,[25] CoAs[23] and RuAs[23]); hexagonal NiAs type (for MnAs and NiAs)[26]; tetragonal NbAs-type structure (for NbAs and TaAs)[27]. Apart from the interesting magnetic properties associated with them, the arsenides have also gained attention following the recent discovery of Fe- based superconductors containing both FeP/FeAs tetrahedral layers with intercalating layers of oxides / alkali metals /alkaline earths. [28] It was observed that magnetic ordering plays an important role for of these superconducting transition metal pnictides. Superconductivity was typically observed at the vicinity of the magnetically ordered phase and tuning the magnetic properties through doping or introducing lattice deformities was found to have a profound effect on the superconductivity. Transition metal pnictides nanoparticles are thereby interesting owing to the interesting magnetic properties which can offer valuable insight into the structure – property relationship.

In the past, nanostructuring of transition metal arsenide have been explored before by Lu et. al.[29] who have made FeAs nanoparticles sonochemically from transition metal chlorides and arsenic while Zhang and coworkers[30] made FeAs nanocrystals from reductive recombination of $FeCl_3$ and $AsCl_3$ at 150-180 °C. Pnictate precursors have been previously used to synthesis these pnictides however only bulk forms were recovered by such a process. [31] However, these reports did not provide any details about the magnetic nature of the EAs nanoparticles and also the morphology was very ill-defined. All of these methods involved toxic precursors or solvents. Since sustainability and green synthesis of nanomaterials has been one of the greatest concerns amongst researchers these days, there's a need for developing synthesis protocols for these functional nanostructures using less toxic reagents. To this cause, regulated/ minimal usage of hydrocarbon based solvents in synthetic methods has been pushed as a way to synthesize "green" nanoparticles. We have devised one such approach which does not involve any solvent at the time of synthesis. Rather it takes advantage of the reducing capability of the capping agent and the basic environment at the synthesis conditions. This approach is a proof that solvents in much nanoparticle synthesis may be redundant and can be totally eliminated if clever reaction precursors and conditions are applied. Hence, with this method reported in this article we can move one step closer to the sustainability cause for synthesis methods which involve solvent based nanoparticle synthesis approaches. This was the key motivation behind developing this process. It should be noted however, that minimal solvents are required during the purification step due to the magnetic nature of these nanostructured transition metal arsenides.

EXPERIMENTAL

Synthesis: The synthesis of EAs nanoparticles was carried out in a N_2 filled glove box containing less than 1 ppm of O_2. 1 mM of triphenylarsine (TPA) and 5 mM of HDA was weighed and added to a three-neck round bottom flask equipped with a magnetic stir bar and air condenser. The mixture was slowly heated to 325° C during which the reactants slowly melted and the colorless mixture refluxed in its own vapors. 1mM of $Fe(CO)_5$ / $Co_2(CO)_8$/ $Mn(CO)_5$ / $Cr(CO)_6$ maintained at room temperature was then injected using a syringe pump or as solid into the hot HDA+TPA mixture. Upon addition of the carbonyl precursor the solution immediately turned blackish with rapid evolution of gases. After 5 min the gases subsided and the black solution was left to reflux for variable length of time. After desired refluxing time, the heating was stopped and reaction was cooled down to room temperature.

Purification: The as-synthesized product, by virtue of its attraction to a magnet, was purified through simple magnetic filtration. The isolated product was washed at least 3-4 times with ethanol and hexane using ultra-sonication to remove excess HDA and any unreacted precursors. The powder collected from the bottom of the centrifuge tube was dried in air. The yield of the product was in excess of 90% compared to the amount of $Fe(CO)_5$ / $Co_2(CO)_8$/ $Mn(CO)_5$ taken as the precursor. The product was characterized further through powder X-ray diffraction (pxrd), scanning and transmission electron microscopy (SEM and TEM respectively), XPS, EDAX. It should be noted here that of all the arsenides prepared by this methods, only the CrAs nanoparticles did not yield a solid precipitate. The product containing Cr-arsenide formed a black suspension which remained as a stable dispersion.

Characterization: *PXRD*: The as-synthesized powder was finely ground and used for powder X-ray diffraction (PXRD), which was carried out on a Philips Xpert diffractometer scanning from 5° to 90°. *TEM:* A Tecnai F20 microscope operating at 200 kV was used for transmission electron microscopy (TEM) while a dual beam Helios FIB microscope was used for scanning electron microscopy (SEM) and STEM studies. Samples for TEM and STEM were made by dispersing as-synthesized arsenide nanoparticles in ethanol by ultra-sonication for 30 min and adding drops from the diluted dispersion on a carbon coated 200 mesh Cu TEM grid followed by drying in air.

RESULTS AND DISCUSSIONS

The synthesis was carried out by a facile *hot- injection* redox reaction under inert conditions. Figure1 shows the general scheme of the reaction protocol. In here, the
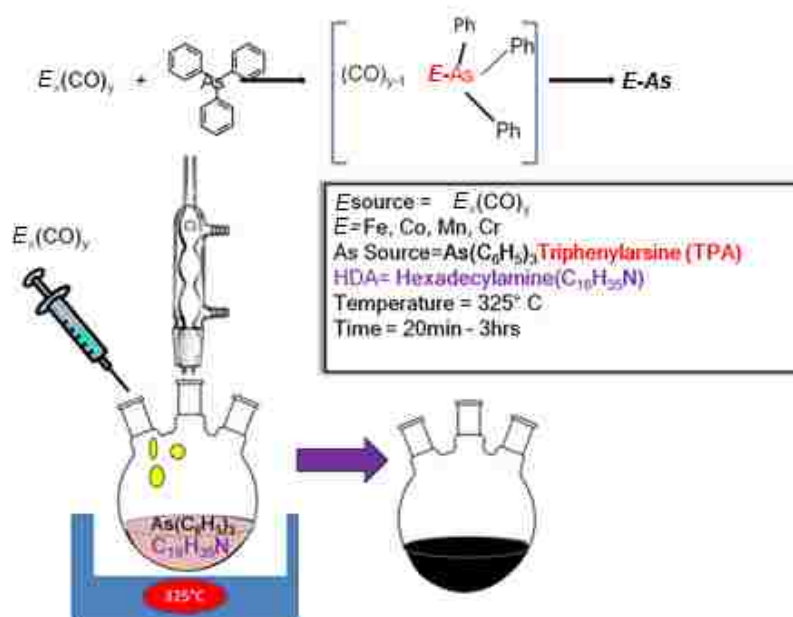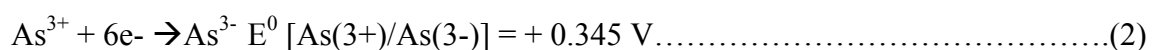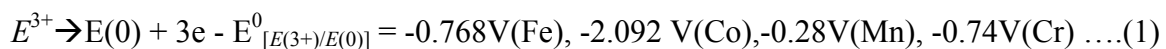

Figure1: A schematic describing the synthesis protocol for the *E*As nanostructures through hot-injection technique

central idea was performing the *hot-injection* of the transition metal carbonyl in the presence of an arsine precursor. Arsenic precursor by itself was not sufficient to generate nanomorphologies. It is known that very commonly used surfactant, hexadecylamine (HDA) containing a C-16 chain melts at 45 ºC and Triphenylarsine (TPA) melted at around 60 ºC. The mixture of TPA and HDA was heated to high temperatures. Under these conditions the melt behaved as a solvent by itself. The concept is similar to the flux-mediated synthesis conditions for solid state reactions where a low-melting reagent is used as a flux to facilitate reactant diffusion and intimate mixing. After conducting several blank experiments without the metal precursors an appropriate temperature range was selected for injecting the metal carbonyls. This temperature was 325 ºC and was based on the fact that at this temperature the HDA + TPA mixture remained colorless and had just started to reflux vigorously. Various stoichiometric combinations ranging from 1:1 to 1:10 TPA:HDA were tried. The appropriate combination to yield nanostructures was chosen as a midpoint 1:5. Excess HDA caused excessive froth buildup whereas 1:1 did not leave enough liquid phases for the metal carbonyls to react. When the TPA+HDA mixture was at the appropriate refluxing temperature, metal carbonyl was injected into the hot reaction mixture. It was also observed that the precursor oxidation state was important in the sense that it must be in the elemental or 0 oxidation state to guide the appropriate redox chemistry (Table 1). This was verified by many reactions involving precursors other than the carbonyls like acetylacetonates, halides etc. When iron acetylacetonte was used as a metal source it resulted in impure products with Fe_2As and $FeAs_2$ as impurities. Metal halides like $FeCl_3$, $CoCl_2$, $MnCl_2$ on the other hand, were very sluggish in reacting and the reactions never proceeded to completion.

Mechanistically it can be expected that during initial stage of the reaction, ligand exchange takes place as soon as $E_x(CO)_y$ is added into the mixture of TPA and HDA as seen in figure 1, the CO ligand is displaced by the $As(C_6H_5)_3$ to form an intermediate complex $[(C_6H_5)_3As-E(CO)_{y-1}]$ with generation of free CO. This kind of ligand exchange with phosphines and arsines is very favorable since they act as electron donating Lewis bases. The intermediate formed, in principle, can behave as a single source precursor for both E and As. It brings the As and E close enough as would be expected than the traditional solid state methods of EAs synthesis. Proximity of As and E in this intermediate renders the possibility of an internal redox between As and E. The driving force is the difference in the reduction potentials of E^{3+}/E and As^{3+}/As^{3-} couples as shown in Eqs.1 and 2 respectively. The presence of amine (HDA) in the mixture makes the reaction medium slightly basic, thereby decreasing the reducing ability of the arsine compound. Since the As^{3+}/As^{3-} has a more positive reduction potential, it acts as a stronger oxidizing agent thereby oxidizing $E(0)$ to E^{3+} while itself being reduced to As^{3-}.

Temperature also plays a definitive role in this ligand exchange and internal redox reactions, since it was observed that at low temperature, the product contained a mixture of FeAs and $FeAs_2$ (which contains Fe in the +2 oxidation state). The lower valent arsenides were also obtained as impurities (e.g. $CoAs_2$ for the CoAs system) under low reaction temperature. The reactions can be summarized as follows:

$E^{3+} \rightarrow E(0) + 3e - E^0_{[E(3+)/E(0)]} = $ -0.768V(Fe), -2.092 V(Co),-0.28V(Mn), -0.74V(Cr) ....(1)

$As^{3+} + 6e- \rightarrow As^{3-}$ E^0 [As(3+)/As(3-)] = + 0.345 V...(2)

Where, Tm = Fe, Co, Mn, Cr, respectively.

Figure 2(A) shows the PXRD pattern of the FeAs, nanoparticles along with its comparison with the standard pattern reported in JCPDS file card number 01-076-0458. These nanoparticles were found to be highly crystalline and as-synthesized nanoparticles crystallized in the MnP structure-type. The morphology of the product was studied in details through STEM and TEM. TEM image in figure 2(B) shows the high degree of monodispersity of the as-synthesized FeAs nanoparticles. The diameter of these
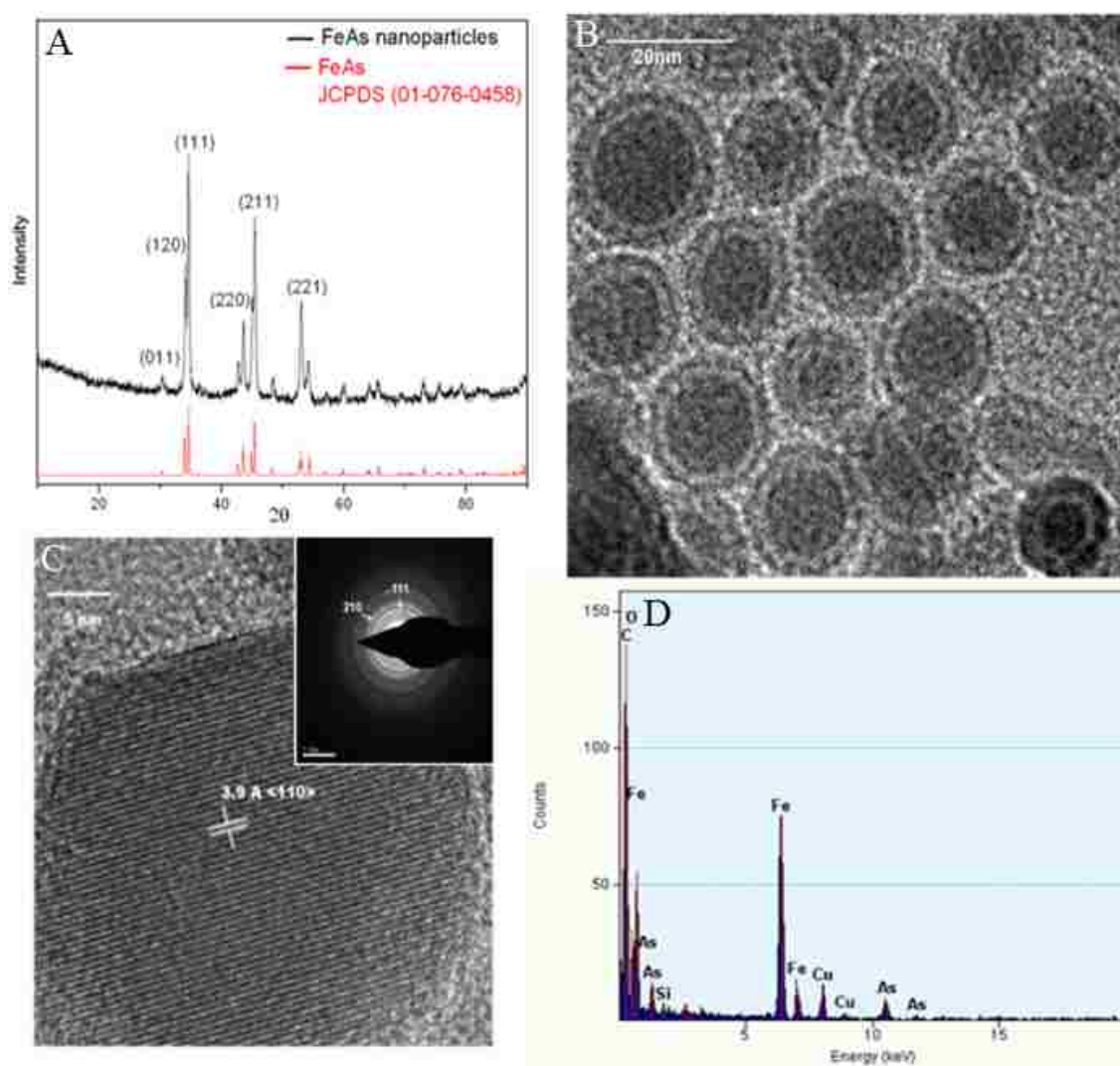

Figure 2: (A) PXRD pattern of FeAs nanoparticles.(B) STEM image of FeAs nanoparticles.(C) HRTEM image of a single nanoparticle.(D) EDS analysis of a nanoparticle

nanoparticles was calculated from Scherer equation to be 13 nm. Figure2(C) is the HRTEM of a single FeAs nanoparticle and the inset shows the corresponding diffraction pattern suggesting polycrystalline nature. Figure2 (D) shows the corresponding EDS pattern confirming As and Fe presence in the ratio 1:1within the nanoparticle. As was apparent from the TEM images, the particles contained a core and a shell. The shell was found to consist mainly of carbon while the core contained Fe and As as confirmed by EDS point and line scans. No other phase of FeAs or any other impurity was detected. The size of the nanoparticles was dependent on the refluxing time. When the temperature of $Fe(CO)_5$ addition was reduced to 250°C a mixture of $FeAs_2$ and FeAs was obtained.

Figure 3(A), to (D) shows PXRD, STEM, TEM and XPS image images respectively of CoAs nanoparticles. The PXRD pattern suggests that pure phase CoAs nanoparticles (JCPDS-01-077-1351) were formed by this method. It was noted that this method in the case of CoAs yielded one dimensional nanostructures within the first 20 min of introducing the $Co_2(CO)_8$ Into the reaction mixture. The propensity to form nanowires was seen to be much higher with CoAs. For obtaining the CoAs nanoparticles the reaction conditions were further altered by injecting a solution of Co_2CO_8 mixed with oleylamine. This altered the phase and solubility of the precursor resulting into nanoparticles as seen in figure 3(B) whereas figure 3(C) shows the nanowires morphology obtained without addition of oleylamine.
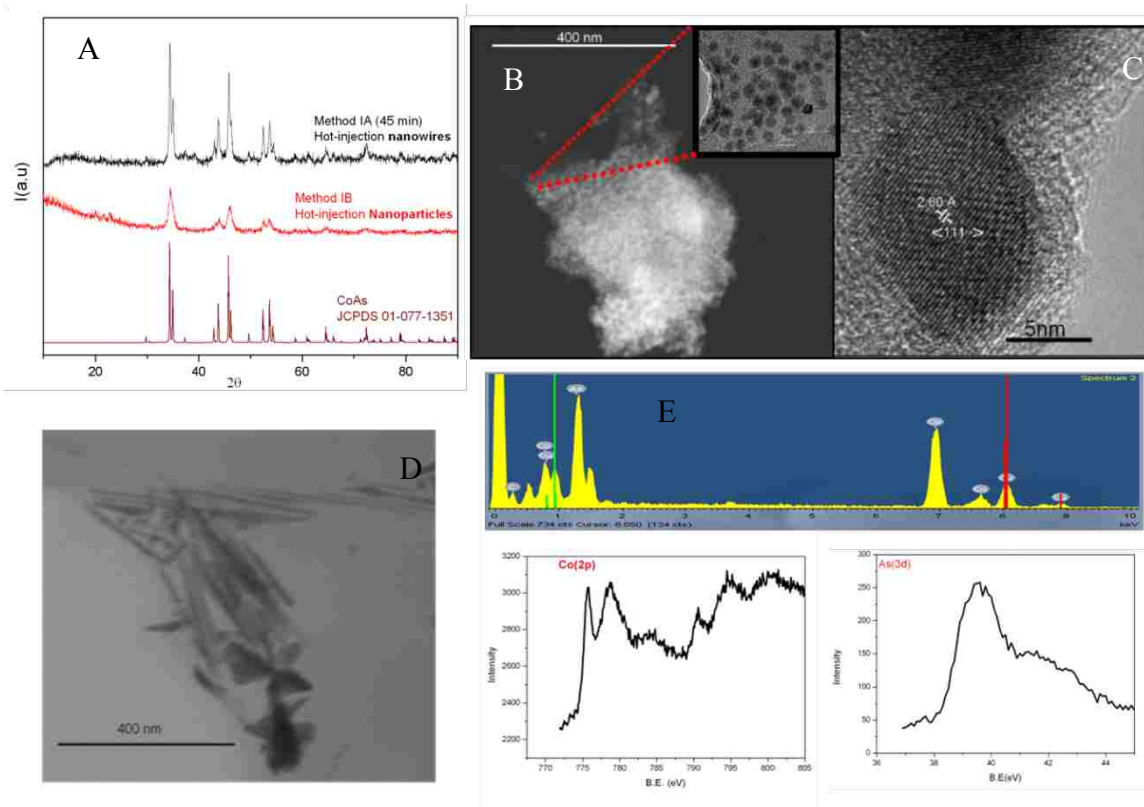
Figure 3: (A) PXRD of CoAs nanostructures (B)Low magnification TEM image (C) HRTEM of a single nanoparticle of CoAs (D) Low magnification STEM of CoAs one dimensional nanostructures(E) EDS spectra and XPS of Co and As.

Figure 4 shows the PXRD for MnAs nanoparticles and the comparison with reported MnAs pattern (JCPDS- 0072-1065). It should be noted that there were few unidentified peaks corresponding to impurities observed in the pxrd pattern. Inset in the figure shows the STEM image. The size range of the MnAs nanoparticles was considerably smaller that the FeAs and CoAs systems. Synthesis and magnetic properties of MnAs has been previously explored by Brock et al. MnAs nanoparticles have magnetostructural properties and are known to have high electromotive force.
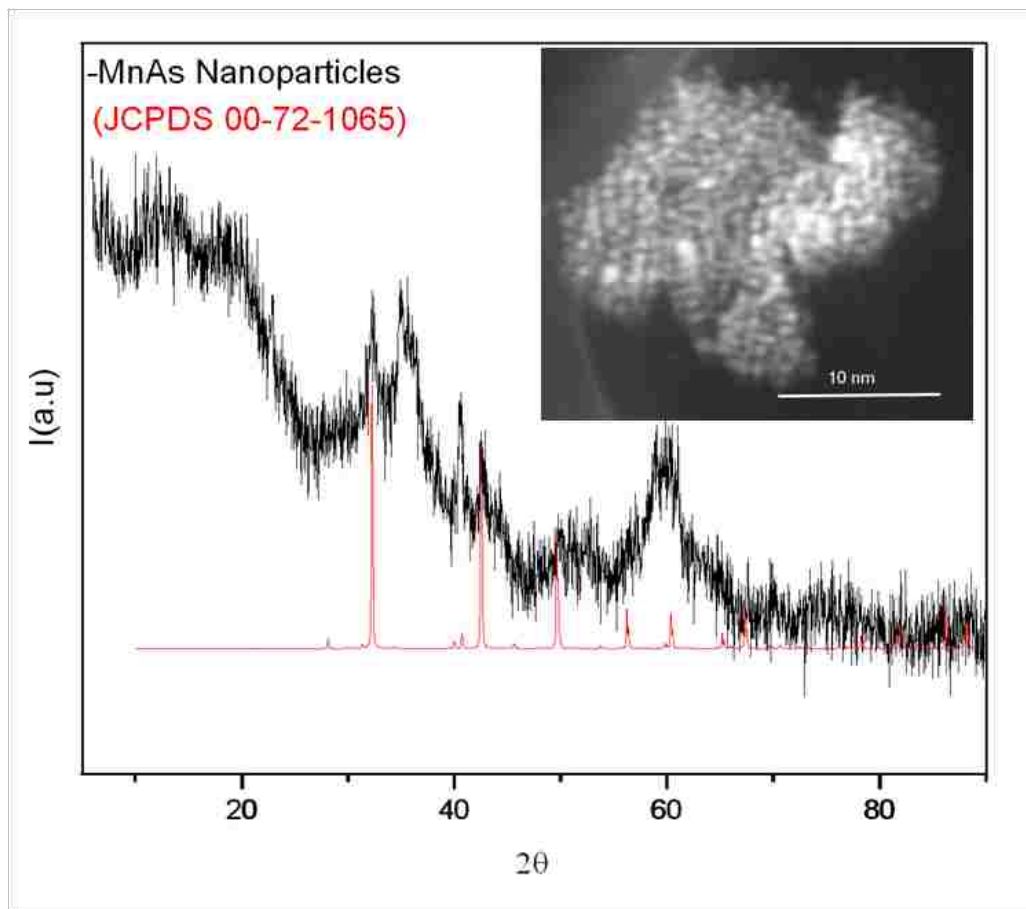
Figure 4: PXRD pattern of MnAs (inset shows STEM image of nanoparticles).

CrAs is a ferromagnetic semiconductor. [21] Figure 5A shows the HRTEM image of the ultra-small CrAs nanoparticles/ quantum dots. Since these nanoparticles are almost of the size of quantum dots hence isolation of these as powders was difficult. The quantum dots preferred to disperse well in the solution of various polar solvents like ethanol, dichloromethane giving a green solution. So in order to characterize these nanoparticles, we performed EDS and photoluminescence (PL) spectroscopy. Figure 5B shows the PL spectra of the CrAs. There was a strong absorption peak at 481nm which corresponds to 2.5 eV. Band gap of bulk CrAs is1.8 eV, indicating that there is a considerable quantum confinement in the nanoparticles resulting in a blue shift of the absorbance band.
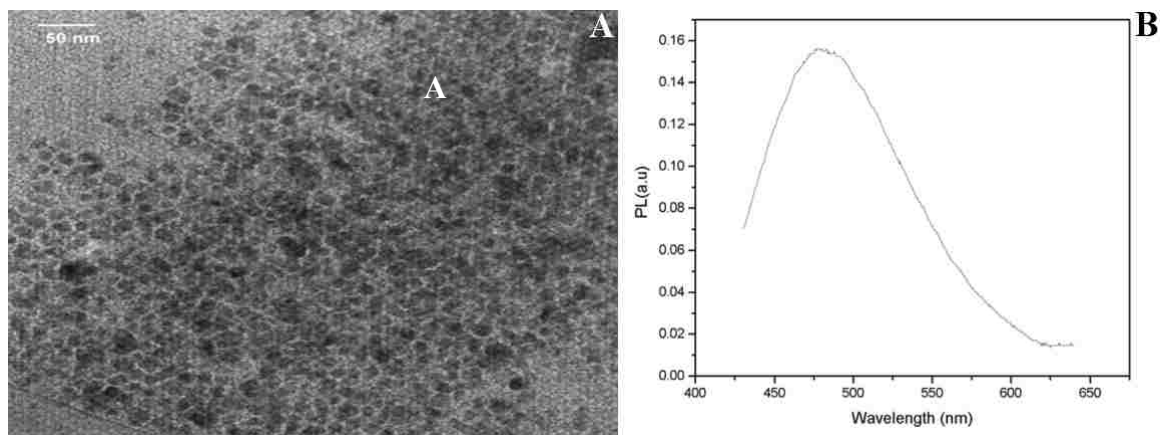
Figure 5(A) HRTEM image of CrAs quantum dots (B) PL spectra).

These nanostructured transition metal arsenides also exhibited novel magnetic properties. The FeAs and CoAs nanostructures were attracted to the lab magnet to variable extents. From figure 6A and B it can be seen that the FeAs and CoAs nanoparticles were ferromagnetic at low temperatures and superparamagnetic at high temperatures, respectively. A detailed study of these magnetic properties have been discussed by the authors in separate publications.[17]
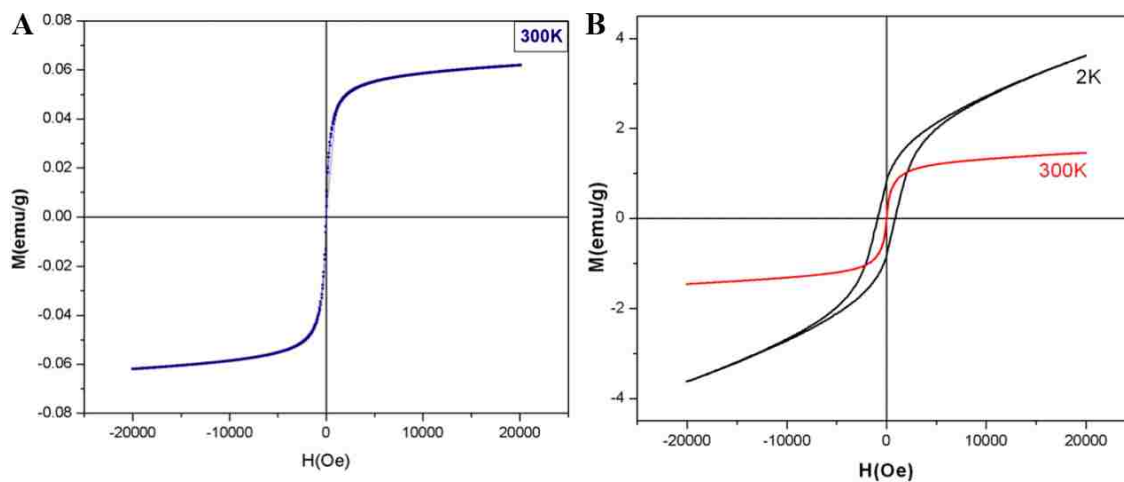
Figure 6(A) (B) M vs H curve for FeAs and CoAs nanostructures showing superparamagnetism

By conducting several experiments with variable reaction parameters and detailed observation, we have hypothesized a mechanism that can very well explain the evolution of morphology for these nanostructures. The conversion process starts with a burst of nucleation at t = 0 following the addition of $E_x(CO)_y$ forming a E-rich nuclei capped with HDA. TPA then starts reacting at the surface of the nuclei and the initial layers of EAs formed coat the nuclei. At conditions of constant high temperature (300°C) As diffuses deeper into the nuclei thereby promoting conversion of the core to EAs. Depending on the critical radius and stability of the nuclei it can then redissolve and re-precipitate. Continuous dissolution and precipitation will cause different morphologies to emerge. We have observed that the propensity towards formation of one dimensional nanostructures increases as the d electrons availability increases i.e. as we proceed from left to right in the series (Cr to Co). CoAs forms nanorods whereas CrAs forms extremely small quantum dots. Also it can be said the formation of the carbonaceous shell depends on the catalytic ability of the transition metal and the FeAs nanostructures exhibited the most predominant carbonaceous shell. A pictorial representation of this growth mechanism is shown in Figure 7 for EAs.

CONCLUSIONS

We have successfully devised a method for the synthesis of nanostructured transition metal arsenides. The novelty of this method is the one step facile precipitation of the monoarsenides of the 3d transition element series. The chemistry behind this conversion is very simple ad involves simple redox chemistry between the metal carbonyls and arsine precursor aided by the amine surfactant which provides a slightly

basic medium. Authors are also trying to apply this technique to the main group metals arsenides like InAs, GaAs, which are used for optoelectronics.
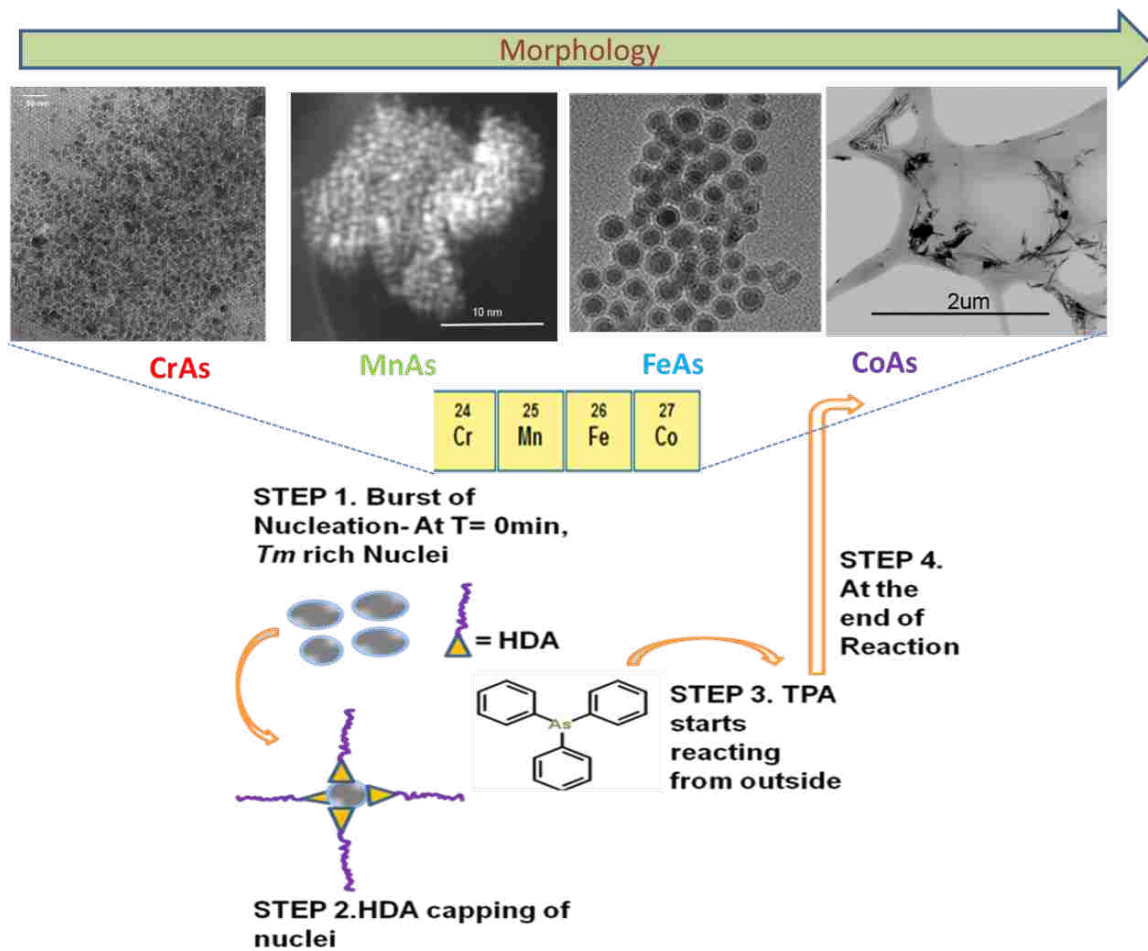

Figure7: Growth mechanism of the *E*As nanostructures

NOTES AND REFERENCES

1.   Marzin J-Y, Gérard J-M, Izrael A, Barrier D, Bastard G. Photoluminescence of single InAs quantum dots obtained by self-organized growth on GaAs. Phys. Rev. lett. 1994;73:716.

2.   Howe A-T, Fensham PJ. Electronic properties of binary compounds of the first-row transition metals. Q Rev, Chem Soc.Rev. 1967;21:507-24.

3.   Suchet J. Crystal Chemistry and Semiconduction in Transition Metal Binary Compounds: Elsevier; 2012.

4.   Bichat MP, Gillot F, Monconduit L, Favier F, Morcrette M, Lemoigno F, Doublet ML. Redox-Induced Structural Change in Anode Materials Based on Tetrahedral (MPn4)x- Transition Metal Pnictides. Chem. Mater. 2004;16:1002-13.

5.   Xie W-H, Liu B-G, Pettifor D. Half-metallic ferromagnetism in transition metal pnictides and chalcogenides with wurtzite structure. Phys. Rev. B. 2003;68:134407.

6.   Chioncel L, Katsnelson M, De Wijs G, De Groot R, Lichtenstein A. Tunable spin transport in CrAs: Role of correlation effects. Phys. Rev. B. 2005;71:085111.

7.   Sanyal B, Bergqvist L, Eriksson O. Ferromagnetic materials in the zinc-blende structure. Phys. Rev. B 2003; 68; 054417.

8.   Häggström L, Gustavsson-Seidel A, Fjellvåg H. A Mössbauer Study of Helimagnetic FeAs. Europhys. Lett. 1989;9:87.

9.   Matsukura F, Ohno H, Dietl T. chapter 1 III-V ferromagnetic semiconductors. Handbook of Magnetic Materials. 2002;14:1-87.

10.   Vetcher A, Kattwinkel A, Kleeberg C, Kraus E, Froebel P, Baerner K. The thermoelectric power of some magnetically ordered transition metal pnictides. Phys. Status Solidi A. 1998;166:843-51.

11.   Zhou, K.; Jiang, S.; Wang, B.; Shi, Y.; Liu, J.; Hong, N.; Hu, Y.; Gui, Z., Combined effect of transition metal phosphide (MxPy, M= Ni, Co, and Cu) and intumescent flame retardant system on polypropylene. Polymer. Adv. Tech. 2014.

12.   Abu II, Smith KJ. HDN and HDS of model compounds and light gas oil derived from Athabasca bitumen using supported metal phosphide catalysts. Applied Catalysis A: General. 2007;328:58-67.

13.   Oyama ST. Novel catalysts for advanced hydroprocessing: transition metal phosphides. J. Catal. 2003;216:343-52.

14.   Stinner C, Prins R, Weber T. Binary and ternary transition-metal phosphides as HDN catalysts. Journal of catalysis. 2001;202:187-94.

15.   Zuzaniuk V, Prins R. Synthesis and characterization of silica-supported transition-metal phosphides as HDN catalysts. J. Catal. 2003;219:85-96.

16.   Chiang R-K, Chiang R-T. Formation of hollow Ni_2P nanoparticles based on the nanoscale Kirkendall effect. Inorg.Chem.. 2007;46:369-71.

17.   Desai P, Song K, Koza J, Pariti A, Nath M. Soft Chemical Synthetic Route to Superparamagnteic FeAs@C nanoparticles with High Blocking temperature: Chem. Mater. 2013;25;1510-1518.

18.   Yang Li, Malik AM, and Paul O'Brien. Synthesis of Single-Crystalline CoP Nanowires by a One-Pot Metal-Organic Route . J. Am. Chem. Soc. 2005;127; 16020-16021.

19.   Perera SC, Tsoi G, Wenger LE, Brock SL. Synthesis of MnP Nanocrystals by Treatment of Metal Carbonyl Complexes with Phosphines: A New, Versatile Route to Nanoscale Transition Metal Phosphides. J. Am. Chem. Soc. 2003; 125:13960-1.

20.   Addamiano A, On the Preparation of the Phosphides of Aluminum, Gallium and Indium. J. Am. Chem. Soc. 1996, 82 ; 1537-1540.

21.   Berger R. Crystallographic Data on New Arsenides and Antimonides of Titanium and Scandium. Acta. Chem Scand. A. 1977;31.

22.   Rundqvist S, Carlsson B. New metal-rich arsenides of niobium and tantalum. Acta Chem Scand. 1968;22.

23.   Saparov, B.; Mitchell, J. E.; Sefat, A. S., Properties of binary transition-metal arsenides (TAs). Supercond. Sci. Technol. 2012; 25 ; 084016.

24.   Selte K, Kjekshus A, Jamison WE, Andresen A, Engebretsen J. Magnetic Structure and Properties of CrAs. Acta Chem. Scand. 1971;25:1703-14.

25.   Selte K, Kjekshus A. Crystal structure of FeAs. Acta Chem Scand. 1969; 23: 2047-2054.

26.   Motizuki K. Recent advances in the theory of magnetism of nickel monoarsenide-type transition-metal chalcogenides and pnictides. J. Magn. Magn. Mater. 1987; 70:1-7.

27. Willerström J-O. Stacking disorder in NbP, TaP, NbAs and TaAs. J.Alloys Compd. 1984;99:273-83.

28. Shein IR, Ivanovskii AL. Electronic properties of novel 6 K superconductor LiFeP in comparison with LiFeAs from first principles calculations. Solid State Commun. 2010;150:152-6.

29. Lu J, Xie Y, Jiang X, He W, Du G. A safe sonochemical route to iron, cobalt and nickel monoarsenides. J. Mater. Chem. 2001;11:3281-4.

30. Zhang X, Wang C, Qian X, Xie Y, Qian Y. Synthesis of nanocrystalline iron monoarsenide via a reductive recombination pathway. J. Solid State Chem. 1999;144: 237-9.

31. Stamm KL, Garno JC, Liu G-y, Brock SL. A general methodology for the synthesis of transition metal pnictide nanoparticles from pnictate precursors and its application to iron-phosphorus phases. J.Am.Chem.Soc.. 2003;125:4038-9.

IV. ONE POT SYNTHESIS OF $Co(CO_3)_{0.5}$. OH 0.11 H_2O NANOWIRES AND THEIR CONVERSION TO Co_3O_4 NANOWIRES

Prachi Desai, Manashi Nath[*]

Department of Chemistry, Missouri University of Science and Technology, MO 65401

ABSTRACT

Co_3O_4 nanowires were synthesized using a hydrothermal technique using cobalt carbonyl $(Co_2(CO)_8)$ and hexadecylamine $(C_{16}H_{35}N)$ as cobalt source and reducing agent/ surfactant respectively. The reaction proceeds via a carbonate intermediate. We have been able to isolate the intermediate as $Co(CO_3)_{0.5}$. (OH) 0.11 H_2O. The as-synthesized nanowires change in morphology and composition after annealing at 200 °C yielding the Co_3O_4 nanowires which are morphologically thinner, smoother and highly magnetic in nature. The Co_3O_4 nanowires are 10nm in diameter and micron long. The nanowires are antiferromagnetic and a much lower $T_N = 19K$ is observed as seen in the ZFC. Here, in this report we discuss the simple two step method, and the magnetic properties of Co_3O_4 nanowires. The importance of Co_3O_4 nanowires lie in the areas such as supercapacitors , lithium ion battery cathodes and as photocatalysts.

INTRODUCTION

Co_3O_4 is a p- type magnetic semiconductor(1) finding diverse applications in Lithium ion batteries(2) for energy storage, gas sensors (2) electrochromic devices(3) and heterogeneous catalysts (4,5) supercapacitors(6) etc. In the bulk state tricobalt tetraoxide, the oxide is antiferromagnetic (AFM), TN Neel temperature being 40K.(7) The formula unit for Co_3O_4 is described AB_2O_4 (A → Co^{2+}, B → Co^{3+}) and exhibits a normal spinel crystal structure with occupation of tetrahedral, A sites by Co^{2+} and octahedral B sites by

Co^{3+}. Its magnetic moment arises due to Co^{2+} ions largely because of spins, with a small contribution from spin–orbit coupling. (8)

Nanostructured Co_3O_4 presents itself as a better option in comparison to bulk owing to high surface area and variable morphology crucial to enhancing functionality in many devices. The methods of synthesis for Co_3O_4 nanowires can be classified into synthesis from Co and its oxidation or via precursors involving basic carbonate intermediates such as $Co(CO_3)_{0.35}(NO3)_{0.2}(OH)_{1.1}$ $1.74H_2O$ (6) and $Co(CO_3)_{0.5}(OH)•0.11H_2O$. (9) In literature, hydrothermal route has known to yield such precursors of cobalt carbonate hydroxide. Recently, sodium chloride salt was used to synthesize single-crystalline nanowires into a chrysanthemum-like hierarchical assembly of $Co(CO_3)_{0.5}(OH)•0.11H_2O$. (10) Other reports also show $Co(CO_3)_{0.5}$. OH 0.11 H_20, the basic cobalt carbonate in its nanoform has shown great potential, serving as a precursor for porous Co_3O_4 nanowires upon annealing at lower temperatures. Many methods have been developed to isolate the precursor and further anneal it to yield nanoparticles, nanocubes, nanospheres , nanoplatelets and nanowires of Co_3O_4 which mostly involved using urea as a base to reduce the Cobalt precursor into intermediates that are further annealed at low temperatures. (11) Reports of other shape-controlled synthesis of cobalt carbonate/hydroxide intermediates involving three different structures, viz., 1-dimensional (1D) needle-like nanorods, two-dimensional (2D) leaf-like nanosheets, and three-dimensional (3D) oval-shaped microparticles, were synthesized through varying parameters such as precursor (cobalt acetate) concentrations and volume ratio of polyethylene glycol to water.(1, 12, 13,14) In this article we report formation of $Co(CO_3)_{0.5}$. OH 0.11 H_20 by cobalt carbonyl $Co_2(CO)_8$ and Hexadecylamine,

$C_{16}H_{35}N$ as starting materials for conversion into Co_3O_4 nanowires on annealing. The ZFC W data suggests anti-ferromagnetic nature in these wires. The Neel temperature 20K is much lower than that predicted for other nanowires systems. The existence of a much lower T_N suggests that these nanowires are not core shell also there is no or very little exchange bias in surface spins thereby inducing an early onset of paramagnetism.

EXPERIMENTAL

All of the chemical reagents were of analytical grade and used without further purification in these experiments. The synthesis was carried in a Teflon autoclave. 1 mM $Co_2(CO)_8$ and 5mM of Hexadecylamine was added. The contents were sealed in air and kept in high temperature oven (280°C) for a period of 12- 24 hrs. The autoclave was cooled to room temperature and then purified using ethanol, hexane and ultracentrifugation. The collected powder was dried and analyzed by PXRD (Phillips Xpert) , STEM (Helios nano)and TEM(FEI F20). Part of the product was annealed in air at 200°C for 7 h to yield the Co_3O_4 nanowires. Magnetic moment and isothermal magnetization was collected from a SQUID magnetometer and the vibrating sample magnetization (VSM) option of physical property measurement system (PPMS) respectively

RESULTS AND DISCUSSIONS

Figure 1(A) shows the PXRD pattern of the precursor cobalt carbonate hydroxide hydrate, $Co(CO_3)_{0.5}.OH$ 0.11 H_2O matched to the phases (JCPDS # 00-048-0083) and Figure 1(B) is the low magnification STEM image of a bundle of the cobalt

hydroxyl carbonate, $Co(CO_3)_{0.5}$. OH 0.11 H_2O nanowires. During the course of microscopic analysis it was seen that in various samples these nanowires were bundles and sticking to each other in spite of washing with ethanol and water formed such bundles as can be seen in Figure 1(B).
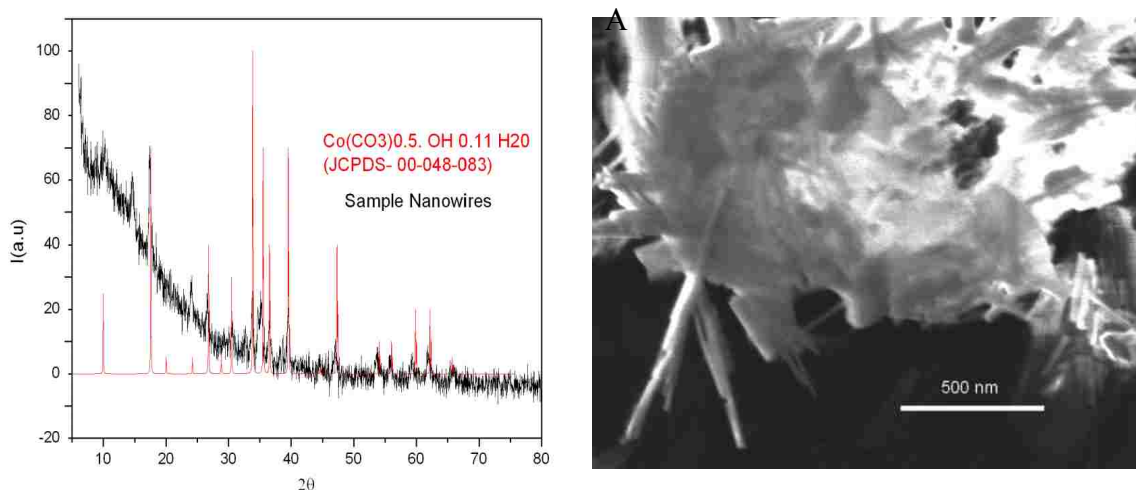

Figure 1: (A) PXRD pattern of the cobalt hydroxy carbonate nanowires and (B) low magnification STEM of cobalt hydroxy carbonate nanowire

The decomposition temperatures was assessed by the thermal analysis. For this purpose we chose the TGA method. Figure 2 (shows the TGA curve of the $Co(CO_3)_{0.5}$. OH 0.11 H_2O nanowires. It shows the TGA heating profile of the cobalt hydroxyl carbonate sample There are two predominant weight loss steps between 167°C -303°C and 303 – 382°C the weight loss stops at around 400 °C. The first weight loss is a slow transformation compared to the second more drastic one. The differential curve shows the maximum weight change occurs at 350°C. Several samples were annealed at 350°C. However, most of the annealing experiments that were conducted at that temperature resulted in deformation of the nanowire morphology of the starting precursor.
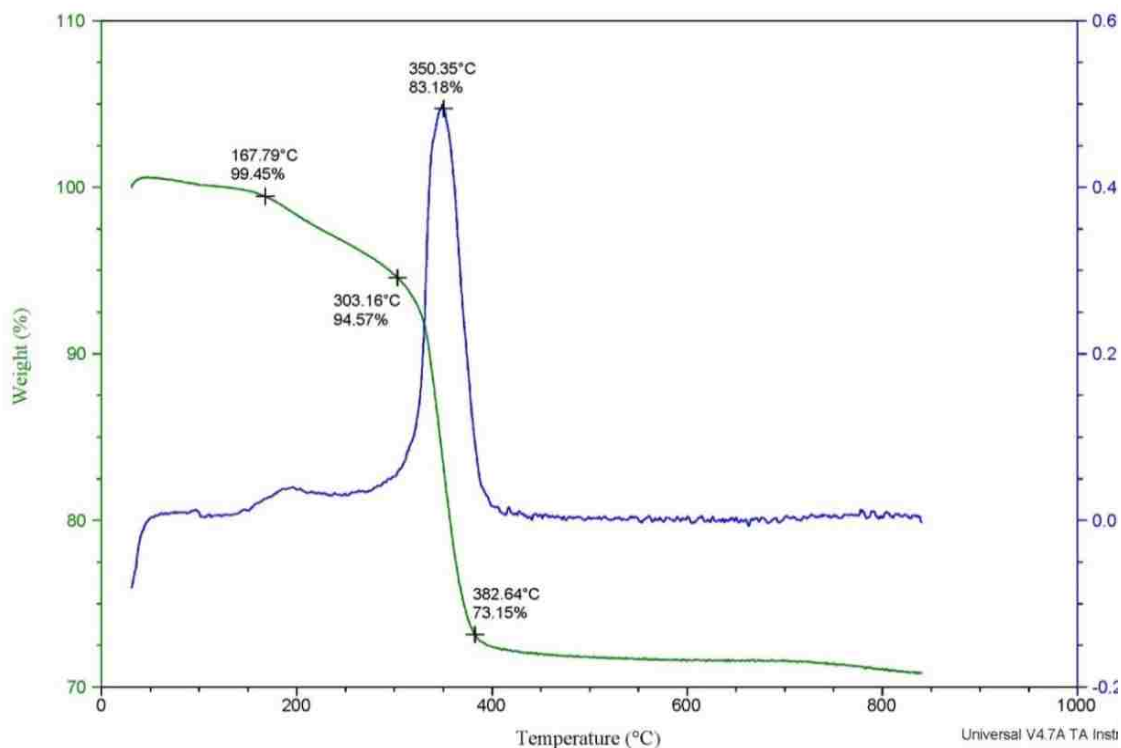
Figure 2: TGA of the cobalt hydroxy carbonate nanowires

In order to preserve the precursor nanowire morphology we chose to anneal them at 200°C for 7h. This low temperature enabled highly crystalline sample formation and gave the nanowires enough time to unbundle without deforming to form individual micron long nanowires as seen in figure 3. Figure 3(A) shows the annealed cobalt oxide Co_3O_4 (JCPDS # 01-074-1657) respectively. All the peaks can be identified and matched to the cubic spinel Co_3O_4 structure (space group Fd3̄m). Some peaks of Co_3O_4 are also visible in the precursor nanowires pattern. The crystallite size is 11nm average as calculated by the Scherrer equation. The morphology and structure of the product were further characterized transmission electron microscopy (TEM).
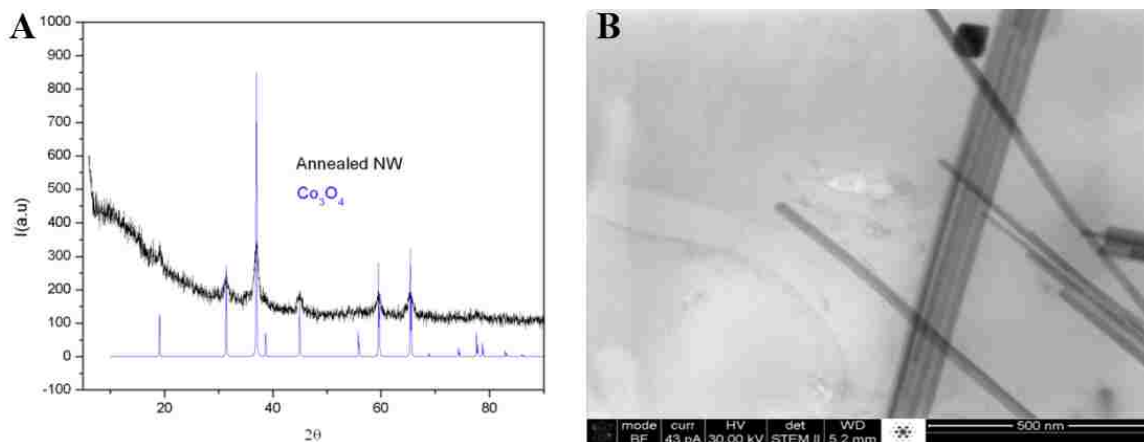
Figure 3: (A) PXRD pattern of Co_3O_4 nanowires after annealing (B) Low magnification STEM image of Co3O4 nanowires after annealing

This bundling effect was reduced after the annealing process. As can be seen in Figure 3(b) shows the low magnification STEM image of the corresponding Co3O4 nanowires obtained after annealing at 200°C the precursor nanowires are highly agglomerated and much thicker when compared to Co_3O_4 nanowires. The core-shell nature of the precursor is evident in Fig 3 (HRTEM). The nanowires are rough in appearance. The nanowires are covered throughout with crystalline oxide which also appears as some impurities in the PXRD. Presumably, they are the crystallites seen on the nanowires structure in TEM Figure 4. Since the annealed sample was magnetic in nature we also performed magnetic studies on the Co_3O_4 sample. magnetic hysteresis measurement of Co3O4wascarried out in an applied magnetic field at room temperature about20 °C, with the field sweeping from -20k Oe to +20k Oe.
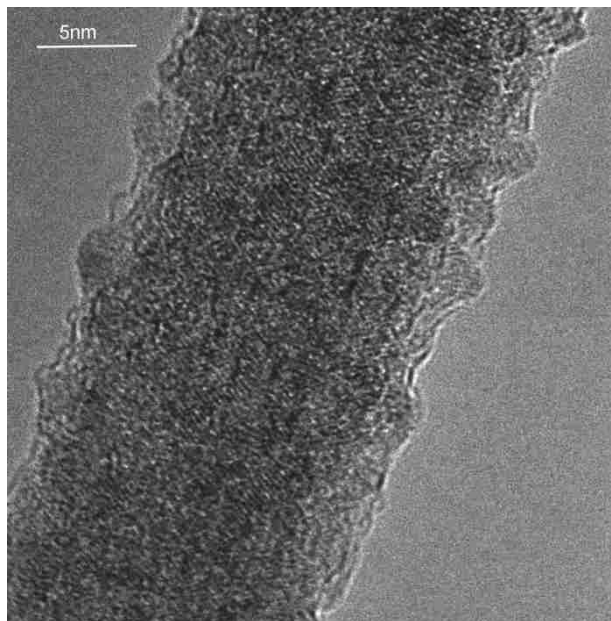
Figure 4: HRTEM of individual Co_3O_4 nanowire

Figure 5(A) is the hysteresis loop of Co3O4 Nanowires at 5K with the inset showing weak ferromagnet behavior at 5K. A very small Coercivity 142 Oe and remnant magnetization of $4.2X10^{-4}$ emu/g is observed. The room temperature hysteresis as seen in Figure 5B does not display ferromagnetic interactions. Figure 6 Magnetization M (emu/g) versus temperature (K) in a magnetic field H = 100 Oe for Co3O4 nanowires. An antiferromagnetic ordering is evident with a Néel temperature $T_N \approx 20$ K The inset shows a fit of the magnetic susceptibility χ from 10 to 200 K to the Curie-Weiss law, $1/\chi$ (g/emu) versus T (K), Curie-Weiss temperature $\theta = -30K$. Thus the anti-ferromagnetic range for this system is small From the ZFC curve an estimate of the Neel temperature can be made. Neel temperature is the temperature below which the material exhibits anti-ferromagnetic ordering. This temperature is estimated to be at 20K for this ensemble of nanowires. The neel temperature of Bulk Co_3O_4 is 40K. at 5K and 300 K.
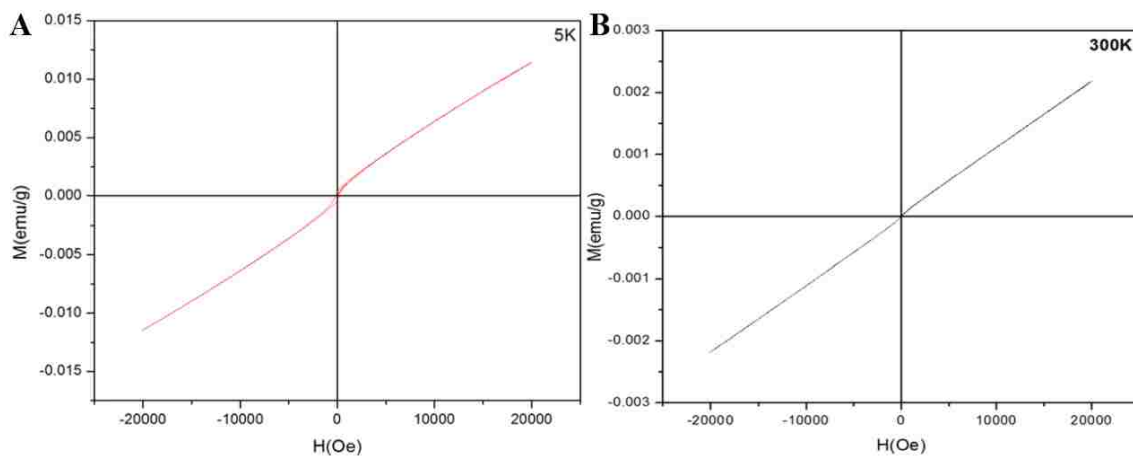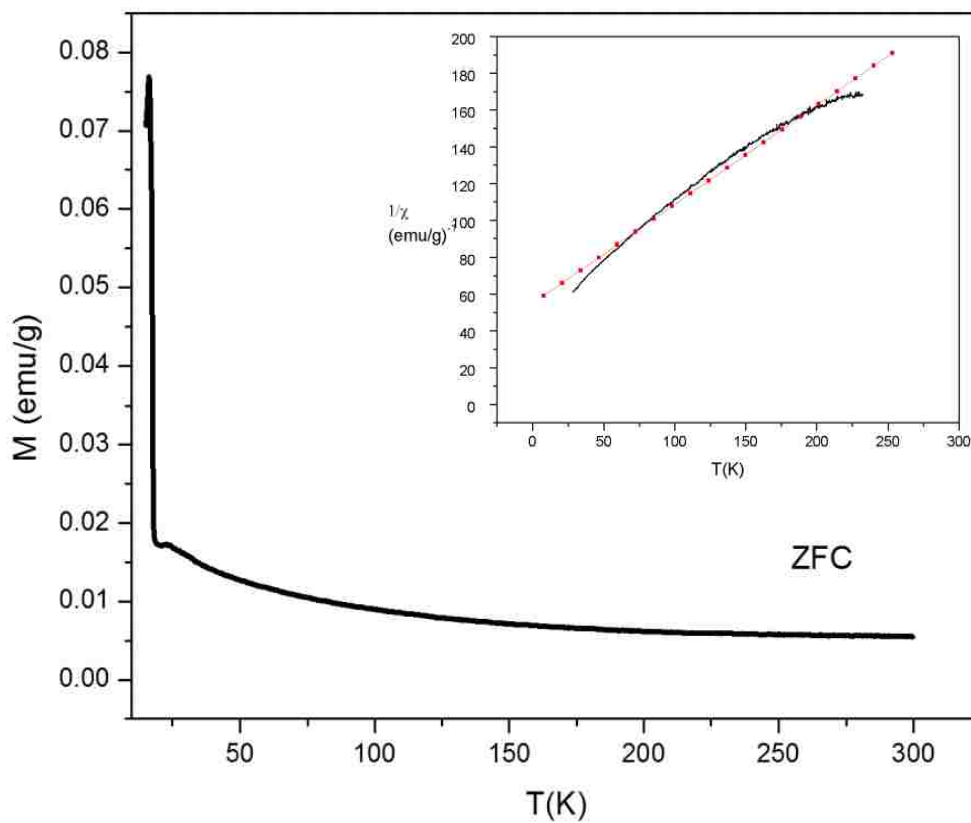
Figure 5(A) M vs H at 5K (B) M vs H at 300 K

Figure 6: M Vs T at 100 Oe. Inset shows the linear fit for $1/\chi$ vs T in the paramagnetic region.

CONCLUSIONS

In summary, we report a new way to synthesize anti-ferromagnetic Co_3O_4 nanowires. The method discussed is fairly simple modification of the solvothermal methods. Only two precursors are needed in this process, $Co_2(CO)_8$ and hexadecylamine. Since many important applications depend of these nanostructures a much easier method like this one serves to establish the growing need of the industry. The other advantage of this method is that fairly old $Co_2(CO)_8$ which may be on the verge of decomposition may be utilized to give such nanostructures.

REFERENCES

(1)   Cao, A.-M.; Hu, J.-S.; Liang, H.-P.; Song, W.-G.; Wan, L.-J.; He, X.-L.; Gao, X.-G.; Xia, S.-H. *J. Phys. Chem. B* **2006**, *110*, 15858.

(2)   Li, W.-Y.; Xu, L.-N.; Chen, J. *Adv. Funct. Mater.* **2005**, *15*, 851.

(3)   Shim, H.-S.; Shinde, V. R.; Kim, H. J.; Sung, Y.-E.; Kim, W. B. *Thin Solid Films* **2008**, *516*, 8573.

(4)   Sun, Y.; Lv, P.; Yang, J.-Y.; He, L.; Nie, J.-C.; Liu, X.; Li, Y. *Chem. Comm.* **2011**, *47*, 11279.

(5)   Ren, Z.; Guo, Y.; Zhang, Z.; Liu, C.; Gao, P.-X. *J. Mater. Chem. A* **2013**, *1*, 9897.

(6)   Song, Z.; Zhang, Y.; Liu, W.; Zhang, S.; Liu, G.; Chen, H.; Qiu, J. *Electrochim. Acta* **2013**, *112*, 120.

(7)   Salabas, E. L.; Rumplecker, A.; Kleitz, F.; Radu, F.; Schüth, F. *Nano Lett.* **2006**, *6*, 2977.

(8)   Roth, W. *Journal de Physique* **1964**, *25*, 507.

(9)   Desai P, Pariti A, Nath M. Synthesis and Magnetic Properties of CoAs Nanostructures. NanoResearch (submitted)

(10)   Xiong, S.; Chen, J. S.; Lou, X. W.; Zeng, H. C. *Adv. Funct. Mater.* **2012**, *22*, 861.

(11)   Yang, G.; Gao, D.; Zhang, J.; Zhang, J.; Shi, Z.; Zhu, Z.; Xue, D. *RSC Adv.* **2013**, *3*, 508.

(12)   Wang, D.; Wang, Q.; Wang, T. *Inorg.Chem.* **2011**, *50*, 6482.

(13)   Wang, X.; Tian, W.; Zhai, T.; Zhi, C.; Bando, Y.; Golberg, D. *J. Mater. Chem.* **2012**, *22*, 2331

(14)   Wang, Y.; Zhong, Z.; Chen, Y.; Ng, C. T.; Lin, J. *Nano Res.* **2011**, *4*, 695

SECTION

2. CONCLUSIONS AND REMARKS

This research focused on designing novel syntheses of inorganic nanomaterials with properties like superparamagnetism, superconductivity, and semi-conductivity. These nanomaterials in principle have various applications in electronics, memory devices, and magnetic instruments. The synthesis of the "nanoparticulate" LiFeAs an iron–based superconductor was attempted by the "*sacrificial template method*" For this purpose a solvent-less, facile, and highly reproducible hot injection method for synthesis of FeAs nanoparticles was developed. We were the first to synthesize and discover superparamagnetism in the core shell nanoparticles of FeAs coated with carbon (15nm). The method that we developed used wet chemistry and organometallic precursors. The nanoparticles obtained are easily purified by solvent exchange and application of electromagnets. Interestingly, such materials can be exploited to develop novel applications such as magnetic recording media and magnetic refrigerants.

When this method was used as the starting point for testing the sacrificial template approach as described in the introduction. FeAs layers were used as sacrificial templates and Li+ ions were intercalated into these layers. The system is a ternary layered compound with alternating stacks of Li+ and [FeAs]- layers. This ternary phase acts as a superconductor at temperatures below 18K. By making nanostructures of LiFeAs, we shall be in a better position to answer fundamental questions like weather or not nanostructuring aids to superconductivity and if at all there is an increase in Tc. Although

recent experiments have indicated that the phase formation can be achieved but maintaining morphology of the starting nanoparticles maybe tricky and crucial step. The nanoparticles at synthesis temperatures of 750 °C are still in 1-100nm range. The Mossbauer studies have suggested similar chemical shifts as in literature phase of LiFeAs.

APPENDIX A.

CONVERSION OF FeAs@C NANOPARTICLES TO LiFeAs

Introduction

Interest in LiFeAs high temperature nanostructured superconductors stems from the fact that after FeSe it is the least complex system to address synthetically. Reductive lithium intercalation is a well addressed topic in literature that can be used to convert the basic structural motif of FeAs into LiFeAs. Designing routes to nanostructured LiFeAs involve limiting the use of three elements making the synthetic path much easier. These can behave as model systems in understanding the superconductivity of these pnictides at the nanoscale.

Applications of the high temperature superconductors depend on the magnitudes of parametrics like critical temperature, critical field, and critical current. The critical temperature the temperature below which the material enters the superconducting state (Tc) for the bulk LiFeAs is 18K. Superconducting cables, magnetic levitation, MRI, SQUIDS, magnetic shields and energy storage are present themselves as arenas for applicability of these superconducting nanomaterials.

Methods

In practice, solid state synthesis is the main technique which yields bulk LiFeAs at 800ºC. Figure A1 shows the principle of the approach taken. It involves the pre-synthesized nanoparticles of FeAs@C as discussed in paper 1 and reacting with metallic lithium or other Lithium sources under various conditions. In this study, we have undertaken three routes for the synthesis of LiFeAs nanoparticles. These were the solid state route, in-situ synthesis and electrochemical synthesis. These are described as follows
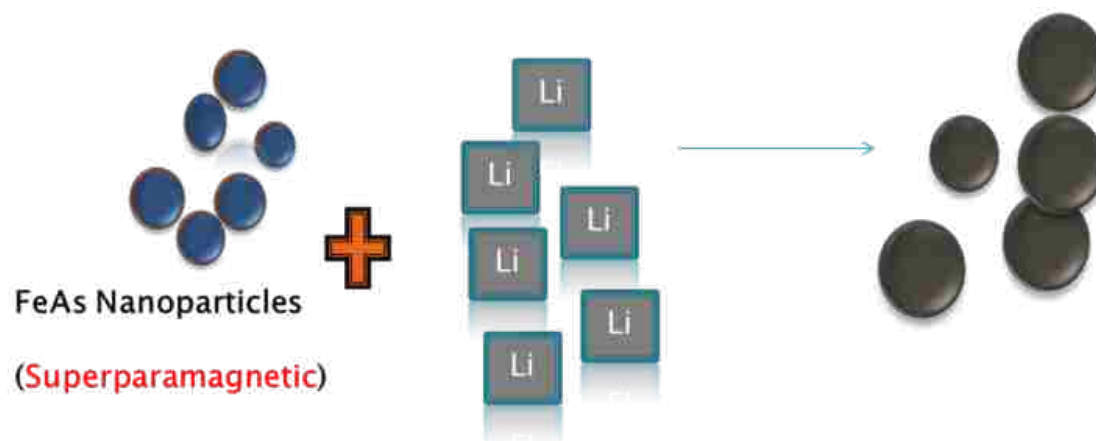
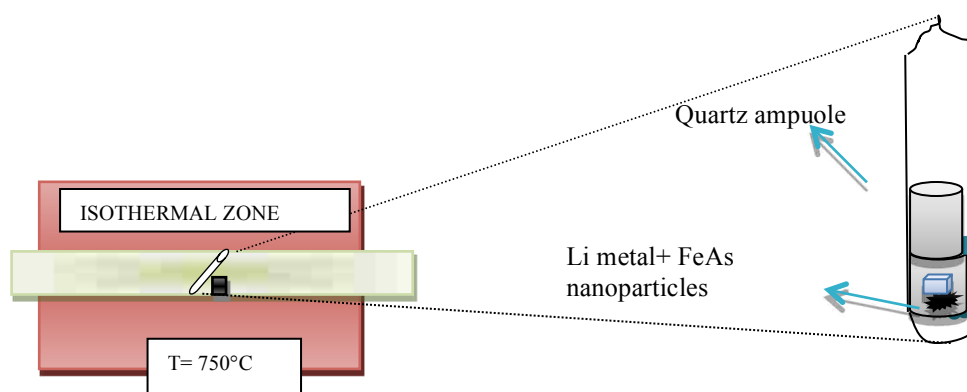Figure A1: Idea behind the sacrificial template approach

Figure A2: Schematic of the solid state synthesis route.

Table 1 shows the reaction stoichiometric conditions that were at 750ºC and the results obtained for the conditions employed using FeAs (nanoparticles) as a sacrificial template with Li metal as shown in figure A2. All handling was done in an Argon glove box. The nanoparticulate powder of FeAs@C were weighed and transferred into a graphite crucible. Several modifications were made to the design and finally it was concluded that in order to prevent Li loss the crucible must be covered with another

crucible. The crucible assembly was loaded in to a quartz tube whose ends were then sealed under minimal N_2 exposure in the Schlenk line. After the sealing the ampoule was transferred to a furnace which was evacuated and heated to 750 ºC at the rate of 5ºC / min under vacuum and cooled with the same rate.

Table 1: Reaction conditions for solid state synthesis

FeAs nanoparticles(mg)	Li metal (mg)	Mass Ratio	Time(H)	Temp°C	XRD
10.5	10	1.05:1	48	750	LiFeAs + LiO
21.3	3.0	7:1	48	750	FeAs
34.0	33.3	1.02:1	48	750	LiFeAs + FeAs
11.3	9	1.25:1	48	750	FeAs + As
34.2	36.6	1:0.94	72	500	Fe+Li$_2$O+C
20.0	23.8	1:0.84	24	750	FeAs2+Li5FeO4
37.9	34.5	1.09:1	30	750	LiFeAs (2 phases) + Li$_2$O
119.8	Na= 47.2	2.52	40	800	NaFeAs + FeAs

Lithium electrochemical Insertion In the electrochemical insertion process FeAs pellets were made and used in electrochemical reactions as shown in the figure for Route 3 description. Coin cells were also assembled by the usual way with pasting FeAs@C + PVDF slurry (in NMP). Carbon black powder which is traditionally added to the slurry

for improved conductivity was omitted. Lithium foil was used as a cathode and FeAs acted as the anode for the discharge / lithium insertion process. Initially low currents were applied from 0.3µA- 5 µA. Later it was figured that C/20- C50 rate was found most appropriate. The cut off voltage were in the 0.01-3.0V range.
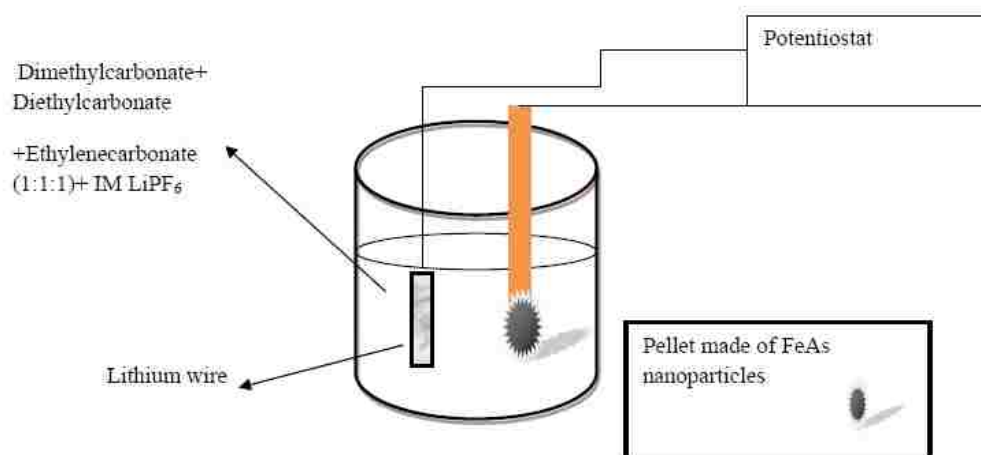

Figure A3: Principle of electrochemical insertion in FeAs@C nanoparticles

Results and Discussions

Based on the results of the above methods we figured that the solid state method works the best for nanostructured LiFeAs. However, it also suffers from some problems like sintering and incomplete conversion of FeAs@C nanoparticles to LiFeAs and has no control on the obtained phases and side products. Route 2 was the most unsuccessful where the FeAs@C nanoparticles did not convert at all in most experiments and hence not discussed here. Route 3, the electrochemical insertion showed promise by good discharge curves but no conversion into LiFeAs. Indirect signs of Fe^{3+} reduction to Fe^{2+} was seen by the PXRD containing phases of Fe_2As. We also realized due to the highly

sensitive nature of LiFeAs the reactions require absolutely no moisture, air and N_2 exposure.

Route 1: The sacrificial template found partial success as it can be seen that when the mass ratios of FeAs : Li were 1.05: 1 *i.e.* (1: 17, mole ratio) LiFeAs appeared as a phase in the PXRD. This shown in PXRD of sample- SS-LiFeAs-6. The pattern can be ascribed to JCPDS 01-087-1981.
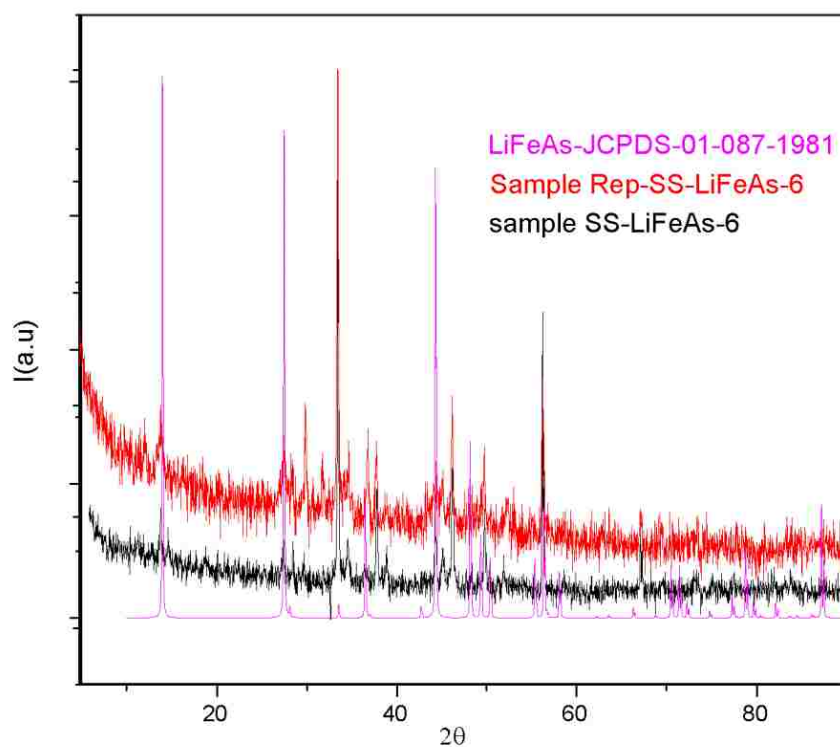

Figure A4: PXRD pattern of sample SS-LiFeAs-6 with matching LiFeAs

FigureA5 shows the TEM images it is evident that the starting core shell morphology of FeAs @C nanoparticles is lost however, larger sizes nanocrystals have taken its place. This method can be considered as a processing method for nanoparticles owing to the increase in size. It is well known that coalescence, agglomeration of
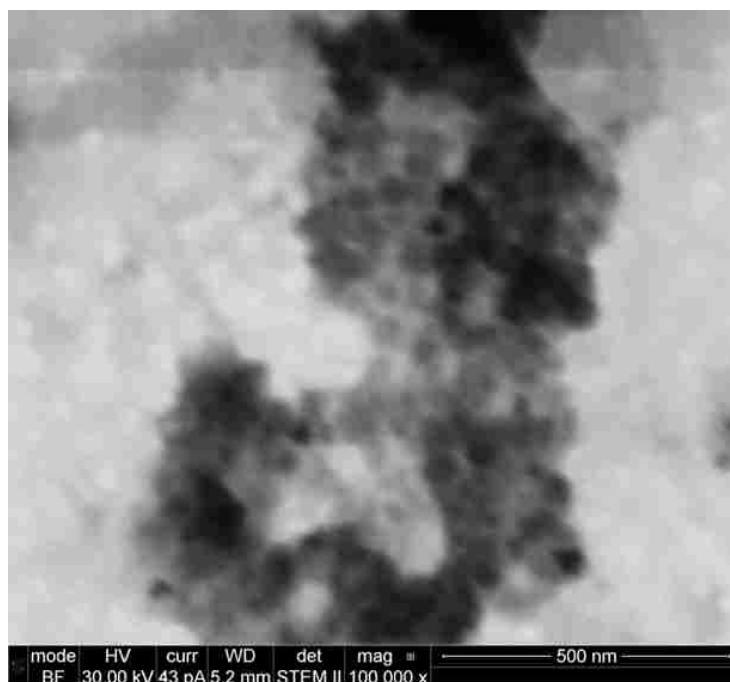
Figure A5: Low magnification TEM of SS-LiFeAs-6

particles and sintering may be the factors that are responsible for gain in particle size and change in particle morphology more so happening during the processing of the nanomaterials. Figure 3 shows the Low magnification TEM of the nanoparticles containing LiFeAs. The low magnification image shows signs of grain growth via necking. These nanoparticles were highly sensitive to air. The particle ensemble can be matched to LiFeAs and Li_2O. These results bring us one step closer to the realization of LiFeAs as nanoparticles.
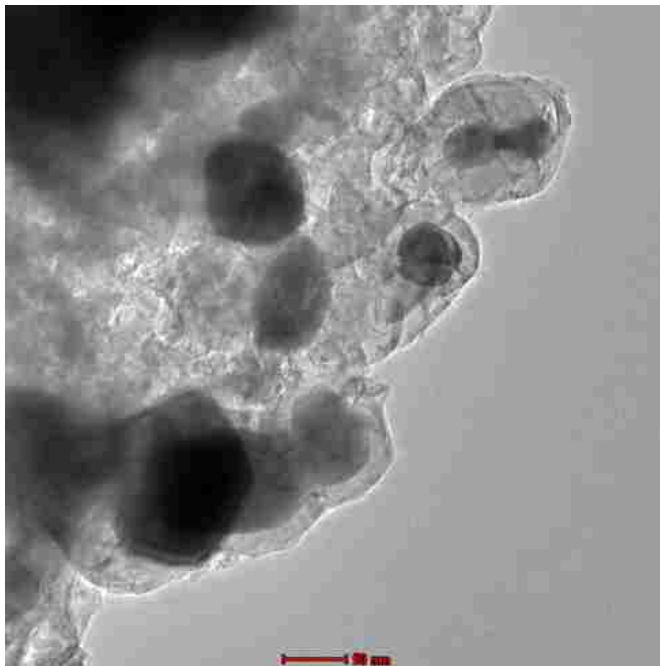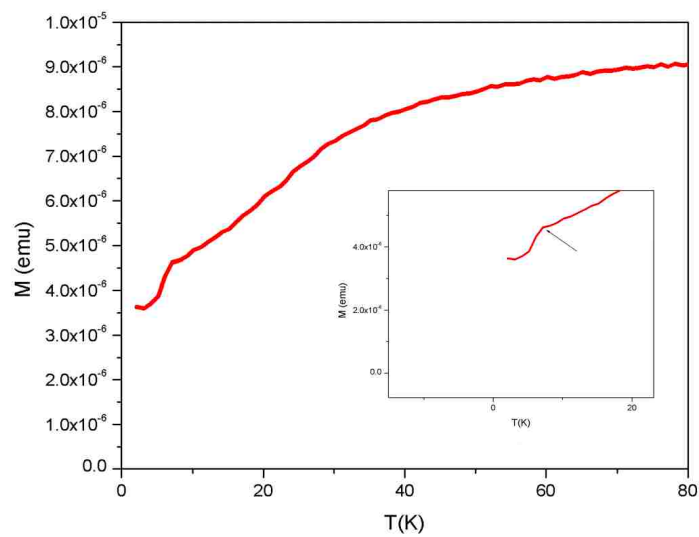
Figure A6: HRTEM of LiFeAs-SS-6

Figure A7: M vs T curve of SS-LiFeAs-6

Figure A7 is the M vs T curve for these nanoparticles under no field. At 7K there is a drop in magnetization. Since the sample is impure and has several other peaks the magnetization does not go below zero i.e. a true diamagnetic superconducting state not achieved.

Route 3: We found that FeAs can be a good anode material for lithium ion batteries since the attributes of a good anode is high specific capacity, no SEI formation, operating voltages less those 1.5 V vs Li less volume change. Figure A8 shows the discharge curve of FeAs. During the discharge process the Li+ ions are inserted into the FeAs. It can be seen that the discharge process took 2.2 hrs. @ -6 μA current. The theoretical specific capacity of FeAs bulk (not coated with C) is 205mAh/g. The observed capacity was 12mAh/g. Clearly the capacity fade was due to the presence of the thick C coating on the surface of the nanoparticles. The non-graphitized coating provided hindrance to the Li^+ ions in the nanoparticle. The choice of current / C rate applied to the anode fluctuated as well. A low current would stop the battery tester abruptly. After the discharge process the coin cell was opened and the Cu foil was recovered. The powder on foil was examined by PXRD. Figure A9 shows the PXRD pattern, it shows traces of Fe_2As. This showed incomplete conversion. However, LiFeAs peaks were missing.

.
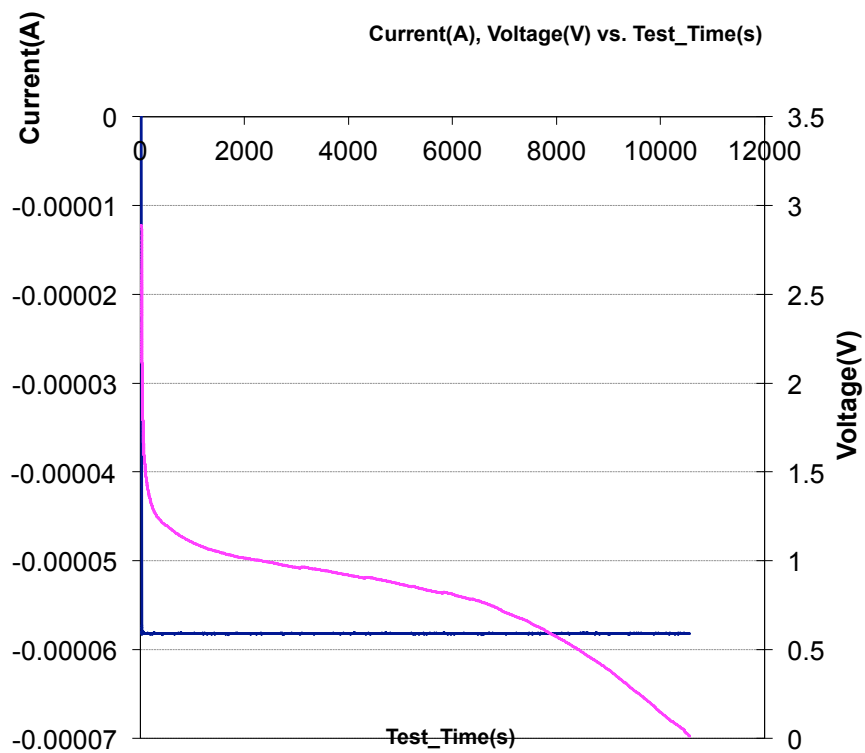
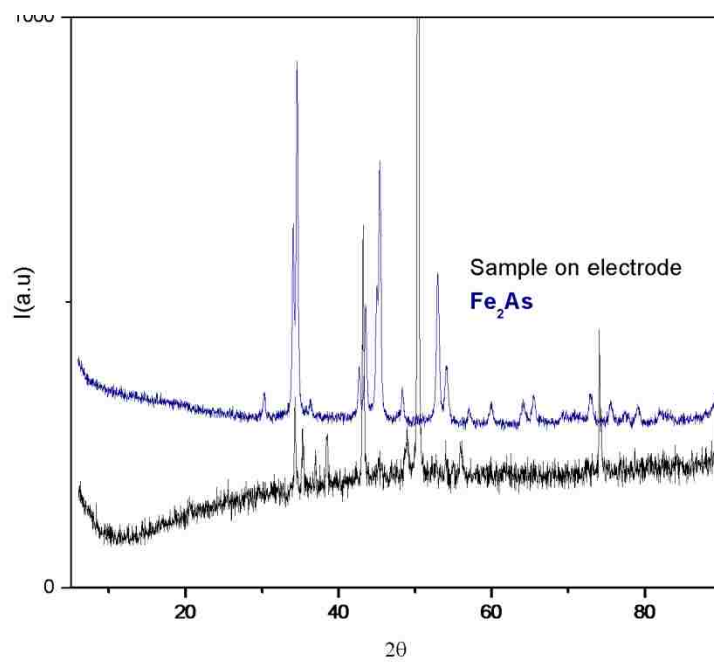FigureA8: Discharge curve of coin cell anode.

Figure A9: PXRD pattern of coin cell cathode

APPENDIX B:

OPTIMIZATION OF Bi_2Se_3 ELECTRODEPOSITION

Introduction

In 1980's it was discovered that electrons when confined to 2 dimensions under an applied magnetic field exhibits topological order, underlining the Quantum Hall Effect. Topological insulators are a class of materials that are effective insulators in bulk but conduct electricity on their surfaces. Recently 3D materials have also shown this order where the magnetic field has been attributed to the one generated by spin orbit coupling. The presence of surface metallic states that can give rise to dissipation less charge transport which being the most ideal situation for energy transport. This is possible due to scattering promoted by grain boundaries and impurities restricted to the bulk states. The topological states remain invariant to them. The Bi_2Se_3 topological insulator can also be induced to become a bulk superconductor, with T c~3.8 K, by copper intercalation in the van der Waals gaps between the Bi2Se3 layers.

Since nanostructured materials have high surface to volume ratio, in this perspective it would be interesting to evaluate nanostructures of these topological insulators as dissipation less charge transport elements. Nanostructures of compounds like Bi_2Se_3, Bi_2Te_3, Ag_2Te has been synthesized and evaluated for topological order at various temperatures and magnetic field applied. Other applications of topological insulators include spintronics. Owing to the unique spin texture, the charge current on the surface of the topological insulators supplies a net spin-density, which would be useful in memory or spin-torque devices. Optoelectronics is an emerging area for topological insulators: the excellent transport properties and the linear relation between energy and momentum in some topological insulators make them competitors with graphene

photonics and optoelectronics, for applications such as transparent conductors and wideband photo detectors.
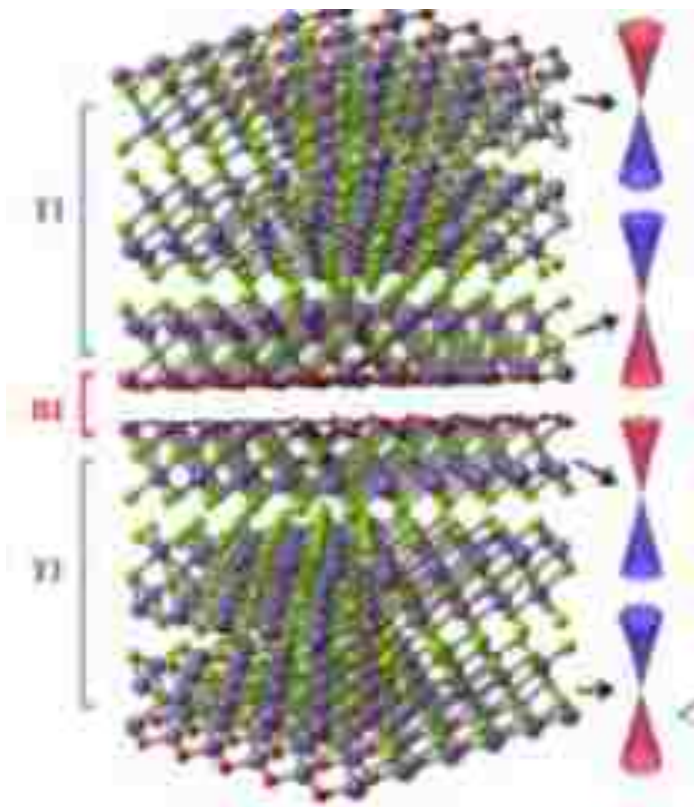

Figure B1 Superlattices of Bi2Se3 and corresponding Dirac cones

The synthesis of Bi_2Se_3 nanopillars on conducting substrates involves using a combination of two methods (1) E- beam lithography and (2) Electrodeposition. Here we report the conditions for electrodeposition of Bi2Se3 as a thin film. At first the conducting ITO pieces were cleaned with acetone and dried. Two layers of PMMA were spin coated on to the conducting side of ITO. The thickness of the PMMA film ranged from 0.25μm to 0.75μm. As shown in scheme 1 using a predefined pattern the PMMA was exposed to an electron beam of known current. The areas which get exposed to the

beam are etched away using 1:3 MIBK: IPA solution. This generated the nano- electrodes needed for the predefined growth of Bi_2Se_3.

In step 2 the ITO with the pattern was connected to the working electrode whereas Pt wire was used as counter electrode. The potentials were measured against an Ag/AgCl electrode. The electrolyte consisted of 1mM solution of $Bi_2(NO)_3.5H_2O$ and SeO_2 in 1 M $HNO_3.N_2$ was bubbled through the solutions to remove any dissolved $O_2.5mL$ of each solution was taken in a beaker and the set up was as shown in figure below. The depositions were carried out at -0.5V for variable times. The substrates were taken out cleaned with water and annealed 200ºC for 15-30 min.
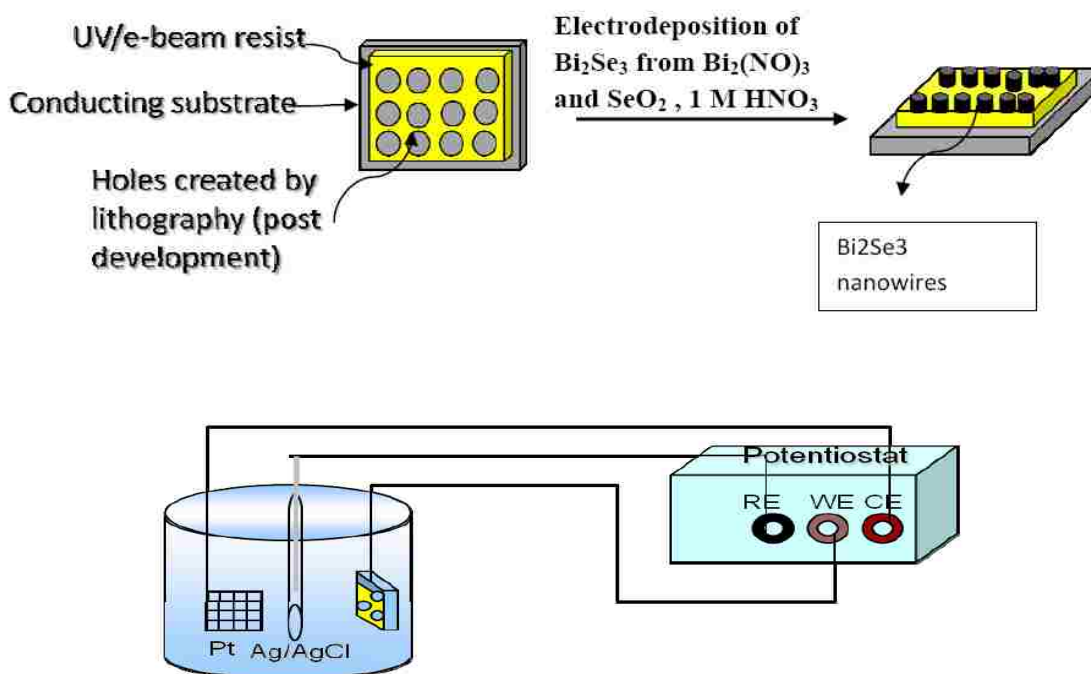

Figure B2: Steps for nanorods electrodeposition on ITO

Preliminary Results and Discussions

Since the ITO was coated with an insulating PMMA the areas which were exposed after the development procedure served as nanoelectrodes. The Bi_2Se_3 is grown on these nanoelectrodes as nanopillars. The choice of appropriate potential is made by running a cyclic voltametry experiment. Figure 3 shows the CV of the solution containing bismuth nitrate and selenium dioxide in 10 mL of water on bare ITO. Figure 4 shows the shows the thin film XRD of Bi_2Se_3 deposited on bare ITO. The film is nanocrystalline which matches to the Bi_2Se_3 phase (JCPDS-01-085-0519). Figure 5 shows the deposited films on patterned substrates for 15 sec.
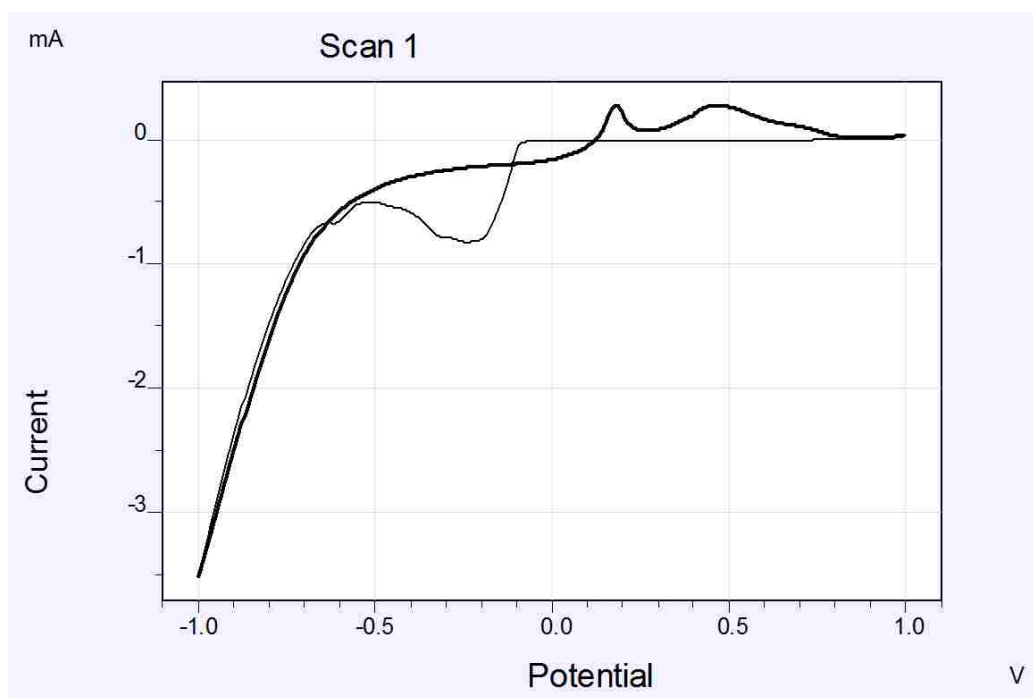

Figure B3: CV of the solution containing Bismuth Nitrate and Selenium dioxide in 10 mL of water
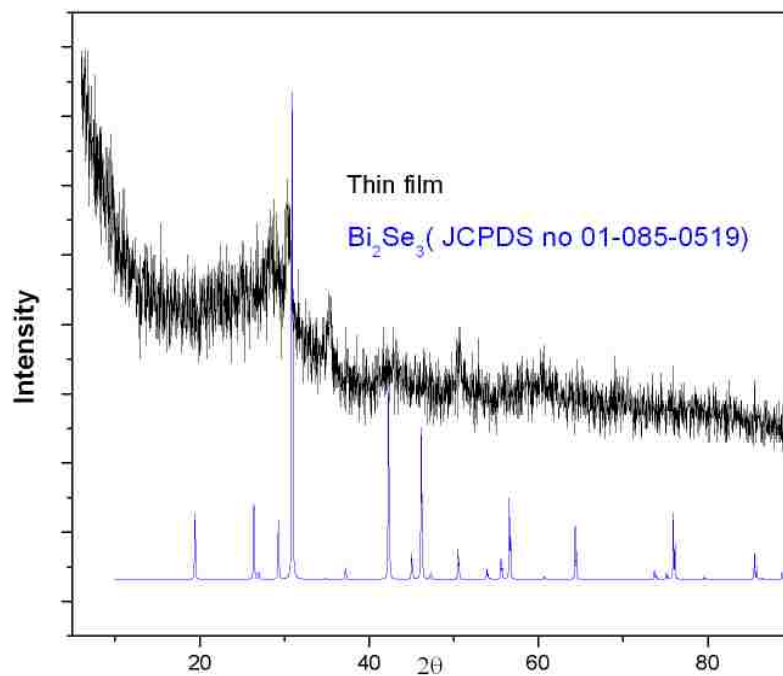
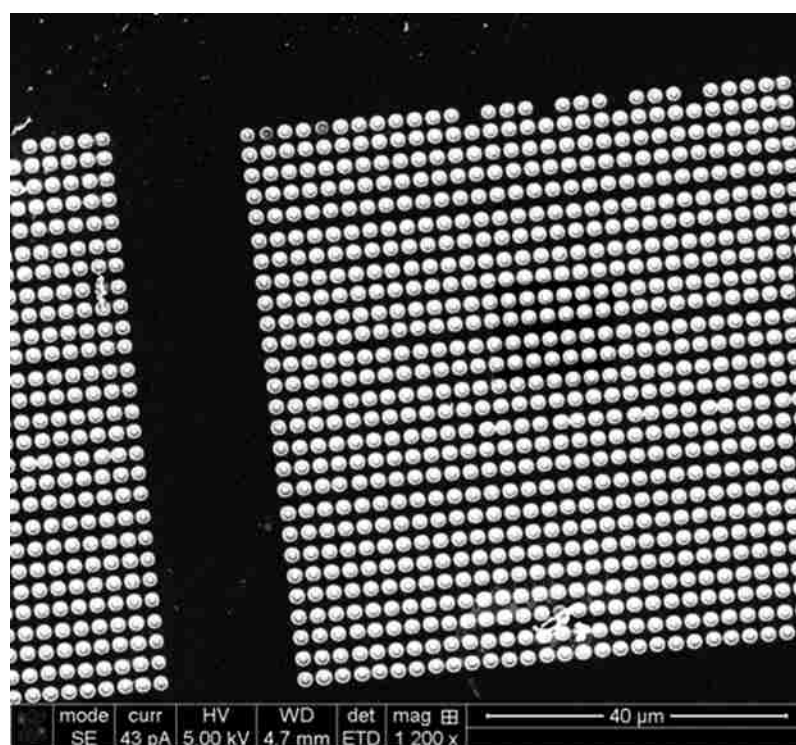Figure B4: PXRD pattern of thin film annealed at 200ºC

Figure B5: SEM image of Bi:Se deposited on patterns for 15 seconds

VITA

Prachi Desai was born as Prachi Sood in Delhi, India. In 2002, she received the Bachelors in Science (B.Sc.) Chemistry (honors) degree from Miranda House College, University of Delhi, India. At Miranda House College, her interest in chemistry thrived where she represented her college at various inter-college chemistry quizzes and won many prizes. She was also the vice-president of Rasayanika – a chemistry society of Miranda House where she organized events and fund raising for the organization.

From 2005- 2007, after finishing B.Sc. she received Masters (M.Sc.) in Inorganic Chemistry from University of Delhi, Delhi, India. Prachi Desai also completed a second Bachelors in chemical education from Central Institute of Education, University of Delhi, Delhi ,India in the year 2008 for which she was awarded a scholarship prize. Following that she also worked in solid state physics laboratory under the defense research and development organization of India and gained experience in the field of nanotechnology. In 2009 she joined PhD under Dr. Nath at Missouri University of Science and technology where she undertook synthetic inorganic chemistry of nanomaterials.